6-20-2022 2:00 PM

Deformation Conditions of Quartz-rich Mylonites of the Grenville Front Tectonic Zone and Application to the Crustal Strength

Xueke Chang, *The University of Western Ontario*

Supervisor: Jiang, Dazhi, *The University of Western Ontario*

A thesis submitted in partial fulfillment of the requirements for the Master of Science degree in Geology

Abstract

This thesis analyzes a suite of mylonites from the Grenville Front shear zone exposed southeast of Sudbury, Ontario. Lattice preferred orientations, titanium-in-quartz thermometer, and dynamically recrystallized grain size piezometer measurements were applied to obtain the deformation mechanisms, deformation temperatures (T), and differential stresses (σ), respectively. Results show that these mylonites were formed in the shear zone during the terminal stage of the Grenville Orogeny. The dominant deformation mechanism is by regime 2 dislocation creep. The deformation temperature is between 425-567 °C, and the differential stress is between 56-133 MPa. These results are discussed in the context of wet quartzite flow laws. This study shows that a recently calibrated flow law that considers the pressure dependence of the activation enthalpy is applicable to the Grenville Front shear zone. The thesis also improves our understanding of the Grenville Front deformation zone.

Keywords

Grenville Front, Quartz flow law, Titanium-in-quartz, Dynamic recrystallization, Lattice preferred orientation, Paleo-stress analysis

Summary for Lay Audience

The Earth's crust has a significant impact on our daily life. Studying the crust provides us with a better understanding of tectonic history. Quartz plays a key role in determining the crustal strength as it is abundant. As a result, scientists study how quartz reacts to different temperatures and pressures in experiments and make flow laws that can describe the deformation behavior of quartzite. However, these flow laws do not always produce the same results. This is primarily due to how fluid changes the properties of rocks. Also, we cannot simulate the strain rate, which occurs naturally, in the lab. This is the limitation of working with models. The question is, how do we know the flow laws obtained via experiments can apply to natural quartzite. The solution is analyzing the deformation conditions of quartz in natural shear zones and comparing them with experimentally deformed quartz. If the microstructures are similar, that means similar deformation mechanisms are taking place. This thesis focuses on the deformation conditions of naturally deformed quartz-rich mylonites from the Grenville Front. Deformation temperatures were obtained from measuring the amount of titanium in quartz because titanium concentration has a temperature dependence when Ti is substituted for silicon in quartz. Deformation mechanisms were interpreted by the pattern of quartz c-axes orientation. Dynamically recrystallized grain sizes were measured because they reveal the paleo-stress. The temperatures, stress, and deformation mechanisms were compiled and plotted on a flow law profile to see how well they fit into current flow laws. I propose that the deformation condition of our samples from the Grenville Front can fit with the current flow law. According to the overall observation, I interpret that these mylonites were brought to the surface by a process called exhumation. This thesis enhances our understanding of the Grenville Front deformation and flow law studies.

Acknowledgments

First, I would like to thank my supervisor, Professor Dazhi Jiang. His consistent support, guidance, patience, and encouragement helped me to get through my graduate study here at Western University. Being Dazhi's graduate student and his teaching assistant will be one of the most remarkable things in my life. I would like to thank our visiting scholar, Biwei Xiang, as well. Biwei helped me a lot with the Titanium-in-quartz measurement and the stereographic projection. Without their help, I would not be able to finish the research.

Second, I appreciate my parents. They have been supporting me since I was born. They sent me to schools and support me to learn anything I want. Even when I am away from my hometown, they still encourage me all the time. I always feel better after talking to them and listening to their warm encouragement.

Also, I want to thank Changcheng Li, Lucy Xi Lu (for previous data and discussion regarding the study area), Ziyan Cui (for friendship and discussion about the LPOs), Janek Urbanski (for discussion about the LPOs and DRX), and Maha Alam (for helping me in the field trip). Without you, I was not able to compile so much data together for this thesis.

Last, I feel thankful to all members of the Geology program. It's been a pleasure to study here for two years. The program is a good environment for communication and research; the professors give excellent lectures and presentations; the students are enthusiastic about geology. These all make me feel encouraged and enjoyed learning.

Table of Contents

List of Tables

List of Figures

List of Appendices

Chapter 1

Introduction and thesis outlines

1.1 Introduction to the problem

Quartz is one of the most abundant minerals in Earth's crust, and as such its rheological properties play an essential role in determining the crustal strength (Gleason and Tullis, 1995; Lu and Jiang, 2019; Luan and Paterson, 1992). Laboratory experiments on the creep of quartzite contribute to our understanding of the rheology of the ductile crust (Griggs 1967; Gleason and Tullis, 1995; Kohlstedt et al., 1995; Karato, 2008; Hirth and Tullis, 1992; Lu and Jiang, 2019; Shelton and Tullis, 1981). However, despite many decades of effort, there are still great uncertainties related to quartzite flow laws (Gleason et al., 1993; Gleason and Tullis, 1995; Luan and Paterson, 1992; Lu and Jiang, 2019; Rutter and Brodie, 2004; Tokle et al., 2019). The major uncertainties in the quartzite flow laws are caused by the effect of water - "hydraulic weakening" (Griggs, 1967; Tullis and Yund, 1989) and the influence of other phase minerals (Lu and Jiang; Tullis, 2002). Figure 1.1 (Lu and Jiang, 2019) is a plot of three experimentally determined quartz flow laws (Fukuda and Shimizu, 2017; Gleason and Tullis, 1995; Luan and Paterson, 1992; Rutter and Brodie, 2004). Flow laws by Luan and Paterson (1992) (L&P), Gleason and Tullis (1995) (G&T), Rutter and Brodie (2004) (R&B) and their revisions are plotted, using a strain rate of 10^{-12} s^{-1} and a geothermal gradient of 20 degree/km (Figure 1.1). The revised flow laws are based on Fukuda and Shimizu (2017) (Lu and Jiang, 2019). As the figure shows, these three flow laws predict significantly different flow strengths for the continental crust based on wet quartzites. A well-known contrast between natural deformation and laboratory deformation is the strain rate, which is one of the major challenges in creep experiments. The natural strain rate such as in ductile shear zones is likely in the range of $10^{-12+/-1}$ per second (Lu and Jiang, 2019; McGill et al., 2013; Schulz and Evans, 2000; Sutherland et al., 2006) whereas the lab strain rate is about 10^{-6} per second. To ensure that microstructures of similar deformation mechanisms are compared between natural and experimental deformations, it is critically important to examine the microstructures and deformation conditions of the naturally deformed quartz-bearing rocks (Cross et al., 2015; Heilbronner and Kilian, 2017; Hirth et al., 2001; Kidder et al., 2013; Stipp et al., 2002). The most important conditions for deformation include the temperature, differential stress, and deformation mechanisms. Analyzing these conditions allows us to compare the deformation microstructures generated in both labs and nature so that scientists know whether similar mechanisms were activated (Cross et al., 2015; Zhang et al., 2022). Scientists can then investigate whether the experiment-based flow laws can be applied to the ductile deformation of quartz in natural conditions. Documenting the deformation conditions of quartz in natural shear zones is therefore necessary for a better understanding of not only the flow laws, but also the natural shear zones.

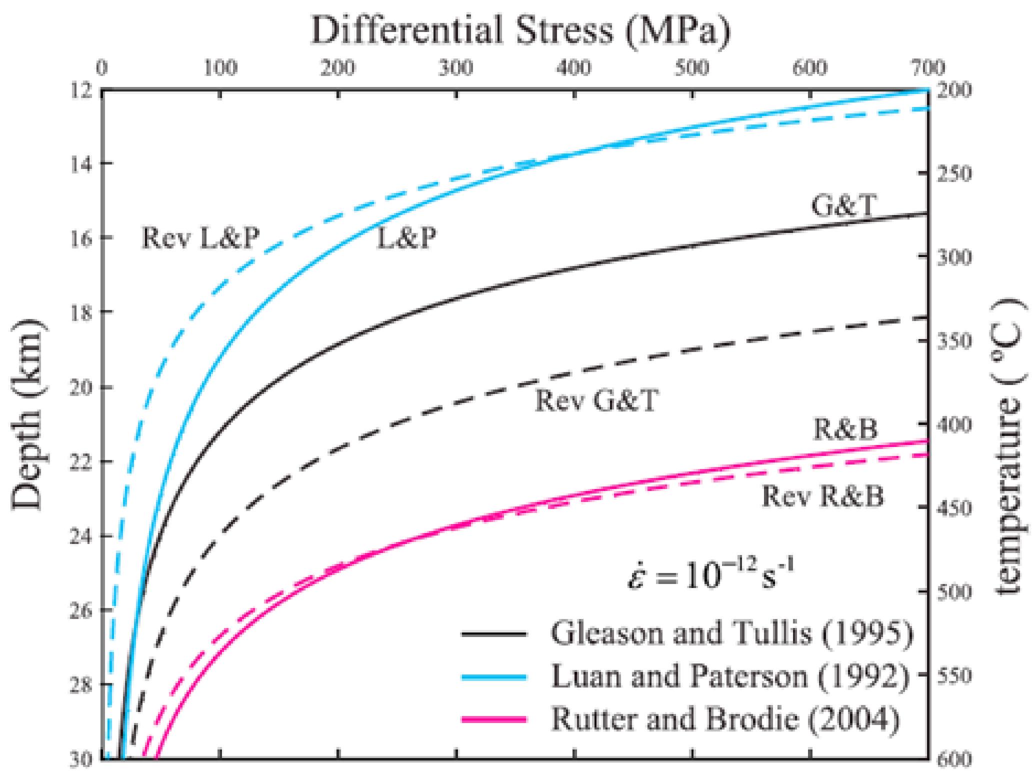

Figure 1.1 Three flow laws compared (Lu and Jiang, 2019).

1.2 Literature review on flow laws

Studies on the quartzite flow laws have been conducted for decades to understand the ductile deformation of the lithosphere (see Gleason and Tullis, 1995; Kohlstedt et al., 1995; Lu and Jiang, 2019 for reviews). These studies usually involve conducting creep experiments on natural or synthetic rocks at different P-T conditions (Gleason and Tullis, 1995; Hirth and Tullis, 1992; Karato et al., 1986; Luan and Paterson, 1992). The deformation behaviors of rocks are expressed by a power law formula, showing the relationship between the strain rate and the differential stress:

$$\dot{\varepsilon} = \mathrm{A} \exp\left(-\frac{Q}{RT}\right) \sigma^{n} \tag{1}$$

where $\dot{\varepsilon}$ is the strain rate (s^{-1}), A is a preexponential parameter ($MPa^{-n} \cdot s^{-1}$), Q is activation energy (kJ/mol), R is gas constant ($J \cdot mol^{-1} K^{-1}$), T is absolute temperature (K), σ is differential stress (MPa), n is stress exponent. This form of flow law is for the dislocation creep of polycrystals (Lu and Jiang, 2019). Since different sets of parameters are calibrated in various experiments, they can predict significantly different flow strength, as shown in Figure 1.1. Therefore, many efforts have been made to explain and reduce the uncertainties among these flow laws.

The flow law of quartzite has been updated by adding a water fugacity term to accomplish the weakening effect caused by the water in rocks (Griggs, 1967; Lu and Jiang, 2019). The previous parameter A has been replaced by $\mathrm{A} \cdot f_w^{m}$ (Fukuda and Shimizu, 2017; Rutter and Brodie, 2004), with A being the pre-exponential parameter (different from A in Equation 1), f_w being the water fugacity (MPa) and m being the exponent of water fugacity. Water fugacity and the exponential term are also determined in experiments (Holyoke and Kronenberg, 2013).

Lu and Jiang (2019) considered the effect of activation volume on the activation enthalpy. The flow law is thus modified by replacing the Q term with Q+PV (Frost and Ashby, 1982), considering this effect:

$$\dot{\varepsilon} = \mathrm{A}\, f_w^{m} \exp\left(-\frac{Q+PV}{RT}\right) \sigma^{n} \tag{2}$$

where P is pressure (MPa), V is activation volume (cm^3/mol), Q is activation energy, Q+PV is activation enthalpy. Equation 2 is now the common type of recently calibrated quartzite flow laws (Lu and Jiang, 2019; Lusk et al., 2021; Tokle et al., 2019).

1.3 Thesis objectives and outlines

Mylonites are rocks deformed in ductile shear zones, preserving microstructures that reflect the deformation conditions. The goal of this study is to analyze the deformation conditions of natural quartz-rich mylonites, which will better constrain and test the quartz flow laws. In the Grenville Front Tectonic Zone (GFTZ) (Davidson, 1984; La Tour, 1981; Li, 2012), excellent quartz-rich mylonites are well exposed about 2 km south of the township of Coniston, east of Sudbury, Ontario. Previous work by Li (2012) and fieldwork by other students from Western's Laboratory for Structural Geology and Tectonics have mapped the area in detail and collected many oriented samples.

In my thesis work, in collaboration with former students Ziyan Cui and Janek Urbanski, and visiting scientist Dr. Biwei Xiang, I investigated the deformation microstructures, differential stress and deformation temperatures of some quartz-rich mylonites from the above-mentioned field area (hereafter referred to as "the study area").

Obtaining the deformation conditions of natural mylonite samples from involved the following processes. First, the lattice preferred orientations (LPOs) of quartz c-axes were measured to examine the dominant slip systems (Bhandari and Jiang, 2021; Oliver, 1996). Open angles of the quartz c-axes were used to estimate deformation temperatures qualitatively (Faleiros et al., 2016; Law, 2014; Oliver, 1996). Second, the deformation temperatures are further determined using the Titanium-in-quartz thermometers (Huang and Audétat, 2012; Thomas et al., 2010; Wark and Watson, 2006). Third, dynamically recrystallized grain sizes were measured to evaluate the differential stress (Hirth and Tullis, 1992; Stipp and Tullis, 2003; Stipp et al., 2002) using the piezometer of Shimizu (2008).

The thesis outlines are as follows: A detailed description and the geological background of the study area and samples are given in Chapter 2. Chapter 3 provides the background of these concepts and methods. The results of the work are presented in Chapter 4. Once these deformation conditions were obtained, they were interpreted and applied to existing flow laws, as discussed in Chapter 5. Finally, Chapter 6 summarizes the findings of this thesis.

Chapter 2

Geologic settings and sample description

2.1 Geologic settings

Research samples for this study were collected from quartz-rich mylonites from the Grenville Front Tectonic Zone (GFTZ) (Figure 2.1). The Proterozoic Grenville Province (pink) is in tectonic contact with the Archean Superior, Churchill, and Nain Provinces to the northwest. The GFTZ is a high-strain zone along with the contact that deformed rocks across the contact. The study area is marked by the red star in Figure 2.1. The brief geologic history of the study area is discussed in this Chapter.

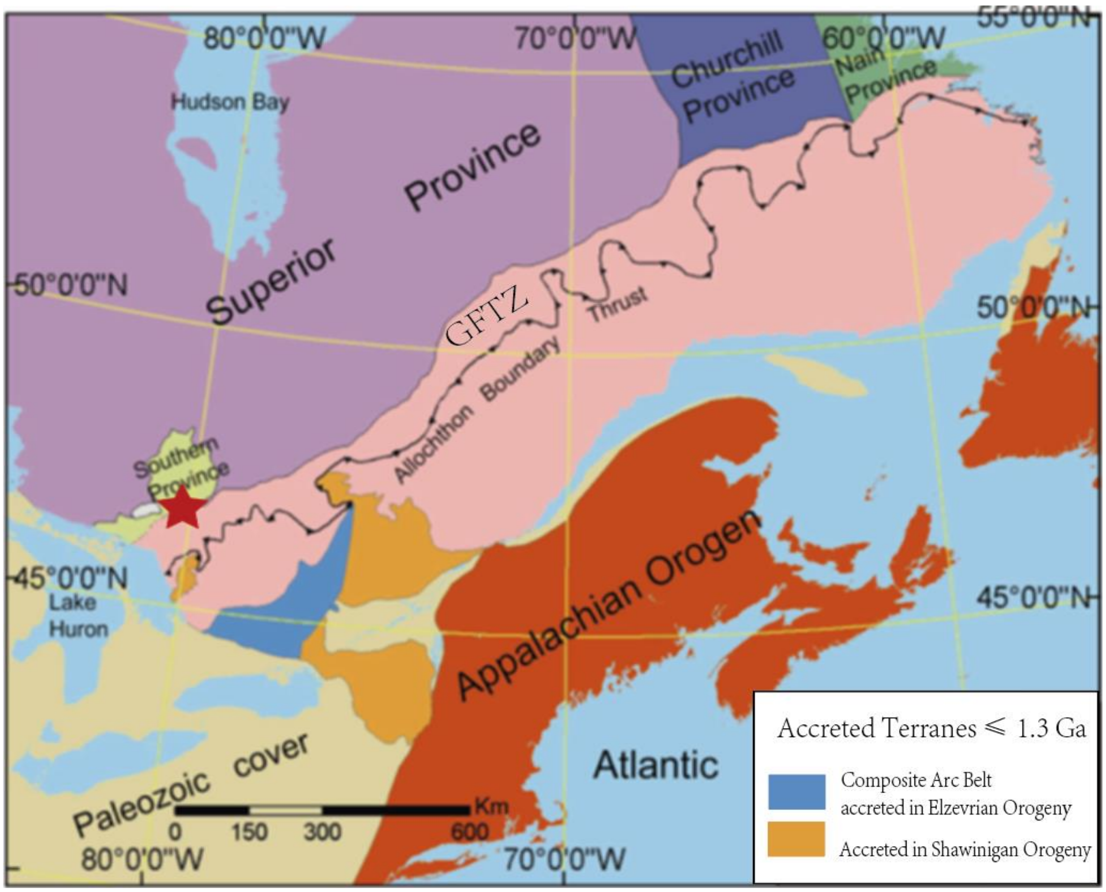

Figure 2.1 Simplified regional tectonic map (from Li, 2012).

The Grenville Province is the youngest geological province (~1.5 Ga) that lies in the southeast of the Canadian Shield and is adjacent to the Appalachian Orogen to the southeast (Figure 2.1; Davidson, 1984; Green et al., 1988; Li, 2012). Rocks in the Grenville Province mostly originated from older crusts, aged from Archean to Mesoproterozoic, and show an overall younging direction toward the southeast of the Grenville Province (Dickin, 1998; Rivers, 1997). Major lithologies of the Grenville Province include migmatites, gneisses, and anorthosites which are highly deformed and metamorphosed (Davidson, 1984; Wynne-Edwards, 1972).

The present configuration of the Grenville Province is mainly due to a continent-continent collision during the Grenville Orogeny, about 1 billion years ago (Moore, 1986). According to Rivers (1997), crustal shortening occurred in the Grenville Province 3 times, at 1.19-1.14, 1.08-1.02 and 1.00-0.85 Ga respectively, all accompanied by high-grade metamorphism.

The entire GFTZ is a roughly 1600 km-long shear zone and is one of the most prominent geologic structures in the Canadian Shield, extending from Lake Huron, southern Ontario to the Labrador Sea to the northeast (Haggart et al., 1993; La Tour, 1981). It has been identified as a multi-phase shear zone (La Tour, 1981), separating the Grenville Province from the Southern Province, Superior Province, Churchill Province, and Nain Province to the northwest (Figure 2.1). Near the study area, the Grenville Province and the Southern Province meet at the GFTZ, which is exposed as a ductile shear zone. I will refer to the shear zone as the Grenville Front shear zone. Some of the rocks in the shear zone are reworked metasedimentary rocks (mostly fine-grained sandstone and siltstone) and mafic dykes derived from the Huronian Supergroup of the geological Southern Province. Other rocks in the Grenville Front shear zone were derived from high-grade gneissic rocks of the Grenville Province.

More specifically, the study area is located between the Baby Lake and the Alice Lake, about 2 km south of the township of Coniston, southeast of Sudbury (Figures 2.2&2.3).

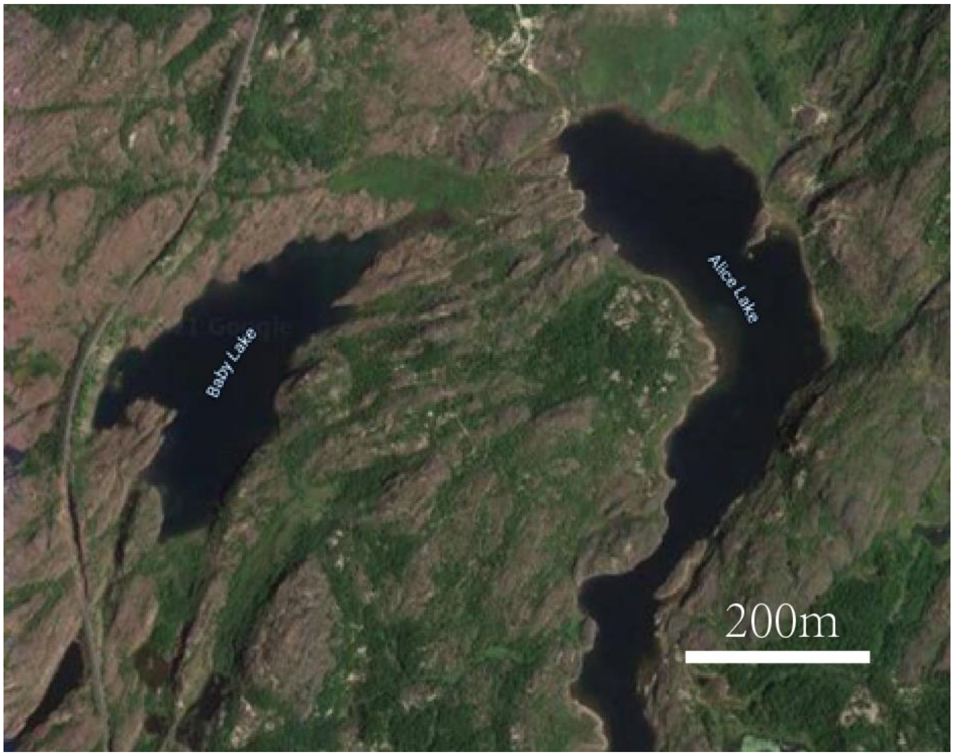

Figure 2.2 Satellite aerial image of the study area.

Figure 2.3A is a detailed geologic map of the study area compiled by Li (2012) and subsequent fieldwork by Lucy Xi Lu and others. In the northwest area of the map, the Mississagi formation metasandstone, which belongs to the Southern Province and forms the footwall of the Grenville Front shear zone, is exposed. The rocks are strongly deformed with a sub-vertical transposition foliation striking approximately at 065. The northwest boundary of the Grenville Front shear zone is now a brittle fault called the Murray fault (represented by black dash line in Figure 2.3A; Corfu and Easton, 2000; Zolnai et al., 1983). Within the shear zone, the rocks are highly mylonitized. They include the mylonitized granites that are about 1749 Ma and about 1464 Ma (Davidson and Van Breeman, 1994; Li, 2012), banded quartz-rich mylonites that are originated from Huronian sedimentary rocks, and variably strained to locally mylonitized mafic rocks (likely the Nipissing diabase). There are also variably strained to mylonitized rock types including meta-pelites, felsic pegmatites, and gneisses. Figure 2.3B is a drone image of part of the study area, demonstrating the location of most quartz-rich mylonite samples. The footwall (northwest) of the Grenville Front shear zone is made of tectonically transposed Mississagi sandstone of the Southern Province. The highly strained rocks in the shear zone consist of, from north to south, a mylonitized granite (~1749Ma), banded mylonites (derived mostly from quartz-rich metasedimentary rocks), a sliver of deformed diabase (most likely the ~2220 Ma Nipissing diabase) sandwiched in banded mylonites, and undifferentiated high-strained rocks. The hanging wall is made of high-grade metamorphic rocks from the Grenville Province.

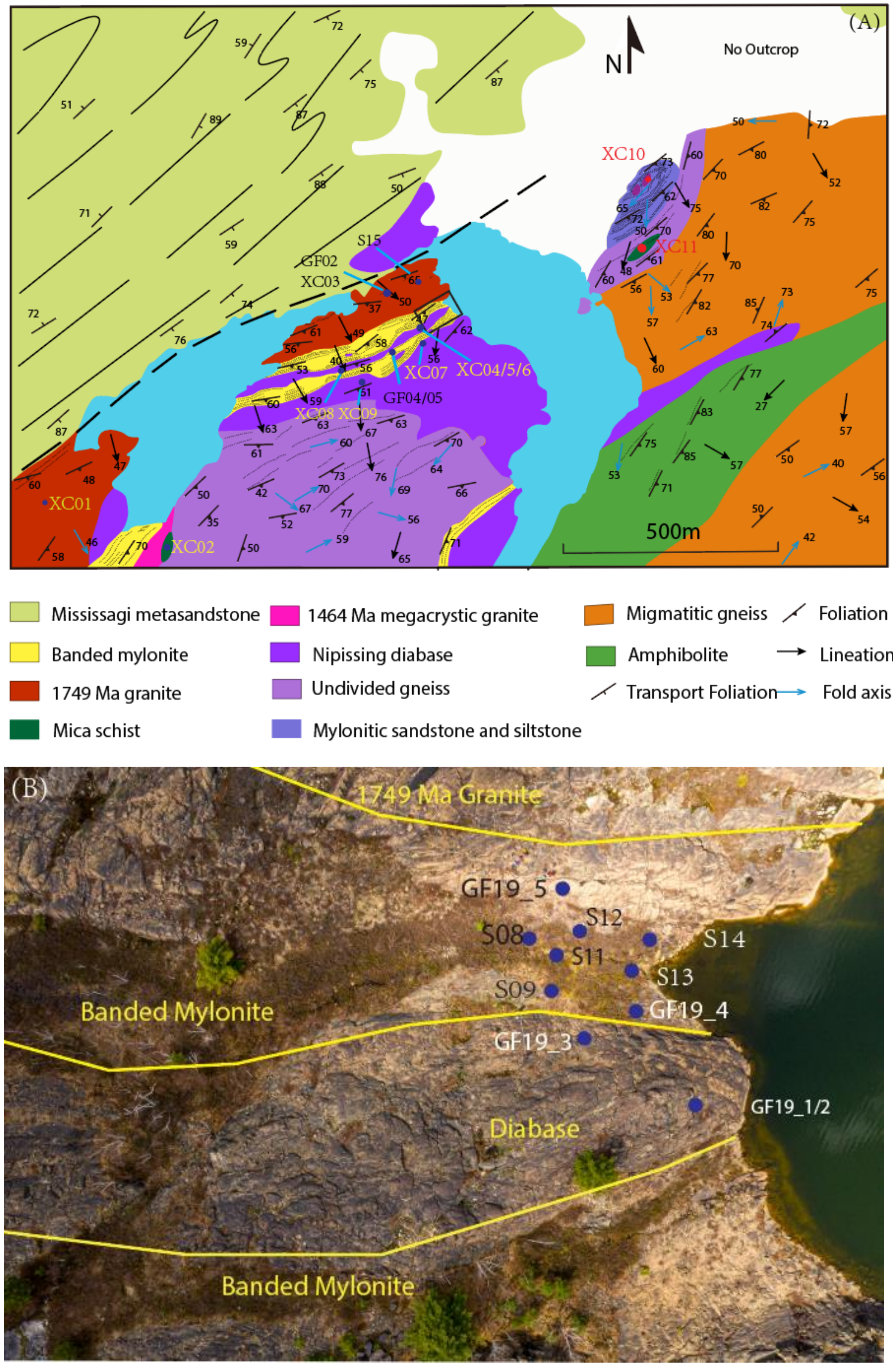

Figure 2.3 Geologic map (A) and satellite image (B) of the study area.

2.2 Sample description

Table 1 summarizes the mylonite samples that were analyzed in this thesis. Although the focus of this study is analyzing the quartz-rich mylonites, some other samples are also described in Table 2, for a better understanding of the shear zone. Samples were all collected from the rock surface. These samples were collected separately by previous students (Changcheng Li, Lucy Xi Lu) and me on different field trips. Samples start with S, GF or GF19 in name were collected separately in different trips, by Lucy Xi Lu. Samples start with XC in name were collected by myself in the trip that I participated in. The compositions were estimated using the microphotographs of the samples. If a mineral composes of 50 % of the area in a microphotograph, then the mineral is estimated to be about 50% of the sample.

Sample	Lithology	Mineral Composition
S08	Quartzo-feldspathic Mylonite	Quartz (60%) + Feldspar (30%) + other minerals like mica, plagioclase, etc. (10% approximately)
S09		
S11		
S12		
S13		
S14		
S15	Mylonitized Granite	Quartz (30%) + Feldspar (50%) + other minerals (20%)
XC01		
GF19-3	Quartzo-feldspathic Mylonite	Quartz (50%) + Feldspar (40%) + other minerals like mica, plagioclase, etc. (10% approximately)
GF19-4		
GF19-5		
XC03	Quartz mylonite	Quartz (100%)
GF02		
GF03	Quartzo-feldspathic Mylonite	Quartz (50%) + Feldspar (40%) + other minerals like mica, plagioclase, etc. (10% approximately)
GF04		
GF05		

Table 1. Lithology and mineral composition of quartz-bearing mylonite samples that are studied in this research.

Sample	Lithology	Description
XC02	Mica schist	Biotite-rich mica schist, possibly originated from the Pecors Formation (Figure 2.4D)
XC04	Gabbro	Anastomosing zones of high strain within the body. In such zones, CPX are deformed, and foliation is well developed. (Figure 2.4E)
XC05	Gabbro	Mylonitized gabbro, rich in clinopyroxene. (Figure 2.4F)
XC06	Gabbro	Rich in clinopyroxene, less deformed, little evidence of grain size-reduction
XC07	Gabbro	Highly mylonitized, rich in clinopyroxene
XC08	Gabbro	Mylonitized gabbro, rich in clinopyroxene with good shape fabric
XC09	Mica schist	Biotite-rich mica schist, the possible origin is the Pecors Formation
XC10	Gabbro	Not very strong deformation of clinopyroxene
XC11	Mica schist	Muscovite-rich mica schist, mica demonstrates perfect cleavage, originated from pelitic rocks

Table 2. Lithology and description of samples from mica schist and gabbro.

A few field photos and microphotographs are shown in Figure 2.4 (detailed microphotographs of the quartz mylonite will be presented in Chapter 4). Figure 2.4A shows banded quartz mylonite and ultra-mylonite (below) and high-strained metasedimentary rocks with less quartz content (above). To the east of Alice Lake, the banded mylonites are also observed but they occur with heterogeneous rock types. They are labeled separately as mylonitized sandstone and siltstone. The southeast corner of this map contains migmatitic gneiss, mica schist, gabbro, and amphibolite. Quartz veins are commonly observed in mylonitic granite, diabase, and gneiss. They are parallel to the mylonitic foliation on cross-sections but intersect the foliation on sub-horizontal exposures. An example is shown in Figure 2.4B, a 10 cm-thick quartz vein located in granite, both demonstrate strong foliation and lineation, dipping toward the southeast. Figure 2.4C shows what banded quartz mylonite looks like in the field. Figures 2.4D, 2.4E and 2.4F are photomicrographs of mica schist and clinopyroxene around the shear zone. These samples all underwent ductile deformation. Quartz grains observed in these samples demonstrate dynamically recrystallization as well. These samples (mica schist, gabbro and quartz-rich mylonites) are possibly deformed by the same generation as the

Grenville Front shear zone. Deformation mechanisms of the clinopyroxene are interpreted to be mechanical twinning and creep. According to Mauler et al. (2000), the major deformation mechanisms for clinopyroxene at low temperature (up to about 500 °C) and high stress are twinning and dislocation glide. At about 500 °C multiple slip systems dominate (Mauler et al., 2000). The gabbro deformation temperatures near this shear zone are around 400-500 °C roughly, by estimation.

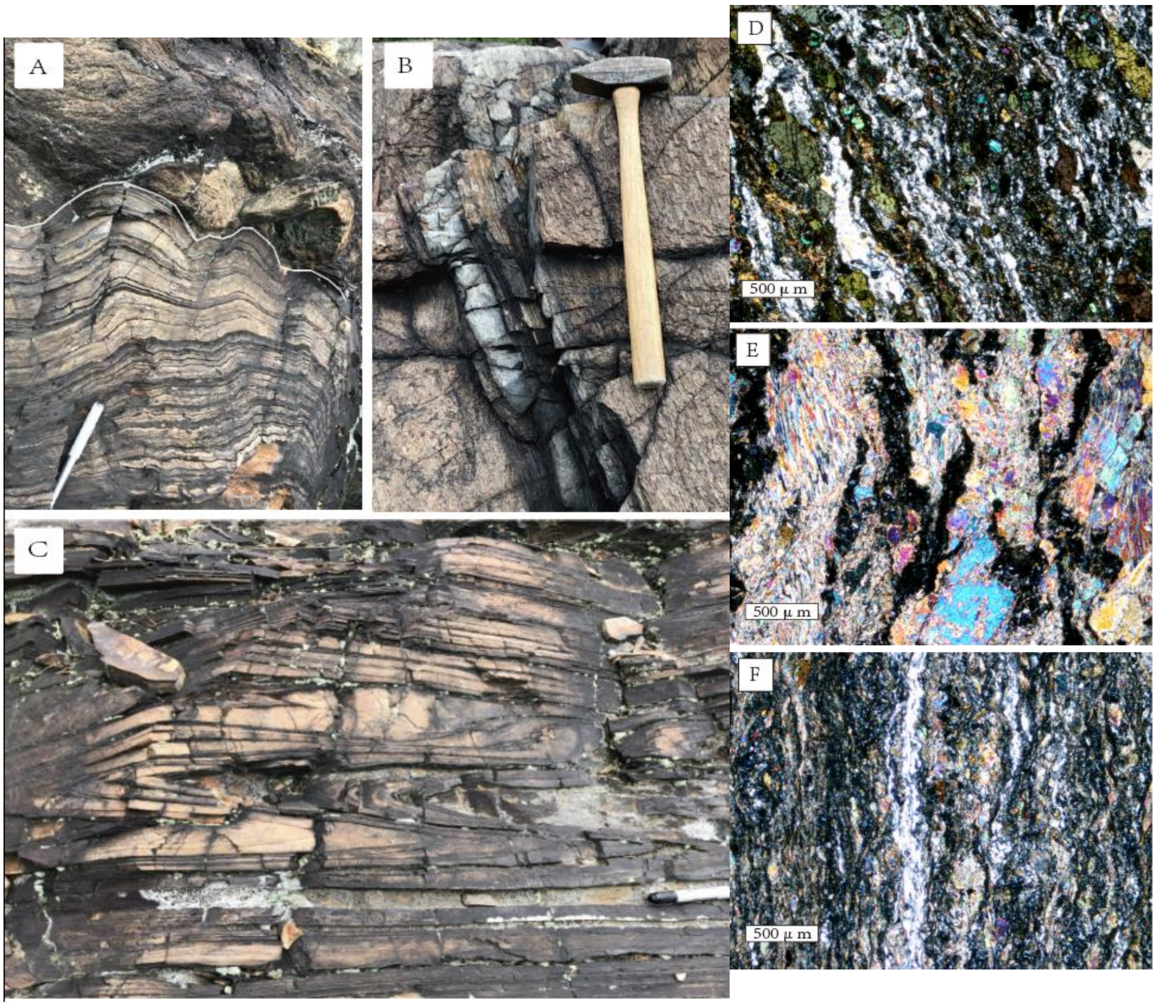

Figure 2.4 Some field photos and microphotographs.

Chapter 3

Background and Methodology

3.1 Background

3.1.1 Lattice Preferred Orientation

Lattice Preferred Orientations (LPOs) of deformed rocks have been used for determining shear sense, constraining deformation temperatures and mechanisms in ductile shear zones (Bhandari and Jiang, 2021; Faleiros et al., 2016; Law, 2014; Oliver, 1996; Schmid and Casey, 1986; Stipp et al., 2002; Wenk et al., 2019). An LPO describes the non-random distribution of crystallographic orientation of mineral grains. LPOs develop mainly due to dislocation creep (Passchier and Trouw, 2005; Tullis, 1977). As the latter depends on deformation conditions (temperature, pressure, fluid activity, etc.), LPO patterns can be used to infer metamorphic conditions during deformation (Figure 3.1).

Dislocation slip occurs on the slip systems. The slip can be imagined as a deck of cards that will 'slip' when the resolved shear stress on the slip plane exceeds a certain value. A slip system is defined by a slip plane and the slip direction (Figure 3.1). Slip planes are usually planes of the greatest atomic density and slip direction is the closed-pack direction. The four major slip systems in quartz are, from low temperatures to high temperatures, basal <a>, rhomb <a>, prism <a> and prism <c>. The naming describes the slip plane plus slip direction, for instance, basal <a> is a slip system which slips on quartz basal plane perpendicular to the c-axis and <a> is the slip direction. The relative activities of these slip systems of quartz give rise to unique final c-axis patterns (Figure 3.1). Various patterns of LPOs can be used to interpret the slip systems activated during deformation. Measuring LPOs allows the interpretation of the deformation mechanism and deformation temperatures qualitatively.

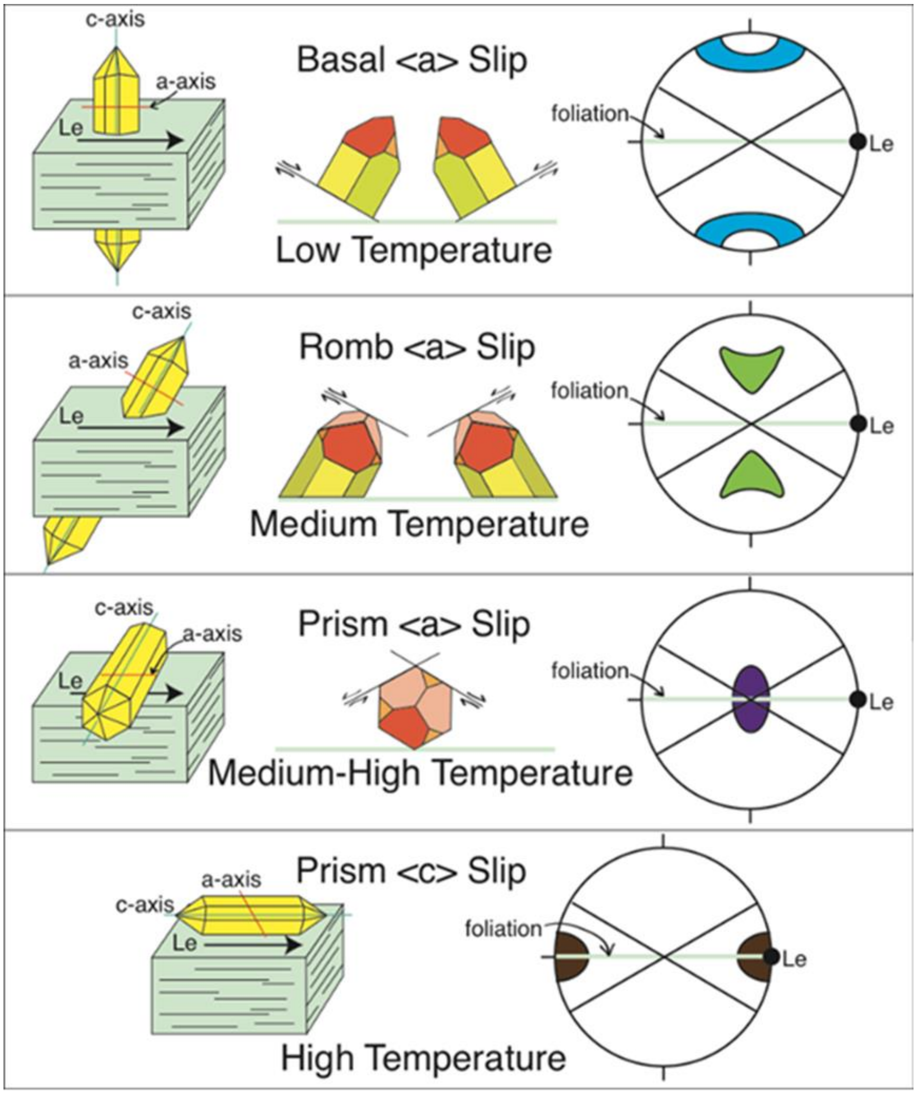

Figure 3.1 Four major slip systems in the development of quartz Lattice Preferred Orientation (Oliver, 1996).

As illustrated in the Flinn diagram, quartz c-axes fabrics from the ductile shear zones often exhibit single girdles or cross girdles (Figures 3.2&3.3). Single girdles mean that there is only one girdle whereas cross girdles usually have one strong girdle and one weak girdle (Figure 3.2). Figure 3.2 illustrates how the geometry of LPO patterns of the quartz a-axes and c-axes relate to the coaxial strain. The inclination of girdles with respect to the mylonitic foliation and lineation can be used to infer the shear sense (Figure 3.3) (Bhandari and Jiang, 2021). Figure 3.3a shows the cross-girdle pattern where the major girdle is normal to the C-foliation or the shear plane, the weaker girdle is normal to the foliation plane; Figure 3.3b and 3.3c demonstrate a single girdle, normal to the foliation plane. The shear sense is dextral in Figure 3.3.

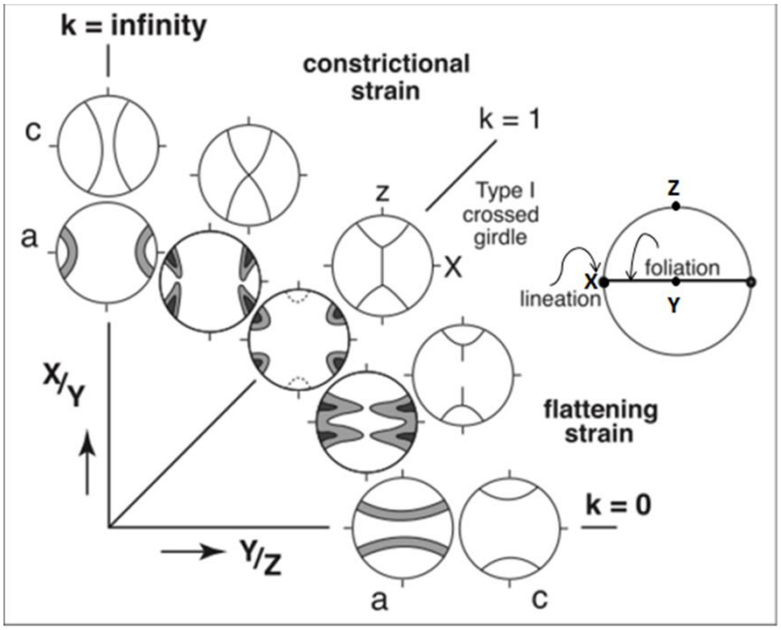

Figure 3.2 The Flinn Diagram (Behrmann and Platt, 1982; Bouchez et al., 1983).

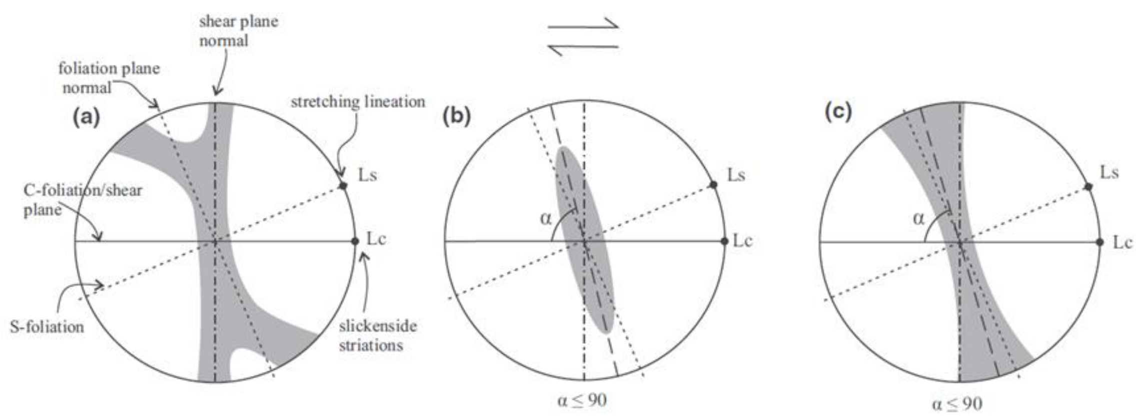

Figure 3.3 Illustration of cross girdles and single girdles of quartz c-axes fabrics in the reference of foliation and lineation (Bhandari and Jiang, 2021).

Open angles of the cross girdles have been shown to correlate with deformation temperatures. (Faleiros et al., 2016; Law, 2014). Faleiros et al. (2016) proposed equations for calculating deformation temperatures, based on open angles. Open angle is the angle bounded between two cross girdles (Oliver, 1996). Equation 3 is used when the temperature is between 250 °C and 650 °, and Equation 4 is used when considering both the pressure effect and the open angle:

$$T = 6.9\ OA + 48 \quad (3)$$

$$T = 410.44 \ln OA + 14.22\ P - 1272 \quad (4)$$

where T is temperature (°C), P is pressure (kbar), and OA is open angle (degrees). However, it should be noted that the OA thermometer is a qualitative method.

3.1.2 Titanium in Quartz thermometers

Titanium is a trace element that can substitute for silicon in quartz. Titanium-in-quartz is a quantitative thermobarometer that enables the investigation of Ti^{4+} substitution of Si^{4+} in quartz and the relationship between Titanium concentration and P-T conditions (Wark and Watson, 2006; Grujic et al., 2011; Huang and Audétat, 2012; Ashley et al., 2014). Ostapenko et al. (1987) pointed out that titanium concentration in quartz varies with changing temperatures. Wark and Watson (2006) proposed that Ti activity is dependent on the presence of rutile. Therefore, the chemical potential of Ti and how much titanium can substitute for silicon vary with temperature. Theoretically, high Ti concentrations correlate to high mineral formation temperatures in rocks (Ehrlich et al., 2012; Wark and Watson, 2006). Wark and Watson (2006) first proposed a mathematical equation describing the temperature-dependent relationship of Ti concentration in quartz. In their experiments, the pressure was fixed at 1.0 GPa and the temperatures range from 600-1000 °C (Wark and Watson, 2006). More experiments have been conducted on pressure effects on Ti concentration since Thomas et al. (2010) examined the solubility of Ti under the effect of pressure variations from 500 MPa to 2.0 GPa. They generated a new expression of the Titanium-in-quartz thermobarometer (Equation 3). In this equation, both the pressure and the temperature are taken into consideration, but the activity of TiO_2 is also a variable (Thomas et al., 2010).

$$RT \ln X_{TiO_2}^{quartz} = -60952 + 1.520 \cdot T - 1741 \cdot P + RT \ln a_{TiO_2} \quad (5)$$

where R is gas constant (8.3145 $J \cdot mol^{-1} \cdot K^{-1}$), T is the temperature (K), P is the pressure (kbar), a_{TiO_2} is the activity of titanium oxide (the ability of TiO_2 to react), and $X_{TiO_2}^{quartz}$ is the concentration of titanium oxide (see the Appendix of Thomas et al., 2010).

Nonetheless, Thomas et al. (2010) were criticized by Wilson et al. (2012) and Huang and Audétat (2012). Wilson et al. (2012) tested the Thomas et al.'s calibration with well-studied rhyolitic volcanic systems and found out that it did not yield reasonable P-T estimates. Huang and Audétat (2012) found out that the Ti concentration is also related to the crystal growth rate (Kidder et al., 2013). Huang and Audétat (2012) concluded that Thomas et al.'s (2010) calibration of the thermobarometer underestimates the crystallization rate in their experiments. Huang and Audétat (2012) gave the following equation (Equation 4), constrained under 1-10 kbar and 600-800 °C:

$$\log \text{Ti} = - 0.27943 \cdot 10^4/T - 660.53 \cdot (P^{0.35}/T) + 5.6459 \quad (6)$$

where Ti = Titanium concentration (ppm), T is absolute temperature, P is pressure (kbar). Both the Thomas et al. (2010) and Huang and Audétat (2012) calibration expressions will be discussed when calculating deformation temperatures in this research.

3.1.3 Dynamically recrystallized grainsize piezometers

Dynamic Recrystallization (DRX) refers to a recrystallization process when new crystal grains nucleate and grow during deformation (Stipp et al., 2002; Stipp and Tullis, 2003). The DRX grain sizes have been used to estimate the differential stress and the temperature of deformation. Dynamic recrystallization is common in natural shear zones and is one major mechanism leading to decreasing grain size in deformed rocks or metals (Shimizu, 2008), is driven by internal strain (Wenk and Christie, 1991), and depends primarily on stress (Twiss, 1977; Stipp et al., 2002; Stipp and Tullis, 2003; Shimizu, 2008). For a deforming system to reduce free energy, grain boundaries favor more deformed grains (Wenk and Christie, 1991). In the recrystallization processes, less deformed grains tend to replace more deformed grains, thus it is easier for the slips to occur (Wenk and Christie, 1991). DRX and the corresponding microstructures in quartz have been analyzed (Hirth and Tullis, 1992; Stipp et al., 2010). Hirth and Tullis (1992) defined the three dislocation creep regimes of dynamic recrystallization in quartz, with distinct microstructures and temperature-strain rate conditions (Passchier and Trouw, 2005). Figure 3.4 illustrates the microstructures corresponding to these three dislocation creeps. Shaded areas represent the substance of a large mineral grain before and after deformation. Strain rate decreases from grain boundary migration to bulging, and temperature rises from bulging to grain boundary migration (Figure 3.4).

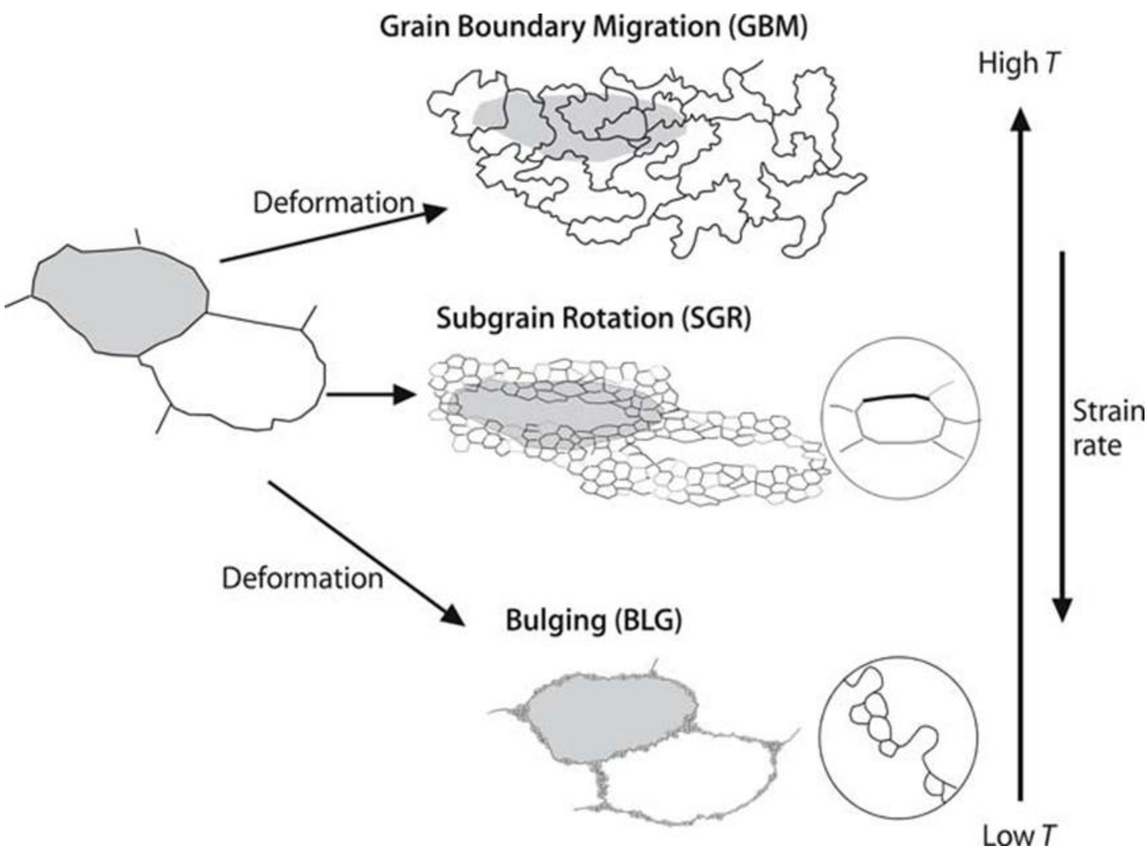

Figure 3.4 Three types of dynamic recrystallization in quartz (from Passchier and Trouw, 2005).

Bulging (BLG), or regime 1, occurs at the low temperature range. It is characterized by non-regular patchy extinction, which is shown in Figure 3.5 by Hirth and Tullis (1992). In this regime, small bulges appear along the grain boundaries. Dislocation climb, in this case, is unlikely to occur, so the major recovery process is strain-induced grain boundary migration (Hirth and Tullis, 1992). Stipp et al. (2002) suggest a temperature range between 300 °C and 400°C for grain boundary bulging. Below 300°C, the dominant mechanism is the cataclastic flow which does not produce recrystallization or preferred orientation in minerals (Wenk and Christie, 1991).

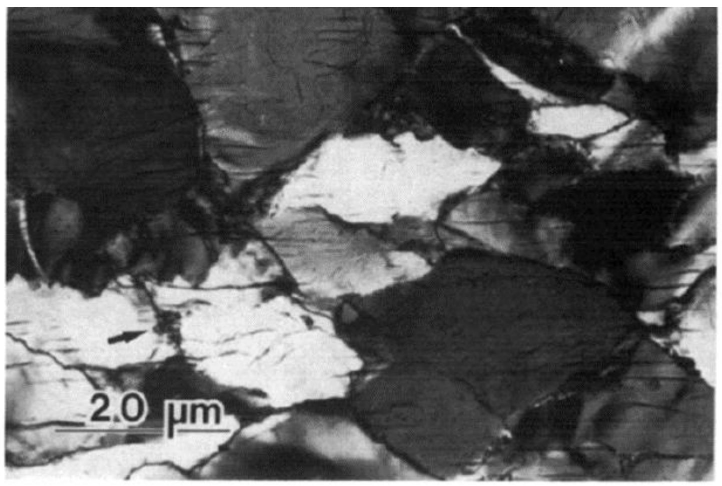

Figure 3.5 Irregular and patchy undulatory extinction microstructure of regime 1 quartz (from Hirth and Tullis, 1992). Arrow points toward the diffuse grain boundary (Hirth and Tullis, 1992).

Subgrain rotation (SGR), or regime 2 (Figure 3.6), occurs when flow stress is reducing (Hirth and Tullis, 1992). During this procedure, subgrains start to nucleate and can be observed around the grain boundary. Sweeping undulatory extinction of extended grains is characteristic of this regime (Hirth and Tullis, 1992). When the misorientation angle between low-angle and high-angle boundaries surpasses the critical angle (10-15°) the subgrain becomes a newly recrystallized grain (Li, 1962; Shimizu, 2008). The estimated temperature range for regime 2 is 400-500 °C (Stipp et al., 2002).

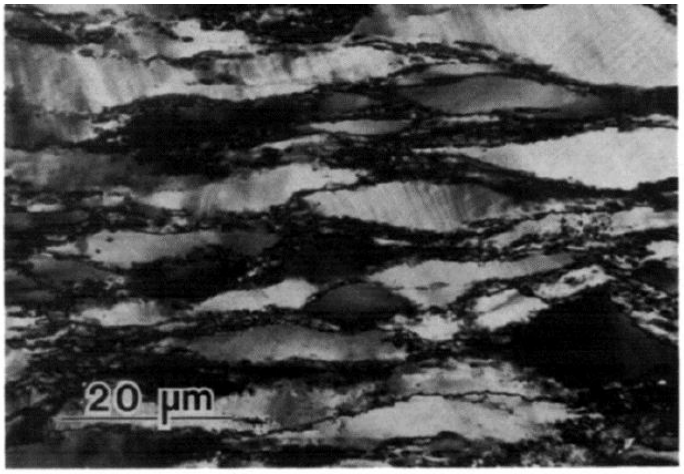

Figure 3.6 Regime 2 of quartz dislocation creep, or subgrain rotation (Hirth and Tullis, 1992).

Grain boundary migration (GBM), or regime 3, contains both grain boundary migration and subgrain rotation mechanisms (Figure 3.7). Grain boundary migration is at a higher rate in regime 3 than in regime 1. The stress is further decreased in this situation (Hirth and Tullis, 1992). Gleiter (1969) described it as a procedure where the absorption and emission of atoms cause the grain boundaries to move, with one emitted from the shrinking grain boundary and absorbed by the other growing grain boundary. GBM occurs in temperatures greater than 500 °C (Stipp et al., 2002). Recrystallized smaller grains completely replace the original grains and the original grain boundaries are entirely reshaped.

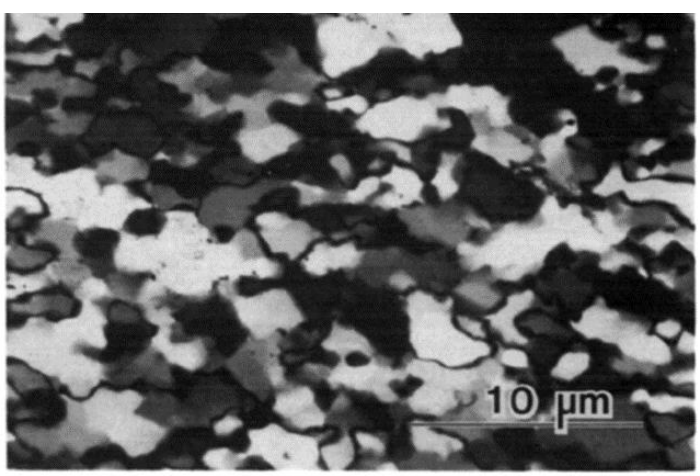

Figure 3.7 Regime 3 or grain boundary migration(from Hirth and Tullis, 1992).

Dynamic recrystallization is thought to be correlated with the differential stress and is sensitive to the deformation conditions in the deep crust (Austin and Evans, 2007; Austin and Evans, 2008; Twiss, 1977; Stipp and Tullis, 2003; Shimizu, 2008). It is suggested that the dislocation density and recrystallized grain sizes correlate with the steady state stress in certain conditions, and therefore stress can be quantified if the relationship is known (Twiss, 1977). A formula can be used to describe the behavior of differential stress and grainsize. As such, the stress is proposed to be a function of grain size, as described in an early paleo-piezometer by Twiss (1977):

$$\sigma = Bd^{-0.68} \quad (7)$$

which is a mechanical formula assuming that the situation of dynamic recrystallization happened in the steady-state and there is no overprinting of recrystallized grains. Differential stress is σ in MPa and d is grain size in mm. For quartz, the parameter B (MPa·mm) is approximately 5.5 (Twiss, 1977).

Nonetheless, more models that examine the stress-grain size relationship have been proposed as the theoretical piezometer by Twiss (1977) does not agree with the observations on changing microstructures in naturally deformed DRX (Shimizu, 2008). Stipp and Tullis (2003) revisited the previous model, investigating whether different dislocation creep mechanisms lead to different piezometers. They suggested the following Equation:

$$d = 10^{3.56 \pm 0.27} \sigma^{-1.26 \pm 0.13} \quad (8)$$

where d is dynamically recrystallized grain size (μm), σ is differential stress (MPa), and the parameter $10^{3.56 \pm 0.27}$ has a unit of μm·MPa.

Both the Twiss (1977) and the Stipp and Tullis (2003) piezometers suggest a negligible temperature-grain size relationship. However, Shimizu (2008) proposed that the temperature effect on dynamic recrystallized grain size can be vital, especially in low-temperature metamorphic conditions. The new d-σ relationship based on the intracrystalline nucleation model was thus developed by Shimizu (2008, 2012) for α-quartz and β-quartz. The transition of two forms of quartzite occurs at 573 °C, below 573°C quartz is in α-form and above 573°C, quartz is in β-form. Their new piezometer is based on subgrain rotation and grain boundary migration mechanisms (Lu and Jiang, 2019) and aligns well with the Stipp and Tullis (2003) piezometer at high temperatures for β-quartz. At low temperature (α-quartz), the Shimizu (2008) piezometer (Equations 9 and 10) generates a higher stress estimation than Stipp and Tullis' model:

$$\sigma = 3.52\times10^{2}\times d^{-0.8}\exp\left(\frac{6.98\times10^{2}}{T}\right) \quad (\alpha\text{-quartz}) \tag{9}$$

$$\sigma = 2.17\times10^{2}\times d^{-0.8}\exp\left(\frac{1.19\times10^{3}}{T}\right) \quad (\beta\text{-quartz}) \tag{10}$$

where σ is differential stress (MPa), T is temperature (K), and d is grain size in μm.

Lu and Jiang (2019) compared the present dynamic recrystallized grain size piezometers, and a summarized diagram of the piezometers and flow laws is shown in Figure 3.8. Piezometers are from Stipp and Tullis (2003), Shimizu (2008, 2012), Cross et al. (2017), Heilbronner and Kilian (2017), and paleowattmeter from Austin and Evans (2007, 2009). The flow laws are from Luan and Paterson (1992), Gleason and Tullis (1995) and Rutter and Brodie (2004). Strain rate estimated for the active plate boundaries is 10^{-12}/s, according to GPS observations on the natural fault zones (Lu and Jiang, 2019; McGill et al., 2013; Schulz and Evans, 2000; Sutherland et al., 2006). There are uncertainties between these flow laws, as discussed earlier. Lu and Jiang (2019) generated the new flow law by adding a water fugacity term and considered the pressure effect of activation enthalpy, which results in uncertainties about pre-existing flow laws by Luan and Paterson (1992) and Gleason and Tullis (1995). Their new adapted flow law is:

$$\dot{\varepsilon} = 6.0\times10^{-15} f_w^{2.7}\exp\left(\frac{-132000+35.3P}{RT}\right)\sigma^{4} \tag{11}$$

where $\dot{\varepsilon}$ is strain rate (s^{-1}), f_w is water fugacity (MPa), R is gas constant ($J \cdot mol^{-1} \cdot K^{-1}$), T is emperature (K), P is pressure (MPa), σ is the differential stress (MPa) and 6.0×10^{-15}

is the pre-exponential parameter ($MPa^{-6.7}s^{-1}$). The deformation conditions of quartzite will be discussed mainly in the context of this flow law.

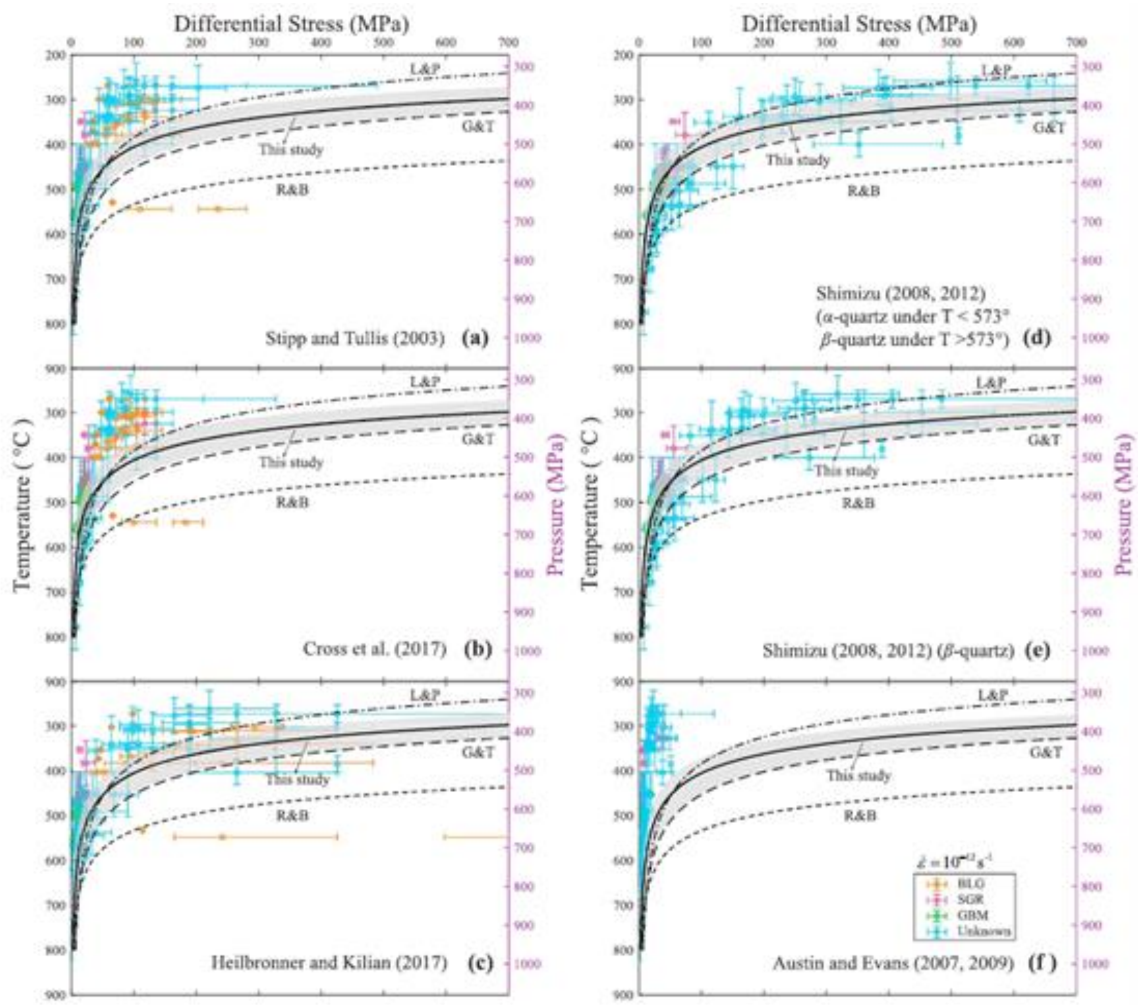

Figure 3.8 Stress profile of some existing quartz DRX piezometers and flow laws by Lu and Jiang (2019).

3.2 Methodology

3.2.1 LPO measurement

LPOs of the quartz-bearing mylonite samples (S08, S09, S11, S12, S13, S14, XC03, GF19-3, GF19-4, GF19-5 and GF05) from the study area were measured using a petrologic microscope with a universal stage (Figure 3.9). The thin sections were cut perpendicular to the foliation and parallel to the lineation.

To measure the quartz c-axis, a four-axis universal stage is used (Figure 3.9). The thin section is being placed on the universal stage, between two glass hemispheres (upper and lower hemispheres) (Figure 3.9). Glycerin is smeared on both sides of the thin section, to ensure that the thin section can be moved smoothly without scratching the hemispheres or the thin section itself.

The four axes of rotation of the universal stage are as follows. The first axis (A1) or the inner ring allows 360° rotation of the thin section around the vertical axis. The second axis (A2) is the N-S horizontal axis that allows the thin sections to be tilted toward the left or right, by up to 85°. The third (A4) is the E-W axis allowing the thin sections to be rotated toward or away from the observer. Finally, the microscope stage (called A5) allows the entire universal stage to be rotated 360° around the vertical axis.

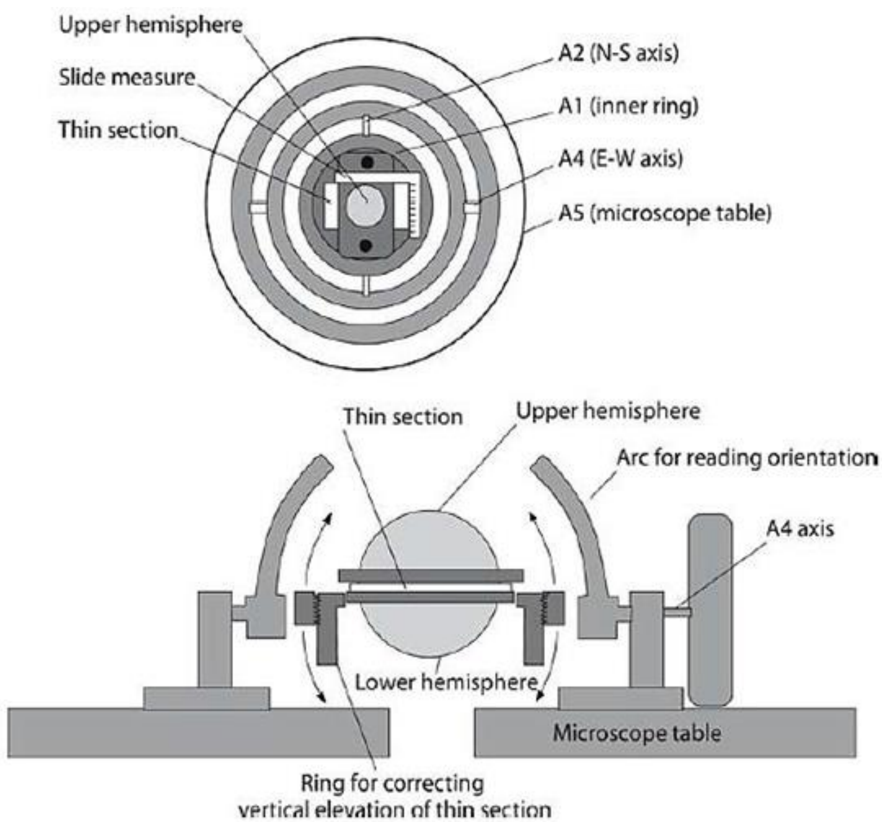

Figure 3.9 Diagram showing the structure of a universal stage used in manual LPO measurement (Passchier and Trouw, 2005).

The processes of calibration are briefly described here. The thin section is assembled on the universal stage which is attached to the microscope and properly centered. An appropriate objective lens for the universal stage with the right magnification is selected to ensure proper measurement of the quartz c-axis. After centering the objective lens, the following calibrations are carried out to ensure that the thin section plane is brought to the same height as all the rotation axes of the u-stage. A mineral grain is selected and is moved to the center of the reticle. Firstly, the center of the lens should focus on the light coming from the bottom of the microscope. Secondly, the horizontal axes and vertical axes are rotated separately to test whether the thin section is at the right height. This is confirmed by rotation around the N-S axis and E-W axis of the u-stage respectively. If the thin section is at the proper height, all grains along the N-S axis will remain sharp in focus when rotation around that axis is performed. And all grains along the E-W axis should remain in focus when rotation around the E-W axis is performed. Otherwise, use the thin-section height-adjustment screw to move the thin section up or down until it is at the proper height. Please refer to Fairbairn (1949, p.264) for detailed steps of the calibrations.

Measuring quartz c-axis fabrics involves the following steps.

Step 1: Move the target grain to the center of the reticle. Rotate the A1 axis (inner ring), until the grain is in optical extinction (with gypsum plate, grains become purple when going to extinction).

Step 2: Rotate around the N-S axis (A2) to see if the grain remains extinct, if the grain lights up, rotate the N-S axis back to horizontal, and then rotate A1 90 degrees for another position of extinction. Rotate the N-S axis and the grain should remain in extinction. Rotate the N-S axis back to horizontal and proceed to step 3.

Step 3: Rotate around the E-W axis (A4) toward or away from the observer for some 30 degrees. If the grain remains in extinction, go to step 4. Otherwise, rotate around the N-S axis until the grain becomes extinct. Return the E-W axis to zero. The grain should remain in extinction while moving the E-W axis back to zero. Proceed to step 4.

Step 4: The final step is to determine whether the c-axis of the grain is in vertical or horizontal orientation. Rotate the microscope stage (axis A5), if the grain remains in extinction, the c-axis is vertical. Otherwise, it is horizontal.

A grain may be in an extinction position before any rotation. If such a grain remains extinct when moving the inner ring, check if it lights up by rotating around the N-S axis and the E-W axis. If the grain lights up, return the N-S axis and E-W axis back to zero and rotate the A1 axis for another position of extinction, then proceed to step 2. If it does not change, do step 4 to determine whether it's horizontal or vertical.

Throughout the measurement, while moving one axis, the other axis should be fixed. When all steps are completed for a grain, record the reading of the inner ring (three digits), the tilt degree around the N-S axis (two digits) on the left or right arc (specify whether the reading is from the left or right arc), and whether the c-axis is horizontal or vertical at the final step. These data were recorded in a Microsoft Excel spreadsheet.

For each thin section, 200 grains were measured to avoid statistical bias. The measurement data are converted to 'trend and plunge' with respect to the sample reference and then plotted on a lower hemisphere equal-area projection using a software called Stereonet. Details of the conversion from the original spreadsheet to the projection are presented in Appendix A.

3.2.2 Titanium in quartz concentration measurement

Because of travel restrictions due to the COVID-19 pandemic, titanium concentrations in quartz (Ti-in-Q) were measured by Dr. Biwei Xiang at the State Key Laboratory of Ore Deposit Geochemistry, Institute of Geochemistry Chinese Academy of Sciences (IGCAS). Dr. Xiang is a Professor from East China University of Technology and was a visiting scholar in the Laboratory for Structural Geology and Tectonics at Western University between September 2019 and August 2020.

The Ti-in-Q measurements were carried out on an Agilent 7900 ICP-MS with a GeoLasPro 193nm ArF excimer laser. The analyses use 10 Hz laser repetition, 12J/cm2 energy density and 44 μm spot size. For every 10 analyses, the external standard of NIST SRM610 or GSE-1G was used and analyzed twice, for quantitative calibrations. An internal standard-in-dependent calibration strategy was applied to the calibrations, with the normalization of the sum of all metal oxides to 100 wt%. NIST SRM612 and GSD-1G were used to monitor the accuracy of the results, showing that most elements have uncertainties lower than 10%. A nature quartz standard was analyzed as well to monitor the accuracy, which suggests values for Ti (57 ± 4 ppm), Al (154 ± 15 ppm), Li (30 ± 2 ppm), Fe (2.2 ± 0.3 ppm), Mn (0.34 ± 0.04 ppm), Ge (1.7 ± 0.2 ppm) and Ga (0.020 ± 0.002 ppm) (Audétat et al., 2015).

3.2.3 Dynamically recrystallized grainsize measurement

The photomicrographs of each thin section were taken using a Nikon microscope with a software called ACT-1. Photomicrographs were viewed in Adobe Illustrator and grain sizes were measured manually using the Ruler Function under the Visualization tab in Adobe Illustrator. The dynamically recrystallized grain size d is described as the diameter of a circle that has the same area as the grain. Diagram showing how to measure is shown in Figure 3.10. For each grain, the approximate length and width were measured, as described in the figure, in AI units. Meanwhile, the actual length of the scale bar in AI units was also measured, thus I can convert the length of grains in AI units to the actual length (Figure 3.10). First, the length of the scale bar in black is measured using the reference lines (the blue lines), given in Adobe Illustrator units, for scale conversion (Figure 3.10). The grain size is also measured using the blue reference lines with respect to the AI units. Then the scale is converted to the actual length.

To avoid statistical bias, 200 grains were measured for each sample. After calculation, the actual length and width were obtained. The size was acquired using the following formula:

$$a \cdot b = [r]^2 \quad (12)$$

where a is length, b is width, r is grain radius. Finally, arithmetic means, and standard deviations of the grain sizes were calculated in the spreadsheet. Piezometers from Shimizu (2008) were used to constrain the paleo-stress based on the average dynamically recrystallized grain sizes.

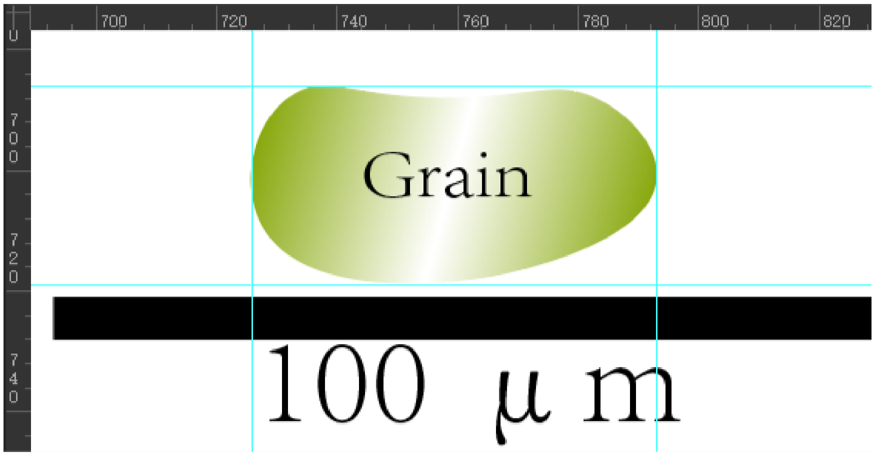

Figure 3.10 An illustration showing how the grain size is measured in Adobe Illustrator.

Chapter 4

Results

4.1 LPO results

The LPOs of quartz-rich mylonites from the study area are shown in Figure 4.1. All samples present clear and consistent LPO patterns, which have the cross-girdle characteristics with the peripheral maxima and the Y-maxima. Diagrams A-J in Figure 4.1 were measured from domains that consist of quartz and feldspar mixture (labeled as the Q+F zone in Figure 4.2). Diagrams K-M in Figure 4.1 were measured from pure quartz domains (labeled as the Q zone in Figure 4.2). In Figure 4.2, a gypsum plate is inserted. Diagram N in Figure 4.1 was measured from a pure quartz vein (see bottom-left in Figure 4.3).

It is shown that some samples (S08 (quartz and feldspar domain), GF19-5, S08 (pure quartz domain), S13 (pure quartz domain), S14 (pure quartz domain) and XC03) have relatively continuous cross girdles (A, J, K, L, M, N in Figure 4.1) whereas others (S09, S11, S12, S13 (quartz and feldspar domain), S14 (quartz and feldspar domain), GF05, GF19-3 and GF19-4) have noticeable gaps in the girdle (B, C, D, E, F, G, H, I in Figure 4.1). To be specific, there is a lack of data points between Y-maxima and peripheral. An example of the noticeable gap is shown in the top-middle diagram in Figure 4.3. The region where data points are missing is indicated by the fan-shaped region. The bottom-middle and bottom-right diagrams in Figure 4.3 demonstrate a more continuous girdle with the interpreted fabric skeleton, which is more consistent with the cross girdle described in Figure 3.3. The samples with noticeable gaps were all measured from the domains that consist of quartz and feldspar porphyroclasts (Figure 4.1).

Abnormal spreading of the quartz c-axes at the peripheral has been observed in samples S11, S12, GF05, GF19-3, and GF19-5 (see Figure 4.1C, D, G, H and J). Figure 4.3 top-middle diagram indicates this phenomenon in GF05, with red arrows pointing toward the region of unusual spreading. This pattern is unlike the normal LPO pattern with a cross girdle. A normal cross girdle usually resembles an ‘X’ (see Figures 3.2, 3.3 and 4.3 bottom-right). Open angles, bounded by data points that represent quartz c-axes orientation, usually form at the top and bottom of the cross girdles (Figures 3.3, 4.3 and 4.4). However, in samples with this abnormal spread, the data points form an ‘arc’-shaped structure near the peripheral, instead of an open angle. In samples that exhibit this phenomenon, their microphotographs (the top-left diagram in Figure 4.3 as an example) demonstrate the quartz ribbon being wrapped around the large feldspar grains.

The gap in cross girdles and the abnormal spreading of quartz c-axes are observed mainly in samples that consist of quartz and feldspar porphyroclasts (Figures 4.1, 4.2 and 4.3). LPOs that were measured from samples with the pure quartz demonstrate a continuous cross girdle and little quartz c-axes abnormal spread.

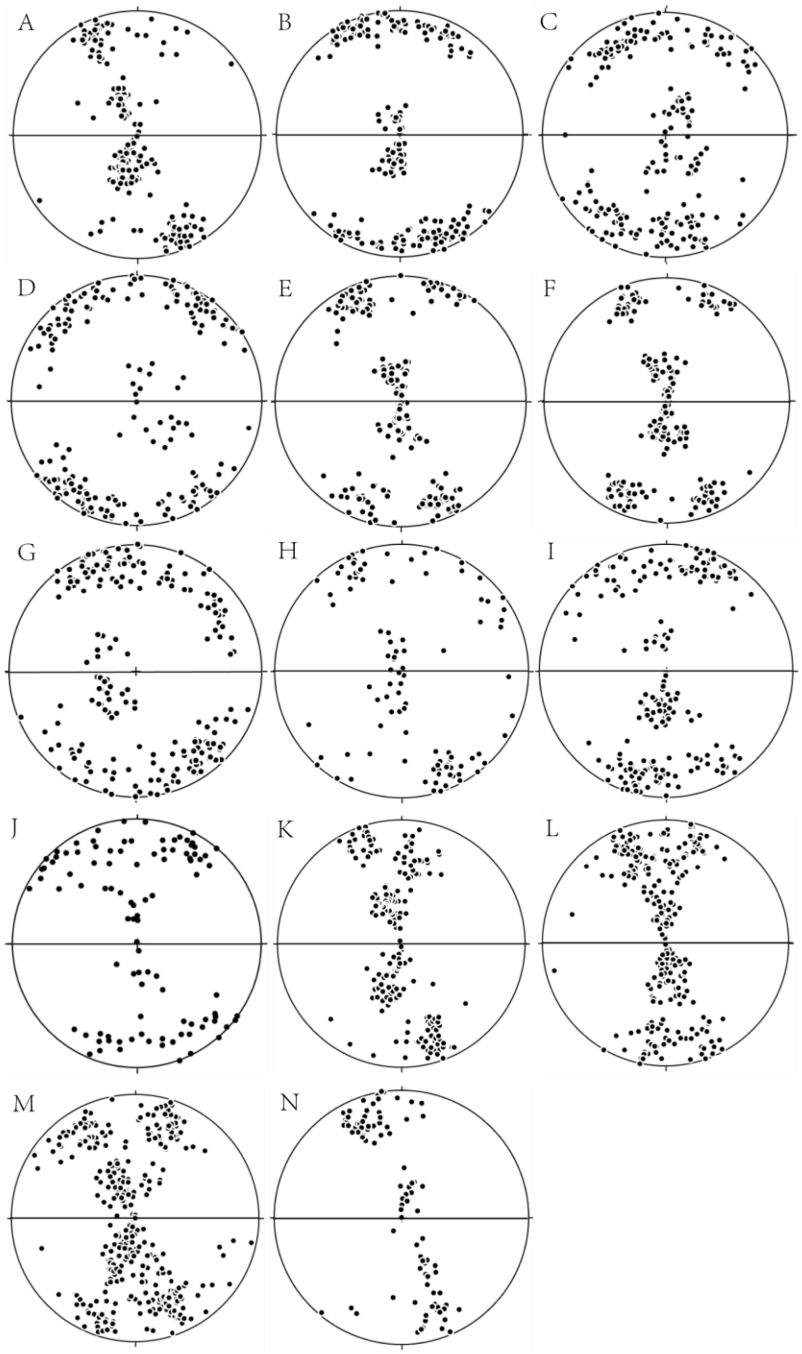

Figure 4.1 A compilation of all the LPO projections.

A) S08; B) S09; C) S11; D) S12; E) S13; F) S14; G) GF05; H) GF19-3; I) GF19-4; J) GF19-5; K) S08, pure quartz domain; L) S13, pure quartz domain; M) S14, pure quartz domain; N) XC03, pure quartz vein. In the projected sphere, the horizontal line represents the foliation plane. LPOs of S08, S13 and S14 were modified from Cui (2020).

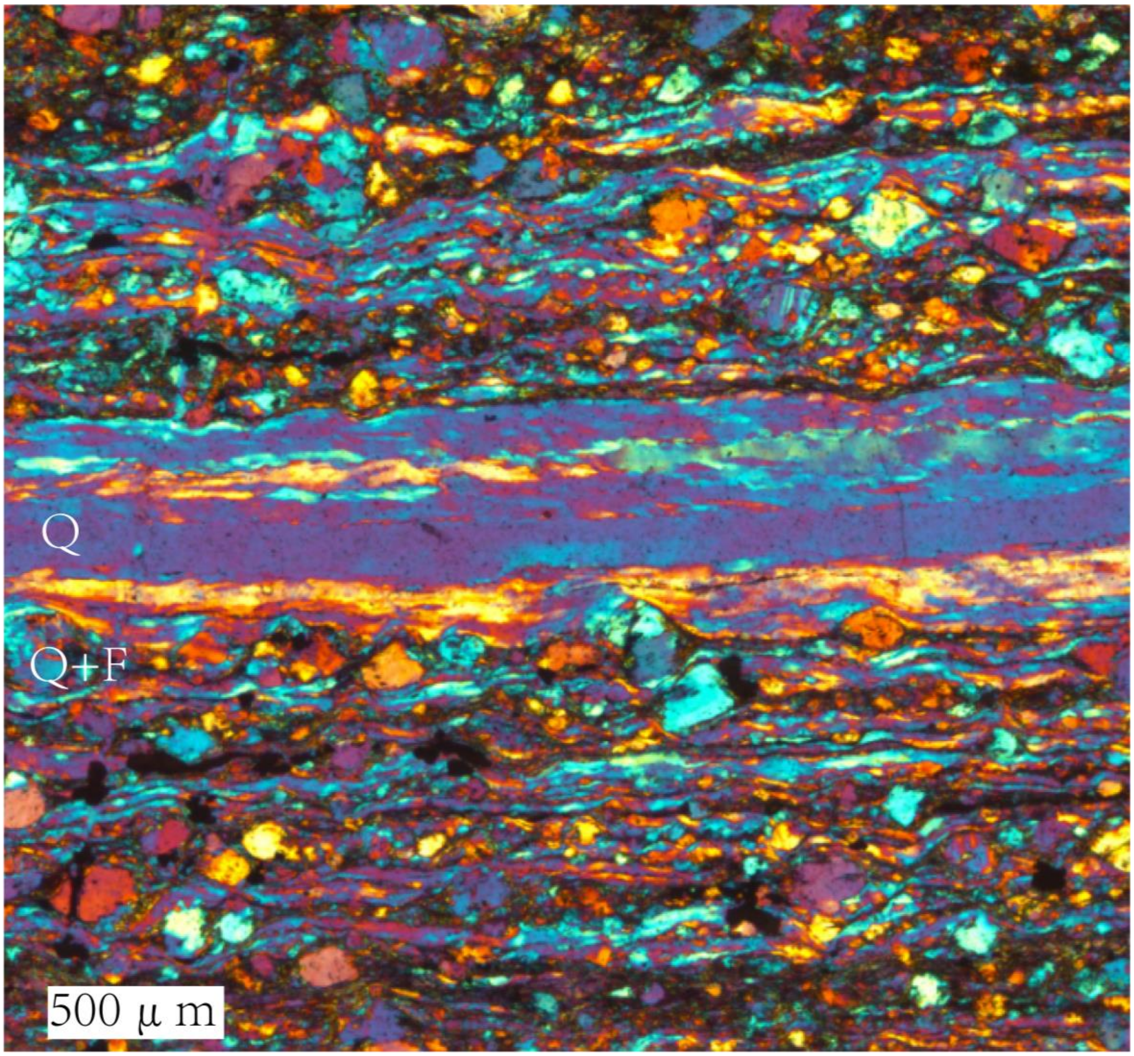

Figure 4.2 A microphotograph of the thin section showing the pure quartz domain and quartz with feldspar mixture domain.

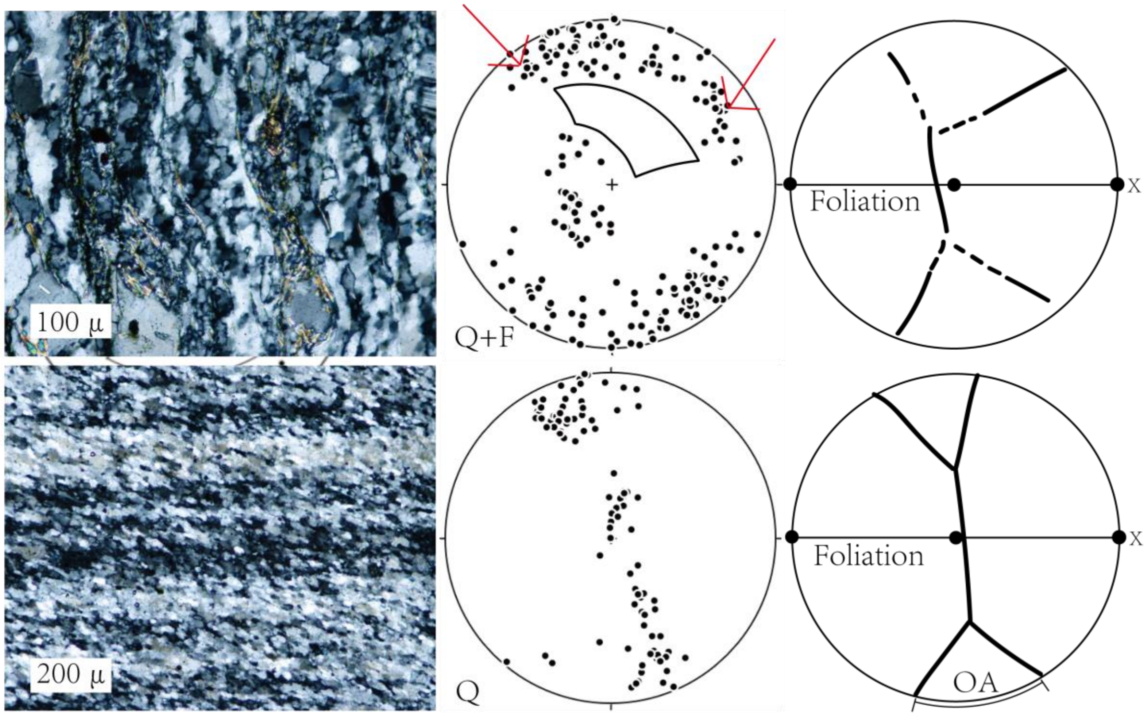

Figure 4.3 Diagrams show examples of 1) relatively continuous cross girdle vs. gaps in cross girdle; 2) abnormal spread vs. normal spread of quartz c-axes.

In Figure 4.3, the top-middle projection is from GF05. The bottom-middle projection is from XC03. Pictures to the left are the microphotographs of the corresponding sample (μ=micron). GF05 is composed of mainly quartz and feldspar porphyroclasts (Q+F) whereas XC03 is composed of 100% quartz (Q). The two diagrams on the right show the reference frame as well as the interpretation of the fabric skeleton for the asymmetric cross-girdles (Cross et al., 2015). The shear plane is represented by the horizontal line, and X represents the direction of lineation. In GF05, most of the c-axes are distributed at the outer edge and near the center, in between, there are gaps, bounded by the fan-like shape (which suggests a weak rhomb <a> slip). In the fabric skeleton, this gap is represented by the dashed line. In XC03, the cross girdle is more continuous. Red arrows point toward where the quartz c-axes spread out unusual in GF05. The abnormal spread results in an extremely large open angle and great uncertainty while measuring the open angle.

The open angle thermometer results are presented in Figure 4.4 and Table 3. The third column in Table 3 is the estimated temperature from Figure 4.4 and the fourth column shows the calculated temperature using Equation 3 (T below 650°C). The fifth column shows calculated temperatures using Equation 4 with P=5.3 kbar. These three thermometers do not yield temperatures of big difference.

Pressure estimation is based on a thermal gradient of 25 °C/km. According to Stipp et al. (2002), the transition between SGR to GBM occurs at 500 °C (see Section 4.3 for identification on the dislocation creep mechanism), which corresponds to 20 km in depth. Based the relationship $P=\rho \cdot g \cdot h$, where ρ is the crustal density (assuming 2700 kg/m^3), g is acceleration due to gravity (assuming 10 m/s^2), h is depth (20000 m), the pressure is 530 MPa or 5.3 kbar approximately. Pressure-dependence on the temperature is weak (1 kbar variation in pressure leads to ±14 °C change in temperature).

In Figure 4.4, the red crosses represent the measurements from samples that are not affected by rigid feldspar porphyroclasts. The blue crosses represent the measurements that are less reliable due to feldspar porphyroclast interruption in samples (please see Chapter 5 for more clarification). The diagram is modified after Law (2014). Longer bars of the cross suggest larger uncertainty. Samples labeled with an asterisk (*) are considered less reliable data due to the abnormal spread of quartz c-axes. There is no significant difference between temperatures estimated in Figure 4.4, Equations 3 and 4. Samples S11, S12, GF05, GF19-3, and GF19-5 yield an extremely large spread in the peripheral c-axes. I notice that the large open angle is due to the quartz ribbons wrapping around rigid feldspar porphyroclasts (Figure 4.2), so these samples are not used in temperature estimation (see Chapter 5 for more clarification). The deformation temperature ranges from 350 to 440 (±50) °C. This is a qualitative estimation.

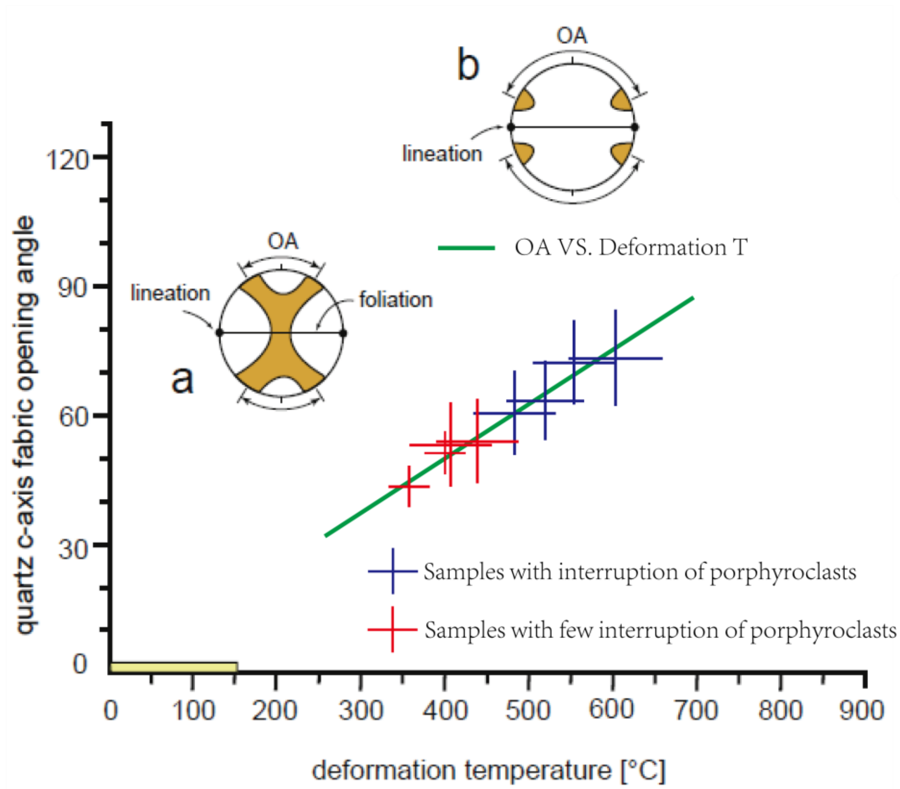

Figure 4.4 Temperature constrained using the open angle thermobarometer of quartz c-axes LPO (Law, 2014).

Sample	LPO Open Angle (°)	Temperature (°C) (Figure 4.4)	Eq. 3 (°C)	Eq. 4 (°C)
S08 (Cui, 2020)	45 (±5)	350 (±25)	359 (±35)	366 (±45)
S09	53 (±10)	435 (±50)	414 (±70)	433 (±75)
S11 *	65 (±10)	515 (±50)	497 (±70)	517 (±65)
S12 *	70 (±10)	550 (±50)	531 (±70)	547 (±60)
S13 (Cui, 2020)	50 (±5)	400 (±25)	393 (±35)	409 (±40)
S14 (Cui, 2020)	50 (±5)	400 (±25)	393 (±35)	409 (±40)
GF19-3 *	65 (±8)	515 (±35)	497 (±55)	517 (±50)
GF19-4	55 (±10)	440 (±50)	428 (±70)	448 (±75)
GF19-5 *	60 (±10)	480 (±50)	462 (±70)	484 (±70)
GF05 *	75 (±15)	590 (±75)	566 (±105)	576 (±80)
XC03	45 (±3)	350 (±20)	359 (±20)	366 (±27)

Table 3. Open angle thermometer results of samples at GFTZ mylonites.

4.2 Titanium-in-quartz results

The titanium concentrations, the standard deviation of concentrations, and the temperatures calibrated using both thermometers are presented in Table 4 and Figure 4.5. Temperatures calibrated is not sensitive to pressure. Calculation shows that a change in 130 MPa in pressure will only result in 20°C change temperature.

If there is rutile in the samples (rutile saturation), the activity of TiO_2 should be set to 1 (Ghent and Stout, 1984). The activity of TiO_2 in metapelites is thought to be from 0.6 to 1 (Ghent and Stout, 1984). No rutile was found in the samples that I studied, but pelites are common both inside and outside the shear zone and in the wall rocks. Therefore, I have considered the activity of TiO_2 in the range of 0.6 and 1. Also, the temperature is relatively insensitive to the variation in TiO_2 activity (Table 5). Table 5 lists temperatures obtained using the thermometer of Thomas et al. (2010) that has the activity term. It turns out that change in activity of 0.4 only results in a 30 °C variation in the temperature approximately. The 0.6 in Table 5 likely represents the lower bound of activity considering the presence of pelites. The 1.0 in Table 4 and Table 5 represents the upper bound.

S14(W) represents the concentration measured from large grains. S14(r) is measurements from grains of small grain sizes. S14 is the only sample that has measurements from two spots within the same thin section. S15 is a sample from 1749 Ma mylonitized granite. Samples labeled with an asterisk (*) are data with less confident level due to the large standard deviation.

The lowest concentration of Titanium in these samples is 0.89 ppm from GF19-5, which is 7.23 ppm lower than the highest value from S14 (W). In S14, the concentrations vary by grain size. The concentration in relatively large grains is higher than the concentration in relatively small grains. Overall, the temperatures estimated using the Huang and Audétat (2012) thermometer are higher than the temperatures estimated using the Thomas et al. (2010) thermometer. The results in Table 4 are plotted as diagrams as well (Figure 4.4). The temperatures constrained using two thermometers from Thomas et al.

(2010) and Huang and Audétat (2012) vary by 80 degrees approximately when the activity of TiO_2 is set to 1.0. Deformation temperatures calculated for samples S14(W) and S15 are significantly higher than the other samples (S08, S09, S13, S14(r), GF19-5, GF04), by almost 100 °C. Temperatures of S15 and S14(r) have large uncertainties due to the large standard deviation of Ti concentrations.

Sample	**Ti (ppm)**	**Standard Deviation (ppm)**	**Huang & Audétat (2012) °C**	**Thomas et al. (2010) °C (a_{TiO2}=1.0)**
S08	1.01	0.30	431.89(±18)	352.86(±18)
S09	1.50	0.53	454.29(±23)	378.20(±23)
S13	2.13	1.27	474.98(±50)	390.10(±50)
S14(W)	8.12	1.62	566.80(±16)	449.77(±16)
S14(r) *	3.54	2.62	507.44(±78)	401.83(±78)
S15 *	9.09	6.14	575.61(±78)	456.85(±78)
GF19-5	0.89	0.22	425.11(±14)	341.40(±14)
GF04	1.10	0.66	436.46(±46)	357.38(±46)

Table 4. A table that shows the concentrations of Titanium and the estimated temperatures in each sample.

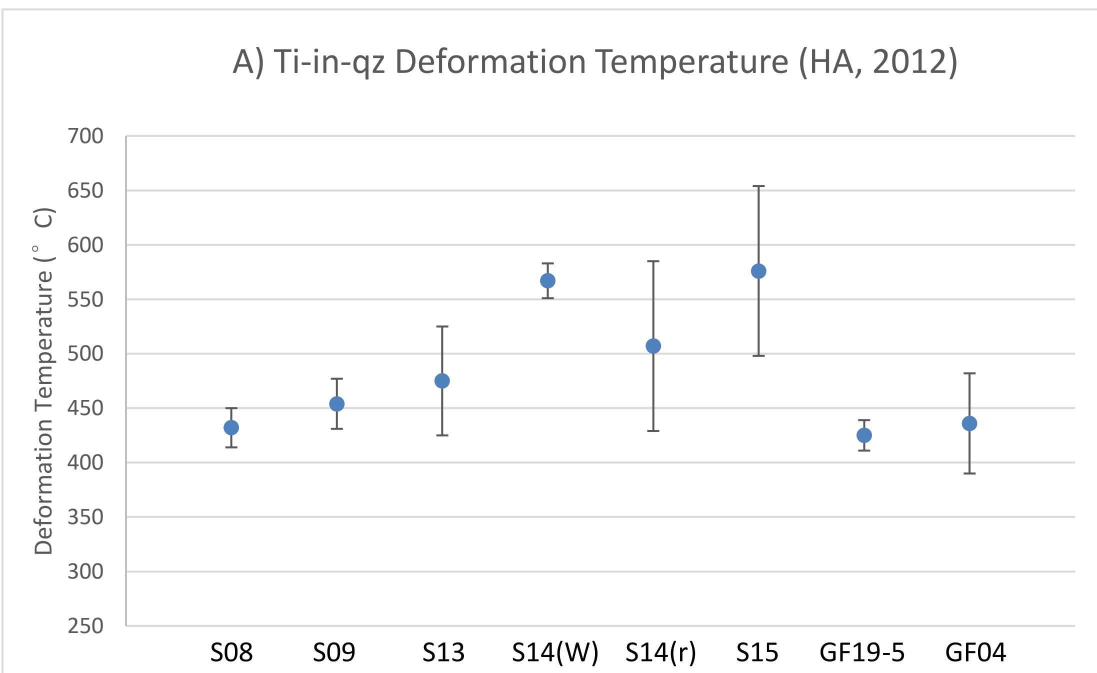

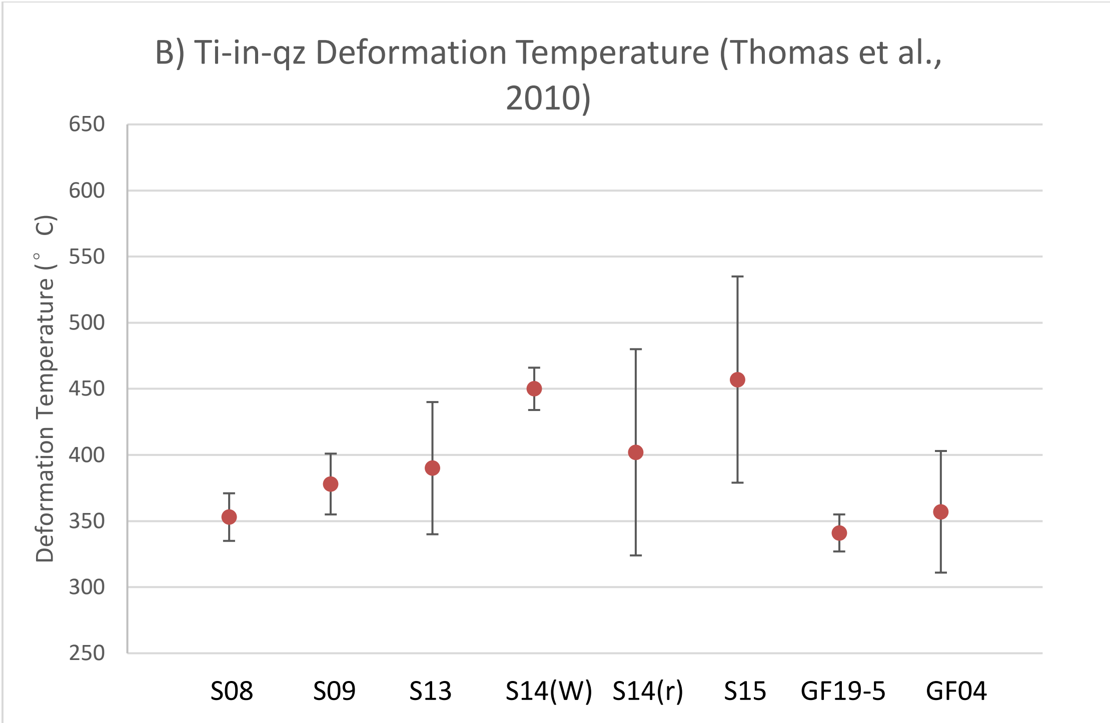

Figure 4.5 Deformation temperatures constrained using two thermometers (Huang and Audétat, 2012; Thomas et al., 2010).

Sample	HA(2012)	a_{TiO2}=0.6	a_{TiO2}=1.0
S08	431.89(±18)	377.51	352.86
S09	454.29(±23)	404.93	378.20
S13	474.98(±50)	417.83	390.10
S14(W)	566.80(±16)	482.85	449.77
S14(r) *	507.44(±78)	430.57	401.83
S15 *	575.61(±78)	490.59	456.85
GF19-5	425.11(±14)	365.14	341.40
GF04	436.46(±46)	382.40	357.38

Table 5. This table shows how the temperatures vary with activity.

4.3 Dynamically recrystallized grain size results

The dynamically recrystallized grain–sizes from seven samples (GF02, GF03, GF04, GF05, S15, GF19-3, and GF19-5) across the northeast of the Grenville Front shear zone are presented in Table 6. Lithologies from these samples vary from pure quartz mylonite, to quartzo-feldspathic mylonites and mylonitic granite. The average grain size (d) ranges from 15 to 45 μm. The largest grain size is from GF04 (quartzo-feldspathic mylonite). The smallest grain size is from mylonitized granite S15.

Sample	Rock Type	Number of grains measured	Average Size (μm)	Standard Deviation (μm)	Median (μm)
GF02	Quartz Mylonite	200	37.38	15.14	35.37
GF03	Quartzo-feldspathic Mylonite	200	36.17	13.68	34.41
GF04		200	44.69	19.10	40.41
GF05		200	24.45	7.90	22.86
S15 (Urbanski, 2021)	Mylonitized Granite	200	15.03	6.10	14.06
GF19-3	Quartzo-feldspathic mylonite	200	23.25	12.53	19.61
GF19-5		200	36.24	15.51	31.99

Table 6. Dynamically recrystallized grain size measurements of GF02, GF03, GF04, GF05, S15, GF19-3, and GF19-5.

Figure 4.6 shows new grains forming at the boundaries of the remnant of the old grains. The dominant dislocation creep mechanism of quartzo-feldspathic mylonites is subgrain rotation (SGR) or regime 2. Minerals outside the quartz domain include mica and feldspar. Notice that at the boundary recrystallized small grains already formed, and at the large grain remnant new subgrains are forming. Mica and some other highly deformed materials are on the left, and remnants of a large quartz grain are on the right. Their sub boundaries are still faint but can be seen. Some grain boundaries show a triple junction structure (a structure where grain boundaries meet each other, forming a 120° angle. In Kidder et al. (2016) this is described as a partial foam texture.

Figure 4.7 shows the microstructures of pure quartz in quartz veins (GF02 and XC03). The dominant dislocation creep mechanisms in the pure quartz are subgrain rotation (regime 2) to grain boundary migration (regime 3). They are samples of 100% deformed and recrystallized pure quartz samples. The thin section is not oriented with the foliation and lineation. The major dislocation creep regime in GF02 is regime 2 (subgrain rotation). In XC03, it is subgrain rotation to grain boundary migration.

Figure 4.8 is a plot of differential stress estimations of samples in this study using different piezometers (Shimizu, 2008; Stipp and Tullis, 2003; Twiss, 1977). Only the α-quartz piezometer is considered in Shimizu (2008) because the deformation temperatures of mylonites fall below the α-β transition temperature (573°C). Differential stress (σ) is plotted against the dynamically recrystallized grain diameter (d).

Table 7 lists the differential stresses calculated using grain size and deformation temperatures. Decreasing grain size is correlated with higher paleo-differential stress. The piezometer of Stipp and Tullis (2003) yields the smallest differential stress whereas the piezometer of Shimizu (2008) calibrates the highest differential stress. Stresses are estimated using three piezometers by Twiss (1977), Stipp and Tullis (2003) and Shimizu (2008). For the Shimizu (2008) piezometer, only α-quartz is considered because the deformation temperature is below 573 °C. For the deformation temperature obtained from the Ti-in-qz thermometer, please refer to Sections 4.2 and 5.2 for a detailed description. Since the calibration of Ti-in-qz is applied here, only samples that have titanium concentration measurements were selected for plotting. An asterisk (*) indicates the data with large uncertainties.

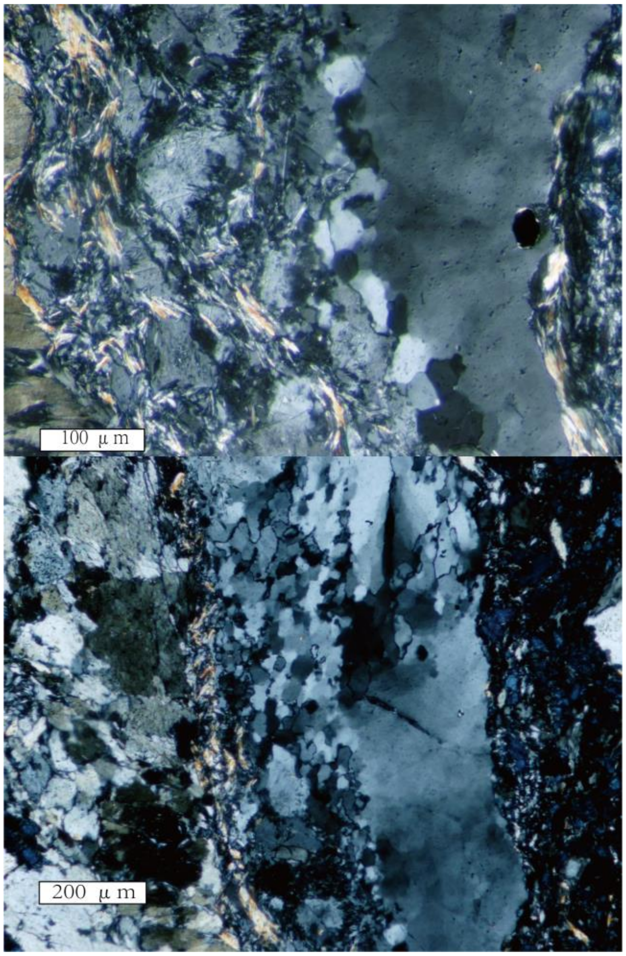

Figure 4.6 Microstructure of GF03.

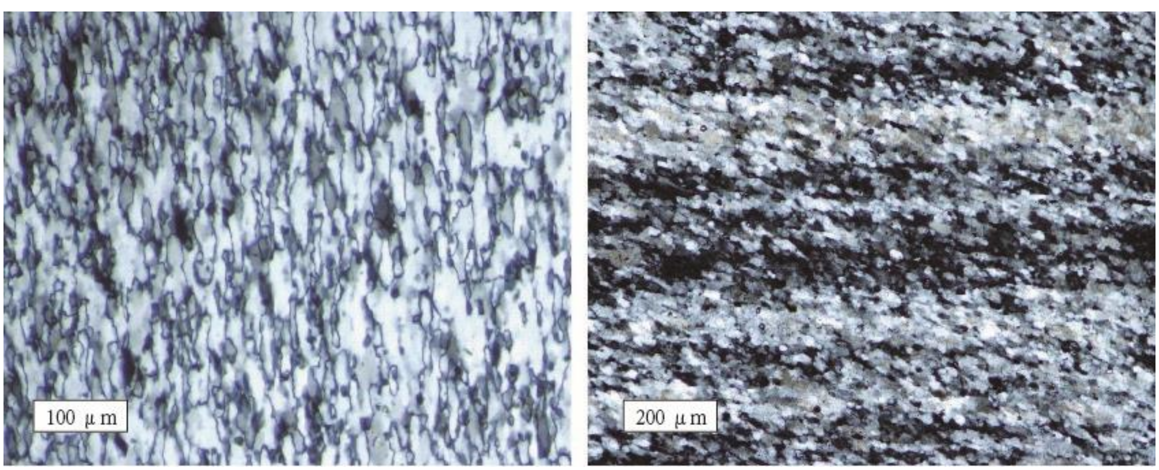

Figure 4.7 Microstructure of GF02 (left) and XC03 (right).

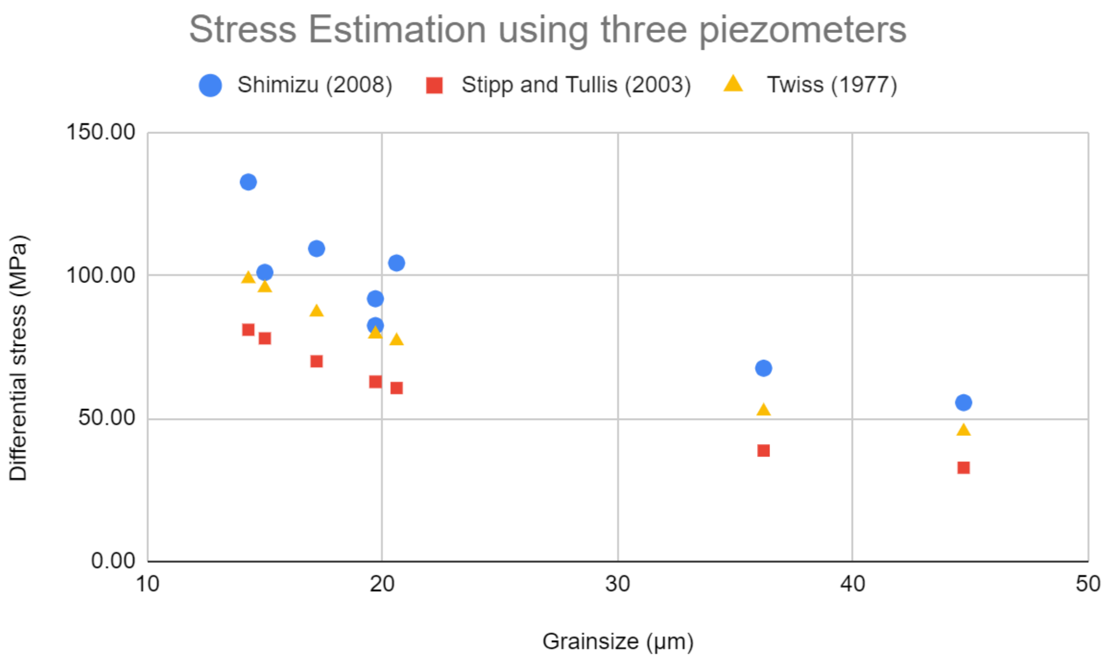

Figure 4.8 Scatter plot that helps visualize paleo-stress (MPa) constrained using three different piezometers (Twiss, 1977; Stipp and Tullis, 2003; Shimizu, 2008).

Sample	d (μm)	σ-Twiss (1977)	σ-S & T (2003)	σ-Shimizu (2008)	Temperature °C
S08	20.6	77.08	60.62	104.33	431.89
S09	14.3	98.79	81.00	132.63	454.29
S13	17.2	87.14	69.95	109.36	474.98
S14(W)	19.7	79.46	62.81	82.45	566.80
S14(r) *	19.7	79.46	62.81	91.83	507.44
S15 *	15.0	95.64	77.98	101.04	575.61
GF19-5	36.2	52.53	38.75	67.55	425.11
GF04	44.7	45.51	32.78	55.53	436.46

Table 7. Dynamic recrystallized grain sizes, deformation temperatures and differential stresses.

4.4 Shear sense of the Grenville Front

There is evidence showing the shear sense (Figure 4.9). Arrows around the porphyroclast indicate the shear direction, which is left lateral. The thin sections are cut perpendicular to foliation and parallel to lineation. The foliation plane is dipping southeast, and therefore the sense of shear in 3D geometry is top-to-the-northwest, with respect to the shear zone (Figure 4.10). The plane represents the shear zone which is striking northeast at 065 and dipping at 70, the thin section is taken perpendicular to the foliation plane and parallel to lineation (Figure 4.10).

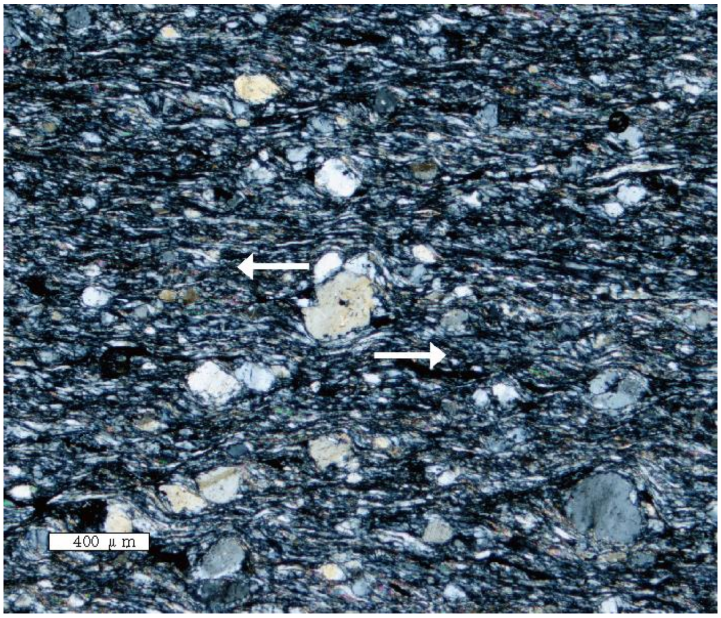

Figure 4.9 Microphotograph of S09, showing a shear sense indicator.

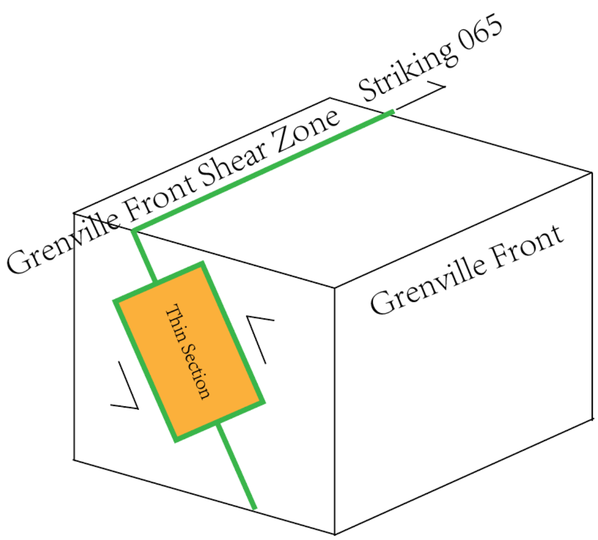

Figure 4.10 An imaginary block diagram showing the orientation of thin sections in 3D geometry.

Chapter 5

Interpretation

5.1 Interpretation of LPO measurements

LPO patterns from samples S08, GF19-5, XC03, S13 (pure quartz domain) and S14 (pure quartz domain) show clear and relatively continuous cross girdles, suggesting that the basal <a>, prism <a> and rhomb <a> slip systems are activated in these samples. The other samples (S09, S11, S12, S13 (quartz and feldspar domain), S14 (quartz and feldspar domain), GF05, GF19-3 and GF19-4) exhibit quartz c-axes at the shear-plane-normal peripheral and Y-maxima, suggesting that basal <a> and prism <a> slip systems are activated, and the gap in the girdle suggests a weak rhomb <a> slip (Figure 3.1). My interpretations regarding slip systems on samples S09, S11, S12, GF05, GF19-3, GF19-4, GF19-5 and XC03 are consistent with previous interpretations on other samples (S08, S13 and S14) by Cui (2020). As described in Chapter 4, LPOs that lack in rhomb <a> slip systems were measured from quartz and feldspar rich domains. An interpretation of this is based on the von Mises Criterion (Mises, 1928). This criterion states that, in polyphase crystals, at least five independent slip systems must be active to deform the crystal uniformly (Groves and Kelly, 1963; Tegart, 1964). If there are not enough independent slip systems operating, cracks may develop, causing failure along the grain boundaries (Cotton and Kaufman, 1991). However, if other deformation mechanisms are available during deformation, fewer slip systems are needed to achieve uniform deformation (Tegart, 1964). In samples with gaps in the girdles, fewer systems are activated than in samples with continuous girdles, suggesting that other deformation mechanisms possibly ‘substitute’ for the rhomb <a> slip system. I believe that the rotation of the second phase minerals, mostly feldspar grains and interface slip, are likely an additional deformation mechanism which promotes the dislocation creep in quartz so that the activation of the rhomb <a> slip is not necessary.

Samples S11, S12, GF05, GF19-3, and GF19-5 demonstrate the abnormal spread of quartz c-axes near shear-plane-normal peripheral (Figures 4.1 and 4.3). These samples all contain feldspar porphyroclasts, and quartz ribbons containing many dynamically recrystallized grains are found to wrap around these feldspar porphyroclasts. This adds an additional rotation of quartz c-axes around the vorticity axis of the shear zone and leads to a greater spread of the peripheral c-axes (Figures 4.3 and 5.1). Note the presence of feldspar grains (Figure 5.1) make quartz grains ribbons wrap around the feldspar grains. This is responsible for the great spread of the peripheral c-axis. The open angle will be increased because of the high concentration of felspar porphyroclasts. This interpretation is consistent with the fact that the sample without feldspar (XC03) does not have an abnormal spread of c-axes (Figure 4.3). The open angles of c-axes are exaggerated in feldspar-rich mylonites, so they cannot be used in the open-angle thermometer. I call for caution in the future use of the thermometer. It should be used where quartz ribbons are unaffected by rigid porphyroclasts. Accordingly, in this thesis, only open angles from the mylonites with little ‘feldspar interruption’ (S08, S09, S13, S14, GF19-4 and XC03) were considered when constraining the deformation temperatures using the open angle thermometer.

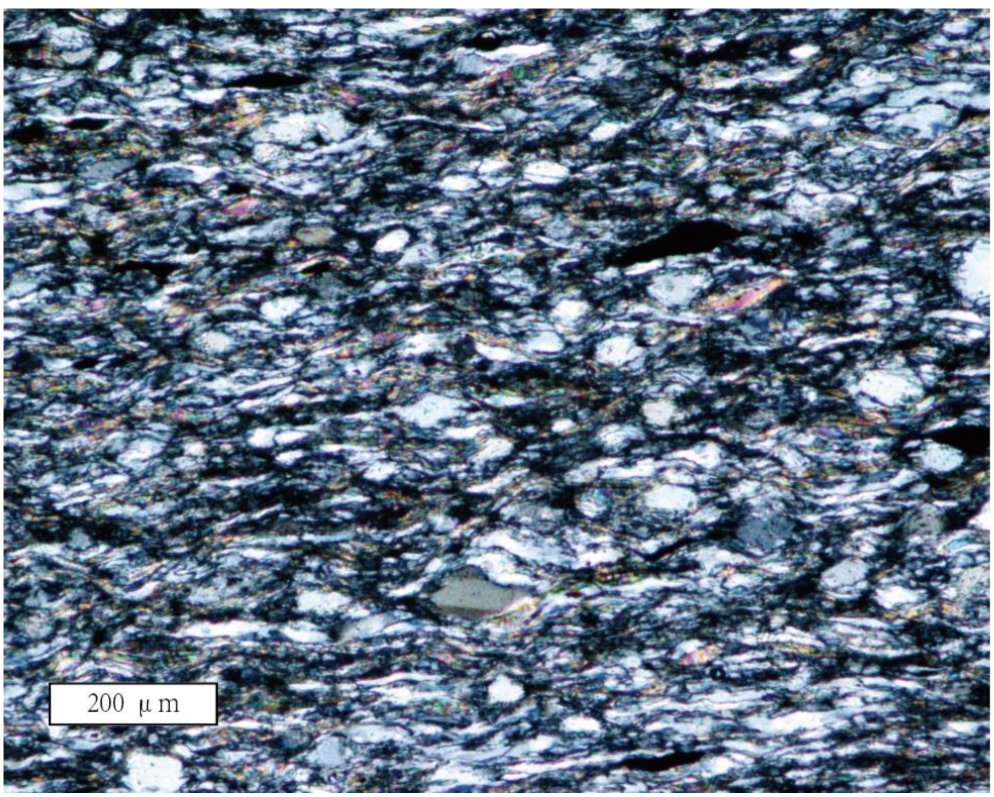

Figure 5.1 Microphotograph of S12.

5.2 Interpretation of Titanium-in-quartz

Our study shows that the temperatures constrained by two calibrations have a significant difference (see Chapter 4). The difference between the two calibrations (Huang and Audétat, 2012; Thomas et al., 2010) has been discussed in previous research as well (Wilson et al., 2012; Cross et al., 2015). Cross et al. (2015) used both calibrations to constrain the deformation temperature of quartz mylonites from the Alpine Fault Shear Zone. As shown in Figure 5.2, their results demonstrate a significant difference in temperatures (about 150 °C) on the same sample from the two thermometers (Cross et al., 2015). Diagrams on the left of Figure 5.2 demonstrate frequencies of Ti concentration, diagrams on the right show temperatures constrained from two calibrations from Huang and Audétat (2012) and Thomas et al. (2010).

In our study, although the difference between these two calibrations is not as large as those obtained by Cross et al. (2015), the Huang and Audétat (2012) calibration would still consistently obtain a deformation temperature higher than the Thomas et al. (2010) calibration (see Table 4).

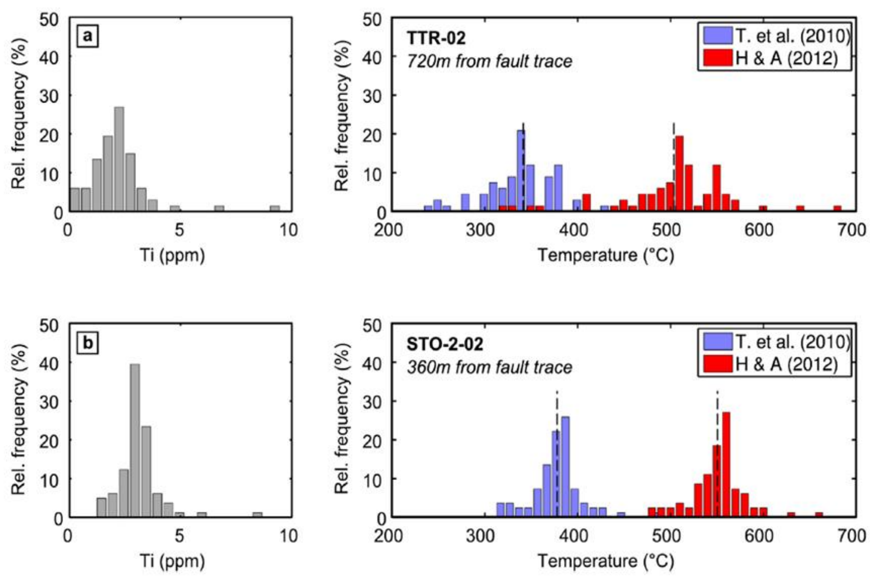

Figure 5.2 Ti-in-qz data and constrained deformation temperatures of two mylonite samples from the Alpine Fault Zone (Cross et al., 2015).

Some researchers have suggested that one of the uncertainties in calibration is the activity of TiO_2 (Grujic et al., 2011; Kidder et al., 2018). Thomas et al.'s (2010) thermometer requires the input of TiO_2 activity. However, the constraints and calibration of a_{TiO2} in rutile-absent samples can be biased and there has not been a clear statement on the limits of Ti-in-qz thermometer application. Huang and Audétat's thermometer does not require the input of TiO_2 activities. They compared three models, MELTS (Ghiorso and Sack, 1995), Hayden and Watson Model (Hayden and Watson, 2007) and Fe-Ti-Oxides Model (Ghiorso and Evans, 2008) to calculate the activity of TiO_2 in quartz and chose MELTS in their calibration (Huang and Audétat, 2012), which results in the most consistent temperatures with natural igneous quartz samples. However, they also conclude that there is no strong evidence showing which model is the most accurate in calculating the activity of TiO_2 (Huang and Audétat, 2012). In our results, these two thermometers still generate different deformation temperatures consistently, independent of TiO_2 activity. The Ti-in-qz thermometer should be used with caution, even though the activity is not strongly related to the discrepancy between the two thermometers.

The uncertainty may also result from extrapolation (Kidder et al., 2013). Samples from this study were deformed at temperatures lower than 600 °C (as prism <c> slip is absent), which is outside the laboratory condition (600-800 °C for Huang and Audétat, 2012; 700-940 °C for Thomas et al., 2012). Thus, the applicability of Ti-in-qz thermometers to the pelitic rocks in lower temperatures has been examined (Haertel et al., 2013; Kidder et al., 2013). Comparisons of Ti-in-qz thermometry with other independent P-T constraints on greenschist facies rocks reveal that both thermometers can constrain reliable deformation temperatures (Cross et al., 2015; Haertel et al., 2013; Kidder et al., 2013).

Discrepancies may also occur due to the various crystal growth rates affecting Ti concentration. The calibration experiments by Huang and Audétat (2012) demonstrate that Ti concentration arises with increasing quartz crystal growth rate. Even at the same growth rate, the absolute Ti concentrations would alter among different samples (Huang and Audétat, 2012). Huang and Audétat (2012) only considered the Ti concentrations from samples of the lowest growth rates in calibration because they are less affected by the growth rate. Thomas et al. (2010) did not consider the effect of the growth rate. Due to this, I interpret that Huang and Audétat's (2012) calibration is more accurate. Therefore, deformation temperatures obtained by Huang and Audétat (2012) are considered in the following flow law analysis.

The titanium concentration variances in one sample are also worth noting (Figure 4.4, S14(W) and S14(r)). Ashley et al. (2014) has reported the phenomenon where titanium concentration was resetting during dynamic recrystallization. In some experiments, recrystallized subgrains contain significantly lower Ti concentrations than their host porphyroclast cores (Ashley et al., 2013; Ashley et al., 2014; Grujic et al., 2011; Kidder et al., 2013). Specifically, it is the thermodynamic factors that redistribute Ti in the quartz during recrystallization, causing Ti abundances to be lower than expected (Ashley et al., 2014). Even though this might be the situation in S14 where the Ti concentration has been reset, there is no strong evidence supporting this interpretation. Another reason for this variance might be that S14(W) and S14(r) were measured on different grain sizes (see section 4.2). Nonetheless, I cannot conclude that the temperature variance is due to grain size unless there are more data that suggest Ti concentration variance in the same sample correlates with grain sizes. I notice that the Ti concentration of S14(r) was measured with great uncertainty, therefore S14(r) should be excluded in further analysis (it is still presented in the following analysis but is marked as data with less confidence). I suggest that the future works may investigate the titanium concentration variation between the dynamically recrystallized grains and their host porphyroclast grains to see whether there is a consistent difference.

The deformation temperatures (Table 4) calibrated using the Ti-in-qz thermobarometer (Huang and Audétat, 2012) ranges from 425 to 576 °C. In Table 4, it is shown that in S14 (r) and S15, Ti concentrations have large uncertainties. Microstructural analysis of the quartz (Section 4.1, 4.2) and clinopyroxene (Section 2.2) also suggest a medium deformation temperature. Therefore, in this study, I suggest that the data from S14(r) and S15 are less reliable (they are still plotted for comparison with other data). Considering the above information, I propose that the deformation temperatures fall within a range from 425-567 °C.

5.3 Piezometric analysis

Microstructures show that the dominant deformation mechanism is regime 2 dislocation creep (Stipp et al., 2002).

In Figure 4.8, the plot of differential-stress reveals the discrepancies among these different piezometric models. The Stipp and Tullis (1977) model yields a consistently lowest estimation of differential stress whereas the Shimizu (2008) model always gives the highest results. The differences in σ obtained by these two piezometers can be as large as 52 MPa (in sample S09). The paleo-stresses obtained in the Grenville Front samples demonstrate a large range, from 56 to 133 MPa (Shimizu, 2008). In the Shimizu model, stress is more sensitive to DRX grain sizes. In comparison, the other two piezometers only obtain a difference of 48 MPa (Stipp and Tullis, 2003) or 54 MPa (Twiss, 1977) between the largest grain size and smallest grain size. What can be inferred is that the differential stress in the ductile crust can be variable even within a short distance. Lu and Jiang (2019) proposed that it is because different assumptions were made by previous authors, and they did not consider the pressure effect and fluid impact. This range could be the real variation in differential stress, uncertainties in the piezometers, or both.

The Shimizu (2008) piezometer is chosen for the flow law analysis in this study as it considers the effect of temperatures and different deformation mechanisms on stress (Stipp and Tullis, 2003). It is also applicable to the SGR mechanism, which is the major dislocation creep regime within the samples. When the temperature rises and the strain rate decreases, the dislocation creep mechanism changes from BLG to SGR and GBM in correspondence (Hirth and Tullis, 1992; Passchier and Trouw, 2005). Twiss's (1977) model is not consistent with the natural samples (Shizimu, 2008), and Stipp and Tullis (2003) failed to consider the temperature and quartz inversion (α-β transition) effect (Shimizu, 2008, 2012). When β-quartz is transformed into α-quartz, activation energy changes with the volume change are possible (Shimizu, 2008). Below 800 °C the temperature effect on grain sizes can also be vital (Shimizu, 2008; Stipp and Tullis, 2003). Thus, I interpret that the Shimizu (2008, 2012) model provides a more reliable estimation. Thus, the differential stresses of GFTZ samples range from 58 to 139 MPa (Shimizu, 2008).

5.4 Applying to flow laws

Based on the interpretation above, the quartz-rich mylonite samples were deformed under 425 to 567 °C, with differential stress ranging from 56 to 133 MPa. I have compiled the differential stress, deformation temperatures and water fugacities of these mylonites in Table 8. With these T-σ relationships, I estimated the strain rates of these samples using flow laws by Lu and Jiang (2019), Tokle et al. (2019) and Gleason and Tullis (1995) (Table 8).

In Table 8, T is in degrees Celsius, σ is in MPa, fw is in MPa, and $\dot{\varepsilon}$ is strain rate in s^{-1}. The three columns of strain rates are from three studies by Lu and Jiang (2019), Tokle et al. (2019) and Gleason and Tullis (1995). The parameters of flow law by Gleason and Tullis (1995) are $A=5.1x10^{-4}$ (corrected by Holyoke and Kronenberg (2010)), n=4, Q=223 (kJ/mol). The parameters of flow law by Tokle et al. (2019) chosen in this thesis are $A=1.1x10^{-12}$, r=1.2, n=3, Q=115 (kJ/mol). The water fugacity was calculated using the calculator by Tony Withers, at https://publish.uwo.ca/~awither5/fugacity/index.htm. S14 (r) and S15 are labeled with an asterisk (*) because of the large uncertainties in temperature estimation.

The Voigt average strain rates are also constrained because the $\dot{\varepsilon}$ (s) represent only the strain rates for quartz deformation, while the other minerals are not deformed and have no strain rates. All three flow laws yield strain rates at $10^{-12+/-2}$ s^{-1} approximately. According to Table 8, the strain rates derived from the flow law by Lu and Jiang (2019) agree well with the crustal strain rate (10^{-13} to 10^{-11} s^{-1}) suggested by many geological studies (Lu and Jiang, 2019). The flow laws by Tokle et al. (2019) and Gleason and Tullis (1995) obtained slower strain rates than the commonly suggested strain rate range for the ductile shear zones.

Sample	T	σ	f_w	ε̇ (/s) (L&J)	ε̇ (/s) (To)	ε̇ (/s) (G&T)	Voigt ε̇
S08	432	104	164	4.63E-12	1.71E-12	1.82E-12	2.78E-12
S09	454	133	185	3.70E-11	7.45E-12	1.53E-11	2.40E-11
S13	475	109	205	4.49E-11	7.99E-12	1.96E-11	2.25E-11
S14(W)	567	82	295	5.48E-10	4.00E-11	3.19E-10	2.47E-10
S14(r) *	507	92	236	8.94E-11	1.21E-11	4.33E-11	8.94E-11
S15 *****	576	101	304	1.68E-09	9.05E-11	1.00E-09	1.09E-09
GF19-5	425	68	158	5.74E-13	3.68E-13	2.21E-13	2.01E-13
GF04	436	56	168	4.68E-13	3.02E-13	1.86E-13	2.34E-13

Table 8. Compilation of differential stress, temperatures, water fugacity and calibration of strain rate using flow laws.

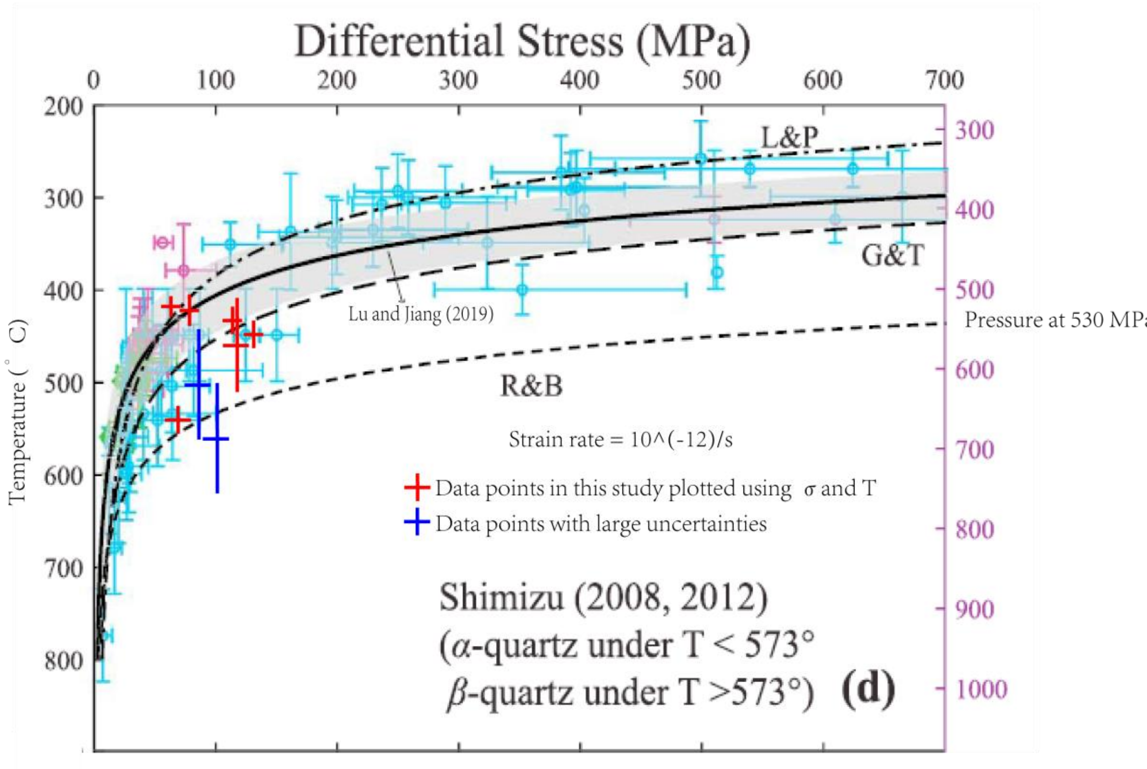

Figure 5.3 Compilation of natural quartzite data to a flow law profile (Lu and Jiang (2019).

Data have been plotted onto the flow laws based on the T-σ relationships (Figure 5.3). The red crosses represent the data points in this study. The deep blue crosses represent less reliable data points due to large uncertainty. The light blue (unknown deformation mechanisms), green (grain boundary migration) and purple (subgrain rotation) crosses represent data of natural quartz samples from earlier studies (Lu and Jiang, 2019). The bars represent uncertainties. The strain rate is set as 10^{-12}/s. The right vertical axis represents the pressure (MPa). In our study, the pressure was estimated to be 400 MPa. Modified after Lu and Jiang (2019). The other three flow laws are from Luan and Paterson (1992) (L&P), Gleason and Tullis (1995) (G&T), and Rutter and Brodie (2004).

As identified in Chapter 4, dislocation creep regime 2 is the dominant mechanism. Most of our data fit well with the flow laws with regime 2, at a strain rate of 10^{-12} s^{-1}. S15 with deformation temperatures higher than 570 °C is slightly out of the range predicted by the flow laws, likely due to less accurate temperature constrain. The flow law by Luan and

Paterson (1992) slightly underestimates the temperature of samples when stress is the same. In the contrast, the Rutter and Brodie (2004) flow law overestimates the temperature. Flow laws by Lu and Jiang (2019) and Gleason and Tullis (1995) are better at predicting the deformation conditions of natural samples. The alignment of deformation conditions between natural quartzite and the quartz flow law implies that similar deformation mechanisms are activated.

5.5 Tectonic synthesis and interpretation

Based on the observation, it is suggested that our samples were deformed during the third generation of deformation, which is identified as D3 (Li, 2012). This generation of deformation took place around 1000-953 million years ago, according to zircon dating by Li (2012), after the D1 (1080-1030 Ma) and D2 (1028-1018 Ma) deformation. D3 is responsible for the shear zone development in this region, and it resulted in F4 folds (please see Li (2012) for more details). The footwall of the Grenville Front shear zone is the Mississagi quartz-rich sandstone in the study area whereas the hanging wall is composed of metamorphosed gneiss and amphibolite. The mylonites studied in this thesis are in the immediate footwall of the Grenville Front shear zone and have recorded the terminal stage of the Grenville Orogeny.

5.6 Limitations on the study

Even though this study comments on the applicability of flow laws by comparing the deformation conditions of natural quartz-rich mylonites with previous experimental data, limitations of the work still exists.

First, determining the deformation conditions involve the calibrations of temperatures, pressures, and grainsizes. The calibrations on P-T-σ conditions can be very different depend on the selection of the thermometers or piezometers. As shown in Chapter 4, the temperatures estimated between the two Ti-in-qz thermometers have significant discrepancies. The temperatures constrained and the conclusion based on temperatures will likely be different if others choose the calibration by Thomas et al. (2010). The differential stress estimation demonstrates the discrepancies between the piezometers as well. These are the limitations on constraining the P-T-σ of the natural samples.

Second, the flow law studies have a limit. This type of studies are based on power law rheology. The flow law formula is relatively sensitive to its parameters (A, m, Q, n). For instance, Lu and Jiang (2019) has obtained a value of 6.0 (±5.0) x 10^{-15} for parameter A. The lower bound and upper bound of this parameter's uncertainty can lead to different crustal density estimation, and this difference can be as large as an order of magnitude.

Chapter 6

Conclusions

In this thesis, I have investigated the deformation conditions of naturally deformed quartz-rich mylonites from the Grenville Front shear zone. The major discoveries and contributions are summarized in this chapter. This thesis promotes the understanding of the ductile deformation of the continental crust by adding new constrained P-T-σ data onto the current flow law profile and examined the applicability of current flow laws. This research also provides a better constrained deformation condition of the Grenville Front shear zone.

The LPOs of the quartz c-axes demonstrate clear and consistent cross-girdles. The LPOs suggest that the major slip systems activated are basal <a>, rhomb <a> and prism <a> in samples having continuous cross girdles. Some samples have clear gaps in the girdles and suggest the lack of rhomb <a> slip. The presence of feldspar grains have acted as an additional deformation mechanism so that rhomb <a> slip is weak. The presence of rigid feldspar grains have also led to the abnormal spread of peripheral quartz c-axes in some of the LPOs. This leads to large open angles of the c-axis pattern. This effect should be considered when applying the open angle thermometer to calculate deformation temperatures.

Deformation temperature was estimated using the Ti-in-qz thermometer by Huang and Audétat (2012), ranging from 425 to 567 °C.

The major deformation mechanism is regime 2 dislocation creep. This deformation mechanism is consistent with the medium temperature range and the active slip systems constrained from LPO data.

The dynamically recrystallized grainsizes are between 45 to 15 μm which yield differential stresses for the deformation between 56 to 133 MPa using the piezometer of Shimizu (2008).

The quartz c-axes patterns suggest that the shear sense is top-to-the-northwest thrusting for the Grenville Front shear zone. This is consistent with previous studies and field observations.

The strain rates estimated based on deformation conditions (P, T, σ) of Grenville Front mylonites fall within the range of 10^{-10} to 10^{-13} s^{-1}. This is consistent with the strain rate on active place boundaries region estimated by modern GPS observations (Lu and Jiang, 2019).

At the strain rate of 10^{-12} s^{-1}, the T-σ relationships of samples from the Grenville Front shear zone fall well within the prediction of the flow law from Lu and Jiang (2019) and Gleason and Tullis (1995). The deformation conditions of quartz-rich mylonites in this study also demonstrate a good consistency with other natural deformed rocks.

References

Ashley K.T., Webb L.E., Spear F.S. and Thomas J.B. (2013) P-T-D histories from quartz: A case study of the application of the TitaniQ thermobarometer to progressive fabric development in metapelites. *Geochem. Geophys. Geosys.* 14, 3821-3843. https://doi.org/10.1002/ggge.20237

Ashley K.T., Carlson W.D., Law R.D. and Tracy R.J. (2014) Ti resetting during dynamic recrystallization: Mechanisms and significance. *Am. Min.* 99, 2025-2030. https://doi.org/10.2138/am-2014-4943

Audétat A., Garbe-Schönberg D., Kronz A., Pettke T., Rusk B., Donovan J. J., and Lowers H.A. (2015) Characterisation of a Natural Quartz Crystal as a Reference Material for Microanalytical Determination of Ti, Al, Li, Fe, Mn, Ga and Ge. *Geostand Geoanal Res* 39 (2), 171. https://doi.org/10.1111/j.1751-908X.2014.00309.x

Austin N.J. and Evans B. (2007) Paleowattmeters: a scaling relation for dynamically recrystallized grain size. *Geol. Soc. Am. Bull.* 35(4), 343-346. https://doi.org/10.1130/G23244A.1

Austin N.J. and Evans B. (2009) The kinetics of microstructural evolution during deformation of calcite. *J. Geophys. Res.* 114, B09402. https://doi.org/10.1029/2008JB006138

Behrmann J.H. and Platt J.P. (1982) Sense of nappe emplacement from quartz c-axis fabrics; an example from the Betic Cordilleras (Spain). *Earth Planet. Sci. Lett.* 59(1), 208-215. https://doi.org/10.1016/0012-821X(82)90126-1

Bhandari A. and Jiang D. (2021) A Multiscale Numerical Modeling Investigation on the Significance of Flow Partitioning for the Development of Quartz c-Axis Fabrics. *J. Geophys. Res. Solid Earth* 126, e2020JB021040. https://doi.org/10.1029/2020JB021040

Bouchez J.L., Lister G.S. and Nicolas A. (1983) Fabric asymmetry and shear sense in movement zones. *Geol Rdsch* 72, 401-419. https://doi.org/10.1007/BF01822075

Corfu F. and Easton R.M. (2000) U-Pb evidence for polymetamorphic history of Huronian rocks within the Grenville front tectonic zone east of Sudbury, Ontario, Canada. *Chem. Geol.* 172, 149-171. https://doi.org/10.1016/S0009-2541(00)00241-2

Cotton J.D. and Kaufman M.J. (1991) A simplified method for determining the number of independent slip systems in crystals. *SCRIPTA METALL MATER* 25, 2395-2398. https://doi.org/10.1016/0956-716X(91)90036-Z

Cross A.J., Kidder S. and Prior D. (2015) Using microstructures and TitaniQ thermobarometry of quartz sheared around garnet porphyroclasts to evaluate microstructural evolution and constrain an Alpine Fault Zone geotherm. *J. Struct. Geol.* 75, 17-31. https://doi.org/10.1016/j.jsg.2015.02.012

Cross A.J., Prior D.J., Stipp M. and Kidder S. (2017) The recrystallized grain size piezometer for quartz: An EBSD-based calibration. *Geophys. Res. Lett.* 44, 6667-6674. https://doi.org/10.1002/2017GL073836

Cui Z. (2020) Quartz C-Axis Fabric Variation in A Grenville Front Mylonite: Implications for Dislocation Slip Systems. Electronic Thesis.

Davidson A. (1984) Tectonic boundaries within the Grenville province of the Canadian shield. *J. Geodyn.* 1, 433-444. https://doi.org/10.1016/0264-3707(84)90018-8

Davidson A. and Van Breeman O. (1994) U-Pb ages of granites near the Grenville Front, Ontario Radiogenic Age and Isotopic Studies: Report 8. *Geological Survey of Canada*, Current Research 1994-F.

Dickin A.P. (1998) Nd isotope mapping of a cryptic continental suture, Grenville Province of Ontario. *Precambrian Res.* 91, 433-444. https://doi.org/10.1016/S0301-9268(98)00062-X

Ehrlich K., Vers, E., Kirs J. and Soesoo A. (2012) Using a titanium-in-quartz geothermometer for crystallization temperature estimation of the

Palaeoproterozoic Suursaari quartz porphyry. *Estonian J. Earth Sci.* 61(4), 195-204. https://doi.org/10.3176/earth.2012.4.01

Fairbairn H.W. (1949) Structural petrology of deformed rocks. Addison-Wesley Publishing Company, Inc. p246.

Faleiros F.M., Moraes R., Pavan M. and Campanha G.A.C. (2016) A new empirical calibration of the quartz c-axis fabric opening-angle deformation thermometer. *Tectonophysics* 671, 173-182. https://doi.org/10.1016/j.tecto.2016.01.014

Frost H. J. and Ashby M. F. (1982) Deformation mechanism maps: The plasticity and creep of metals and ceramics. Oxford, UK: Pergamon Press.

Fukuda J. and Shimizu I. (2017) Theoretical derivation of flow laws for quartz dislocation creep: Comparisons with experimental creep data and extrapolation to natural conditions using water fugacity corrections. *J. Geophys. Res. Solid Earth* 122, 5956–5971. https://doi.org/10.1002/2016JB013798

Ghent E.D. and Stout M.Z. (1984) TiO_2 activity in metamorphosed pelitic and basic rocks: principles and applications to metamorphism in southeastern Canadian Cordillera. *Contrib. Mineral. Petrol.* 86(3), 248-255. https://doi.org/10.1007/BF00373670

Ghiorso M. S. and Evans B. W. (2008) Thermodynamics of rhombohedral oxide solid solutions and a revision of the Fe–Ti two-oxide geothermometer and oxygen barometer. *Am. J. Sci.* 308, 957–1039. https://doi.org/10.2475/09.2008.01

Ghiorso M. S. and Sack R. O. (1995) Chemical mass transfer in magmatic processes. IV. A revised and internally consistent thermodynamic model for the interpolation and extrapolation of liquid–solid equilibria in magmatic systems at elevated temperatures and pressures. *Contrib. Mineral. Petrol.* 119, 197–212. https://doi.org/10.1007/BF00307281

Gleason G.C., Tullis J. and Heidelbach F. (1993) The role of dynamic recrystallization in the development of lattice preferred orientations in experimentally deformed quartz aggregates. *J. Struct. Geol.* 15 (9-10), 1145-1168. https://doi.org/10.1016/0191-8141(93)90161-3

Gleason G.C. and Tullis J. (1995) A flow law for dislocation creep of quartz aggregates determined with the molten salt cell. *Tectonophysics* 247(1-4), 1-23. https://doi.org/10.1016/0040-1951(95)00011-B

Gleiter H. (1969) The mechanism of grain boundary migration. Acta metallurgica. 17(5), 565-573. https://doi.org/10.1016/0001-6160(69)90115-1

Green A.G., Milkereit B., Davidson A., Spencer C., Hutchinson D.R., Cannon W.F., Lee M.W., Agena W.F., Behrendt J.C. and Hinze W.J. (1988) Crustal structure of the Grenville front and adjacent terranes. *Geology* 16, 788-792. https://doi.org/10.1130/0091-7613(1988)016<0788:CSOTGF>2.3.CO;2

Griggs D. (1967) Hydrolytic weakening of quartz and other silicates. *Geophys. J. Int.* 14(1–4), 19–31. https://doi.org/10.1111/j.1365-246X.1967.tb06218.x

Groves G.W. and Kelly A. (1963) Independent slip systems in crystals. The Philosophical Magazine: A Journal of Theoretical Experimental and Applied Physics 8(89), 877-887. https://doi.org/10.1080/14786436308213843

Grujic D., Stipp M. and Wooden J.L. (2011) Thermometry of quartz mylonites: Importance of dynamic recrystallization on Ti-in-quartz reequilibration. *Geochem. Geophy. Geosy.* 12 (6), Q06012. https://doi.org/10.1029/2010GC003368

Haertel M., Herwegh M. and Pettke T. (2013) Titanium-in-quartz thermometry on synkinematic quartz veins in a retrograde crustal-scale normal fault zone. *Tectonophysics* 608, 468-481. http://dx.doi.org/10.1016/j.tecto.2013.08.042

Haggart M.J., Jamieson R.A., Reynolds P.H., Krogh T.E., Beaumont C. and Culshaw N.G. (1993) Last gasp of the Grenville Orogeny: thermochronology of the Grenville Front tectonic zone near Killarney, Ontario. *J. Geol.* 101(5), 575-589. https://doi.org/10.1086/648250

Hayden L. A. and Watson E. B. (2007) Rutile saturation in hydrous siliceous melts and its bearing on Ti-thermometry of quartz and zircon. *Earth Planet. Sci. Lett.* 258, 561–568. https://doi.org/10.1016/j.epsl.2007.04.020

Heilbronner R. and Kilian R. (2017) The grain size (s) of Black Hills quartzite deformed in the dislocation creep regime. *Solid Earth* 8(5), 107-1093. https://doi.org/10.5194/se-8-1071-2017

Hirth G., Teyssier C. and Dunlap J.W. (2001) An evaluation of quartzite flow laws based on comparisons between experimentally and naturally deformed rocks. *Int. J. Earth Sci.* 90(1), 77-87. https://doi.org/10.1007/s005310000152

Hirth G. and Tullis J. (1992) Dislocation creep regimes in quartz aggregates. *J. Struct. Geol.* 14(2), 145-159. https://doi.org/10.1016/0191-8141(92)90053-Y

Holyoke C. W. and Kronenberg A. K. (2010) Accurate differential stress measurement using the molten salt cell and solid salt assemblies in the Griggs apparatus with applications to strength, piezometers and rheology. Tectonophysics 494(1-2), 17-31. https://doi.org/10.1016/j.tecto.2010.08.001

Holyoke C. W. and Kronenberg A. K. (2013). Reversible water weakening of quartz. *Earth Planet. Sci. Let.* 374, 185–190. https://doi.org/10.1016/j.epsl.2013.05.039

Huang R. and Audétat A. (2012) The titanium-in-quartz (TitaniQ) thermobarometer: a critical examination and re-calibration. *Geochim. Cosmochim. Acta* 84, 75-89. https://doi.org/10.1016/j.gca.2012.01.009

Karato S. I. (2008) Deformation of Earth materials: An introduction to the rheology of solid earth. Cambridge: Cambridge Univ. Press.

Karato S. I., Paterson M. S. and FitzGerald J. D. (1986) Rheology of synthetic olivine aggregates: Influence of grain size and water. *J. Geophys. Res. 91*(B8), 8151–8176. https://doi.org/10.1029/JB091iB08p08151

Kidder S.B., Avouac J.P. and Chan Y.C. (2013) Application of titanium-in-quartz thermobarometry to greenschist facies veins and recrystallized quartzites in the Hsuehshan range, Taiwan. *Solid Earth* 4(1), 1-21. https://doi.org/10.5194/se-4-1-2013

Kidder S., Hirth G., Avouac J.P. and Behr W. (2016) The influence of stress history on the grain size and microstructure of experimentally deformed quartzite. *J. Struct. Geol.* 83, 194-206. https://doi.org/10.1016/j.jsg.2015.12.004

Kidder S.B., Toy G.V., Prior D.J., Little T.A., Khan A. and MacRae C. (2018) Constraints on Alpine Fault (New Zealand) mylonitization temperatures and the geothermal gradient from Ti-in-quartz thermobarometry. *Solid Earth* 9, 1123-1139. https://doi.org/10.5194/se-9-1123-2018

Kohlstedt D. L., Evans B. and Mackwell S. J. (1995). Strength of the lithosphere: Constraints imposed by laboratory experiments. *J. Geophys. Res.* 100(B9), 17587–17602. https://doi.org/10.1029/95JB01460

La Tour T.E. (1981) Significance of folds and mylonites at the Grenville front in Ontario: Summary. *Geol. Soc. Am. Bull.* 92(7), 411-413. https://doi.org/10.1130/0016-7606(1981)92<411:SOFAMA>2.0.CO;2

Law R.D. (2014) Deformation thermometry based on quartz c-axis fabrics and recrystallization microstructures: a review. *J. Struct. Geol.* 66, 129–161. https://doi.org/10.1016/j.jsg.2014.05.023

Li C. (2012) An Investigation of Deformation Structures and Their Tectonic Significance Across the Grenville Front Tectonic Zone in the Vicinity of Sudbury, Ontario, Canada. *Electronic Thesis and Dissertation Repository*. 464.

Li J.C.M. (1962) Possibility of Subgrain Rotation during Recrystallization. *J. Appl. Phys.* 33(10), 2958-2965. https://doi.org/10.1063/1.1728543

Lu X. and Jiang D. (2019) Quartz Flow Law Revisited: The Significance of Pressure Dependence of the Activation Enthalpy. *J. Geophys. Res. Solid Earth* 124, 241-256. https://doi.org/10.1029/2018JB016226

Luan F.C. and Paterson M.S. (1992) Preparation and deformation of synthetic aggregates of quartz. *J. Geophys. Res.* 97(B1), 301-320. https://doi.org/10.1029/91JB01748

Lusk A. D. J, Platt J. P. and Platt J. A. (2021) Natural and Experimental Constraints on a Flow Law for Dislocation-Dominated Creep in Wet Quartz. J. Geophys. Res. 126(5), p.e2020JB021302. https://doi.org/10.1029/2020JB021302

Mauler A., Bistricky M., Kunze K. and Mackwell S. (2000) Microstructures and lattice preferred orientations in experimentally deformed clinopyroxene aggregates. *J. Struct. Geol.* 22, 1633-1648. https://doi.org/10.1016/S0191-8141(00)00073-0

McGill S. F., Owen L. A., Weldon R. J. and Kendrick K. J. (2013) Latest Pleistocene and Holocene slip rate for the San Bernardino strand of the San Andreas fault, Plunge Creek, Southern California: Implications for strain partitioning within the southern San Andreas fault system for the last ∼35 k.y. *Geological Society of America Bulletin*, *125*(1–2), 48–72. https://doi.org/10.1130/B30647.1

Mises R.V. (1928) Mechanik der plastischen Formänderung von Kristallen. *J. Appl. Math. Mech.* 8(3), 161-185. https://doi.org/10.1002/zamm.19280080302

Moore J.M. (1986) Introduction: The 'Grenville Problem' then and now. In: Moore J.M., Davidson A., Baer A.J. (Eds.), The Grenville Province. *Geological Association of Canada Special Paper* 31, 1-12.

Oliver D. (1996) Structural, Kinematic and Thermochronometric Studies of the Teslin Suture Zone, South-Central Yukon Territory [Ph.D. thesis]. Southern Methodist University 231.

Ostapenko G. T., Bamarnik M. Y. and Gorogotskaya L. I. (1987) Isomorphism of titanium substitution for silicon in quartz: experimental data. *Mineral. Zh.* 9, 30–40.

Passchier C.W. and Trouw R.A.J. (2005) Microtectonics. Springer, Berlin.

Rivers T. (1997) Lithotectonic elements of the Grenville Province: Review and tectonic implications. *Precambrian Res.* 86(3-4), 117-154. https://doi.org/10.1016/S0301-9268(97)00038-7

Rutter E. H. and Brodie K. H. (2004) Experimental intracrystalline plastic flow in hot-pressed synthetic quartzite prepared from Brazilian quartz crystals. *J. Struct. Geol.* 26(2), 259–270. https://doi.org/10.1016/S0191-8141(03)00096-8

Schmid S. M. and Casey M. (1986) Complete fabric analysis of some commonly observed quartz c-axis patterns. Hobbs B.E., Heard H.C., Mineral and Rock.

Schulz S. E. and Evans J. P. (2000) Mesoscopic structure of the Punchbowl Fault, Southern California and the geologic and geophysical structure of active strike-slip faults. *Journal of Structural Geology*, *22*(7), 913–930. https://doi.org/10.1016/S0191-8141(00)00019-5

Shelton G. L. and Tullis J. (1981) Experimental flow laws for crustal rocks. *Eos, Transactions American Geophysical Union* 62, 396.

Shimizu I. (2008) Theories and applicability of grain size piezometers: the role of dynamic recrystallization mechanisms. *J. Struct. Geol.* 30, 899-917. https://doi.org/10.1016/j.jsg.2008.03.004

Shimizu I. (2012) Steady-state grain size in dynamic recrystallization of minerals. Recrystallization, Prof. Krzysztof Sztwiertnia (Ed.), ISBN: 978-953-51-0122-2, InTech.

Stipp M., Stünitz H., Heilbronner R. and Schmid S.M. (2002) Dynamic recrystallization of quartz: correlation between natural and experimental conditions. *Geol. Soc. Spec. Publ.* 200, 171-190. https://doi.org/10.1144/GSL.SP.2001.200.01.11

Stipp M. and Tullis J. (2003) The recrystallized grain size piezometer for quartz. *Geophysical Research Letters* 30(21), SDE 3 1-5. https://doi.org/10.1029/2003GL018444

Stipp M., Tullis J., Scherwath M. and Behrmann J.H. (2010) A new perspective on paleopiezometry: Dynamically recrystallized grain size distributions indicate mechanism changes. *Geology* 38(8), 759–762. https://doi.org/10.1130/G31162.1

Sutherland R., Berryman K. and Norris R. (2006) Quaternary slip rate and geomorphology of the Alpine fault: Implications for kinematics and seismic hazard in southwest New Zealand. *Geological Society of America Bulletin*, *118*(3–4), 464–474. https://doi.org/10.1130/B25627.1

Tegart W.J.McG. (1964) Independent slip systems and ductility of hexagonal polycrystals. The Philosophical Magazine: A Journal of Theoretical Experimental and Applied Physics 9(98), 339-341. https://doi.org/10.1080/14786436408229197

Thomas J.B., Watson E.B., Spear F.S., Shemella P.T., Nayak S.K. and Lanzirotti A. (2010) TitaniQ under pressure: the effect of pressure and temperature on the solubility of Ti in quartz. *Contrib. Mineral. Petrol.* 160, 743-759. https://doi.org/10.1007/s00410-010-0505-3

Tokle L., Hirth G. and Behr W.M. (2019) Flow laws and fabric transitions in wet quartzite. *Earth Planet. Sci. Lett.* 505, 152-161. https://doi.org/10.1016/j.epsl.2018.10.017

Tullis J. (2002) Deformation of granitic rocks: Experimental studies and natural examples. *Reviews in mineralogy and Geochemistry* 51(1), 51-95. https://doi.org/10.2138/gsrmg.51.1.51

Tullis J. (1977) Preferred orientation of quartz produced by slip during plane strain. *Tectonophysics* 39(1-3), 87-102. https://doi.org/10.1016/0040-1951(77)90090-7

Tullis J. Yund R.A. (1989) Hydrolytic weakening of quartz aggregates: The effects of water and pressure on recovery. *Geophys. Res. Lett.* 16(11), 1343-1346. https://doi.org/10.1029/GL016i011p01343

Twiss R.J. (1977) Theory and applicability of a recrystallized grain size paleopiezometer. *Pure Appl. Geophys.* 115(1-2), 227-244. https://doi.org/10.1007/978-3-0348-5745-1_13

Urbanski J. (2021) Paleostress and Kinematic Analysis from Dynamically Recrystallized Quartz Grains in Mylonites From the Grenville Front Tectonic Zone. Electronic Thesis.

Wark D.A. and Watson E.B. (2006) TitaniQ: a titanium-in-quartz geothermometer. *Contrib. Mineral. Petrol.* 152, 743-754. https://doi.org/10.1007/s00410-006-0132-1

Wenk H.R. and Christie J.M. (1991) Comments on the interpretation of deformation textures in rocks. *J. Struct. Geol.* 13(10), 1091-1110. https://doi.org/10.1016/0191-8141(91)90071-P

Wenk HR., Yu R., Vogel S. and Vasin R. (2019) Preferred Orientation of Quartz in Metamorphic Rocks from the Bergell Alps. *Minerals* 9(5), 277. https://doi.org/10.3390/min9050277

Wilson C.J.N., Seward T.M., Allan A.S.R., Charlier B.L.A. and Bello L. (2012) A comment on: ‘TitaniQ under pressure: the effect of pressure and temperature on the solubility of Ti in quartz’, by Jay B. Thomas, E. Bruce Watson, Frank S.

Spear, Philip T. Shemella, Saroj K. Nayak and Antonio Lanzirotti. *Contrib. Mineral. Petrol.* 160, 743-759. https://doi.org/10.1007/s00410-012-0757-1

Wynne-Edwards H.R. (1972) The Grenville Province in Price R.A. and Douglas R.J.W. eds., Variations in Tectonic Styles in Canada: Geological Association of Canada, Special Paper 11, 263-334.

Zhang L. Zhang B., Zhang J., Wang J., Cai F., Zhao Z., Chen S. and Li X. (2022) The rheology and deformation of the South Tibetan Detachment System as exposed at Zherger La, east-central Himalaya: Implications for exhumation of the Himalayan metamorphic core. J. Struct. Geol. 157, 104559, ISSN 0191-8141. https://doi.org/10.1016/j.jsg.2022.104559

Zolnai A.L., Price R.A. and Helmstaedt H. (1983) Regional cross section of the Southern Province adjacent to Lake Huron, Ontario: implications for the tectonic significance of the Murray Fault Zone. *Can. J. Earth Sci.* 21, 447-456. https://doi.org/10.1139/e84-048

Appendices

Appendix A: Excel formulas that are used to plot Lattice Preferred Orientation.

	A	B	C	D	E	F	G	H	I	J	K	L	M
1	measured data												
2	NO	I-V	S-N	L=1/R=2	H=1/V=2	Color				Plunging	angle		
3	1							90		90	0	L	{N=C, M=30000000FF000000FF0000}

Table A. Spreadsheet used for stereographic projection on LPO measurement. Formulas are given as below.

Column A = Grain Number

Column B = I-V axis reading (three digits)

Column C = S-N axis reading (two digits)

Column D = reading on left (1) or on right (2)

Column E = horizontality of grain (horizontal (1) or vertical (2))

Column F = original color of grain under microscope (blue = 1, yellow = 2, purple = 3)

Take Row 3 as an example, the formulas from Column H to M are listed.

Column H = IF(D3=1,270-B3,90-B3)

Column J = IF(H3<0,360+H3,H3)

Column K = IF(E3=2,90-C3,C3)

Column L = L

Column M =

IF(F3=1,"{N=C,M=3000FF000000FF00000000}",IF(F3=2,"{N=C,M=300000FFFF0000FFFF0000}","{N=C,M=30000000FF000000FF0000}"))

After plugging in measured data, the excel will generate codes that include plunge and trend, and colors. Columns J to M are to be copied into text. file and thus can be projected in Stereonet.

Appendix B: Raw data of quartz c-axes orientation

Sample S09					
NO	I-V	S-N	L/R	H/V	COLOR
1	16	13	R	H	P
2	11	16	R	H	B
3	25	13	L	H	Y
4	359	19	R	H	P
5	22	11	R	H	Y
6	348	19	L	V	P
7	359	14	L	V	P
8	36	7	R	H	Y
9	341	7	R	H	Y
10	334	13	L	H	Y
11	11	9	L	H	B
12	351	28	R	V	P
13	24	19	L	V	B
14	10	1	L	H	P
15	318	17	L	H	Y
16	336	16	L	H	Y
17	330	19	L	H	Y
18	14	28	L	H	B
19	331	11	L	H	Y
20	14	28	R	H	B
21	330	27	R	V	Y
22	6	24	R	H	P
23	18	0	L	H	B
24	17	13	R	H	B
25	4	17	L	H	P
26	36	9	L	H	B
27	11	13	R	H	P
28	11	14	R	V	P
29	13	20	L	H	P
30	2	16	L	H	P
31	21	15	L	H	B
32	357	13	R	H	P
33	32	8	L	H	B
34	323	30	R	V	Y
35	347	11	L	H	Y
36	48	19	L	V	B
37	1	6	R	H	P
38	22	11	R	H	B

39	19	14	L	H	P
40	29	9	R	H	B
41	341	7	R	V	Y
42	319	14	L	H	Y
43	344	22	L	H	Y
44	17	18	R	H	B
45	41	17	R	H	B
46	338	10	R	H	Y
47	22	13	R	H	B
48	350	12	R	H	P
49	6	5	L	H	P
50	346	17	L	H	Y
51	2	17	R	H	P
52	1	18	R	H	P
53	25	23	R	H	B
54	349	8	R	H	Y
55	338	4	L	V	Y
56	358	10	R	V	P
57	26	7	R	V	B
58	32	8	L	H	Y
59	22	12	L	V	B
60	324	13	R	V	Y
61	340	13	R	V	P
62	4	9	L	H	P
63	21	7	L	H	B
64	331	10	R	H	Y
65	2	15	L	H	P
66	0	11	L	V	P
67	8	3	L	H	B
68	342	18	R	V	P
69	23	10	L	V	P
70	334	17	R	V	Y
71	19	2	L	H	B
72	26	6	R	H	B
73	31	4	R	H	B
74	10	9	R	H	B
75	335	12	L	H	Y
76	349	22	R	V	P
77	16	2	R	H	B
78	27	12	R	H	B
79	323	8	R	H	Y

80	359	18	L	H	P
81	58	16	L	V	B
82	324	16	L	H	Y
83	7	2	L	H	P
84	347	20	R	V	P
85	21	0	R	H	B
86	8	20	R	V	P
87	33	3	R	H	B
88	18	7	R	H	B
89	2	12	R	H	P
90	23	14	L	H	B
91	329	9	L	H	Y
92	336	25	R	H	P
93	42	17	L	H	B
94	345	11	L	H	P
95	342	11	L	H	P
96	2	14	R	V	P
97	347	10	R	H	Y
98	358	17	R	H	P
99	357	12	L	H	P
100	337	14	R	H	Y
101	28	9	R	H	B
102	336	5	L	H	Y
103	22	17	R	H	B
104	358	9	L	H	P
105	313	6	R	H	Y
106	18	4	L;	H	B
107	28	5	L	H	B
108	7	10	R	H	P
109	17	13	L	H	B
110	27	8	R	H	B
111	33	14	R	H	B
112	334	9	R	H	Y
113	48	8	R	H	B
114	30	11	R	H	B
115	357	17	R	V	P
116	332	20	R	V	Y
117	1	11	L	H	P
118	14	9	L	V	P
119	25	0	L	H	B
120	332	9	L	H	Y

121	23	9	R	H	B
122	333	11	R	H	Y
123	357	19	L	H	P
124	37	15	R	H	B
125	6	9	L	V	P
126	337	13	L	H	Y
127	347	26	R	V	P
128	31	1	R	H	B
129	21	7	R	H	B
130	3	23	R	V	P
131	30	13	L	H	B
132	327	26	L	H	Y
133	321	17	R	H	Y
134	327	6	R	H	Y
135	27	7	R	H	B
136	44	1	R	H	B
137	19	12	R	H	B
138	71	10	L	V	P
139	351	9	L	H	P
140	25	6	L	H	B
141	351	7	R	H	P
142	36	8	R	H	B
143	351	9	L	H	P
144	20	8	L	H	B
145	350	13	L	H	P
146	30	2	L	H	B
147	27	14	L	H	B
148	6	26	R	V	P
149	340	28	R	V	Y
150	348	22	R	V	P
151	18	18	R	H	B
152	28	15	R	H	B
153	7	0	L	V	P
154	18	18	L	H	B
155	35	8	L	H	B
156	33	5	R	H	B
157	331	6	R	H	Y
158	12	14	R	H	B
159	16	4	L	H	B
160	331	2	R	H	Y
161	15	19	R	H	P

162	2	15	R	H	P
163	3	19	R	V	P
164	28	0	L	H	B
165	19	17	R	H	B
166	356	7	R	V	P
167	24	8	L	H	B
168	17	29	R	H	B
169	327	21	R	V	Y
170	359	3	L	V	P
171	343	13	L	H	Y
172	29	15	R	H	B
173	20	9	L	V	P
174	3	18	R	V	P
175	49	5	R	H	B
176	14	20	R	H	P
177	33	7	L;	H	B
178	22	25	R	H	B
179	44	20	R	H	B
180	358	8	R	H	P
181	13	11	L	V	P
182	47	11	L	H	B
183	3	14	L	H	P
184	328	3	R	H	Y
185	15	14	R	H	B
186	328	22	L	H	Y
187	28	3	L	H	B
188	339	19	R	V	P
189	337	17	L	H	Y
190	35	13	L	H	B
191	349	20	R	V	P
192	25	12	R	H	B
193	328	8	R	H	Y
194	30	10	R	H	B
195	5	23	R	H	P
196	33	1	L	H	B
197	32	19	R	H	B
198	346	10	R	H	P
199	336	10	L	H	Y
200	22	15	L;	H	B

Sample S11					
NO.	I-v	N-S	L/R	H/V	COR
1	38	23	L	H	B
2	90	20	L	H	P
3	302	27	R	H	Y
4	44	26	L	H	B
5	34	17	L	H	B
6	34	24	L	H	B
7	2	17	R	V	P
8	327	22	L	V	P
9	43	11	L	H	Y
10	329	26	R	H	Y
11	328	18	L	V	P
12	16	12	L	H	B
13	52	26	R	V	B
14	297	18	L	V	P
15	86	15	R	V	P
16	336	20	R	V	P
17	24	24	L	H	B
18	32	12	L	H	B
19	18	22	L	H	B
20	339	26	L	V	Y
21	315	1	L	H	Y
22	345	21	R	H	Y
23	359	18	L	H	P
24	316	6	L	H	Y
25	359	23	R	H	P
26	330	19	R	H	Y
27	31	15	L	V	B
28	330	8	L	H	Y
29	320	15	R	H	Y
30	348	25	R	V	P
31	1	33	R	H	P
32	313	13	L	H	P
33	300	26	L	H	Y
34	340	24	L	V	P
35	314	23	R	H	Y
36	2	19	L	H	P
37	318	24	L	H	Y
38	25	29	R	H	B

39	312	24	L	V	Y
40	2	13	R	V	P
41	342	40	R	V	Y
42	16	12	L	H	B
43	307	25	R	H	Y
44	17	17	L	H	B
45	339	24	L	V	Y
46	333	25	R	V	Y
47	348	14	L	H	P
48	323	21	R	H	Y
49	19	25	R	H	Y
50	344	25	L	H	P
51	24	18	L	H	B
52	20	4	L	H	B
53	358	13	R	H	P
54	11	15	L	H	B
55	344	14	R	H	Y
56	14	7	R	H	B
57	310	14	L	H	Y
58	332	9	R	H	Y
59	333	18	L	V	P
60	291	17	L	V	P
61	20	13	L	H	B
62	335	20	L	H	P
63	40	6	R	H	B
64	336	18	L	H	B
65	356	31	L	H	P
66	315	14	R	H	Y
67	331	31	L	V	Y
68	336	1	R	H	Y
69	308	8	L	H	B
70	8	29	R	H	P
71	14	16	R	H	P
72	13	14	L	H	B
73	25	20	L	H	B
74	62	27	R	V	P
75	356	10	R	H	P
76	338	13	L	H	Y
77	49	29	R	V	B
78	323	20	L	V	Y
79	16	1	L	H	B

80	50	28	L	H	B
81	29	23	L	H	B
82	358	20	R	H	P
83	313	14	L	H	Y
84	6	9	L	H	P
85	321	19	L	V	P
86	41	31	R	V	B
87	336	16	R	H	Y
88	19	10	R	H	B
89	333	27	R	H	Y
90	4	22	L	H	P
91	353	31	L	V	P
92	29	43	R	H	B
93	72	29	R	V	P
94	326	3	L	H	Y
95	34	22	L	H	B
96	303	26	R	H	Y
97	319	20	R	H	Y
98	16	27	R	H	B
99	33	31	R	V	B
100	307	16	L	H	Y
101	351	2	R	H	P
102	1	7	R	V	P
103	341	17	R	H	Y
104	24	6	L	H	Y
105	6	8	R	H	P
106	4	21	R	H	P
107	326	29	R	H	Y
108	22	19	L	H	B
109	20	3	R	H	B
110	332	21	R	H	Y
111	338	8	L	H	Y
112	40	29	L	H	B
113	24	31	L	H	B
114	27	16	L	H	B
115	21	11	R	H	B
116	333	24	R	H	Y
117	31	30	R	V	P
118	3	11	R	H	P
119	302	2	R	H	B
120	41	15	L	H	B

121	326	21	L	V	Y
122	20	8	R	H	B
123	326	5	L	H	Y
124	1	15	L	V	P
125	55	5	L	H	B
126	337	19	L	H	Y
127	38	22	L	H	B
128	304	17	R	H	Y
129	344	17	R	H	Y
130	336	13	R	H	Y
131	335	27	R	H	Y
132	296	34	R	H	Y
133	32	22	R	H	B
134	359	2	L	V	P
135	18	31	R	H	B
136	358	24	R	V	P
137	335	12	L	H	Y
138	16	13	R	H	B
139	0	26	R	H	P
140	12	21	L	H	B
141	10	15	R	H	P
142	28	17	R	V	B
143	329	8	R	H	Y
144	327	23	L	H	Y
145	6	23	L	H	B
146	10	27	R	H	B
147	37	15	L	H	B
148	327	28	R	H	Y
149	51	2	L	H	B
150	3	1	L	H	P
151	321	2	R	H	Y
152	16	23	R	H	B
153	307	10	R	H	Y
154	333	28	R	V	Y
155	356	32	R	H	P
156	20	23	R	H	B
157	323	25	R	H	Y
158	44	10	R	H	B
159	35	19	L	H	B
160	334	25	L	V	Y
161	329	1	R	H	Y

162	327	29	L	V	Y
163	308	19	L	V	P
164	20	20	L	H	B
165	352	31	R	H	P
166	28	16	L	H	B
167	1	15	R	H	P
168	26	21	L	H	B
169	39	16	L	H	B
170	358	29	R	H	P
171	323	2	R	H	Y
172	21	10	R	H	B
173	334	20	R	H	Y
174	40	27	R	V	B
175	324	30	R	H	Y
176	15	41	R	H	B
177	2	36	R	H	P
178	354	6	L	H	P
179	34	18	R	V	P
180	343	26	L	H	Y
181	10	16	L	H	B
182	28	20	L	H	B
183	15	31	R	H	B
184	344	19	L	V	P
185	332	24	R	H	Y
186	352	22	R	H	P
187	60	28	R	H	B
188	320	6	L	V	P
189	319	22	R	H	Y
190	322	17	L	H	Y
191	327	18	L	H	Y
192	330	9	L	H	Y
193	357	22	L	H	P
194	349	14	L	V	P
195	43	26	L	H	B
196	32	19	L	H	B
197	331	5	R	V	P
198	324	20	L	H	Y
199	56	28	L	H	B
200	313	13	R	H	Y

Sample S12					
NO	I-V	N-S	L/R	H/V	COR
1	287	28	L	V	P
2	320	22	R	H	Y
3	53	17	R	H	B
4	28	7	L	H	Y
5	319	2	R	H	B
6	319	22	L	H	B
7	305	17	R	H	Y
8	34	17	R	H	B
9	0	0	L	V	P
10	353	18	R	H	P
11	27	19	L	H	B
12	36	11	L	H	B
13	12	11	L	H	P
14	319	2	R	H	B
15	42	1	L	H	Y
16	21	5	L	H	B
17	12	11	L	V	P
18	352	19	L	V	P
19	64	7	L	H	B
20	342	9	L	H	Y
21	38	4	R	H	B
22	331	18	R	H	Y
23	303	0	L	H	B
24	337	17	R	H	Y
25	335	1	R	H	B
26	323	0	L	H	B
27	337	26	L	V	P
28	354	20	L	V	P
29	349	6	L	V	P
30	31	36	R	V	B
31	20	8	L	H	B
32	70	28	L	H	B
33	332	13	R	H	Y
34	319	6	L	H	Y
35	322	7	R	H	Y
36	2	1	L	H	P
37	25	13	R	H	B
38	351	11	R	V	P
39	321	3	R	H	Y

40	328	4	L	H	Y
41	2	4	R	H	P
42	334	25	R	V	P
43	53	5	L	H	B
44	323	24	L	H	Y
45	345	5	R	H	P
46	322	10	R	H	Y
47	358	3	L	H	P
48	334	5	R	H	Y
49	19	22	R	H	Y
50	36	6	L	H	B
51	319	15	R	H	Y
52	29	7	R	H	B
53	345	10	R	H	Y
54	314	22	R	H	Y
55	308	1	R	H	B
56	17	2	R	H	B
57	342	10	R	H	B
58	332	4	L	H	Y
59	331	3	L	H	Y
60	336	5	R	H	Y
61	29	8	R	H	B
62	311	5	R	H	Y
63	32	13	R	H	B
64	49	10	L	H	B
65	306	34	R	H	Y
66	18	20	R	V	B
67	40	17	L	H	B
68	357	16	L	H	P
69	337	0	L	H	B
70	327	20	R	H	Y
71	311	7	L	H	B
72	32	8	L	H	B
73	56	20	L	H	B
74	46	22	L	H	B
75	315	12	R	H	Y
76	64	25	R	V	P
77	310	10	L	H	B
78	32	27	L	H	B
79	334	19	L	V	P
80	328	14	R	H	Y

81	58	43	R	V	B
82	319	8	L	H	Y
83	35	2	L	H	B
84	333	13	R	H	Y
85	47	21	R	V	B
86	322	9	R	H	Y
87	14	7	R	H	P
88	346	22	R	H	P
89	55	6	R	H	B
90	317	27	L	H	Y
91	303	11	R	H	B
92	18	1	L	H	B
93	53	16	L	H	B
94	306	4	L	H	B
95	18	2	L	H	B
96	343	6	L	H	B
97	317	11	L	H	B
98	332	15	L	H	Y
99	326	21	L	H	Y
100	328	10	L	H	B
101	29	1	R	H	Y
102	323	8	R	H	Y
103	328	15	R	H	Y
104	18	15	L	H	B
105	42	21	L	H	B
106	350	17	R	H	Y
107	32	16	R	H	B
108	54	10	L	H	B
109	27	6	R	H	B
110	62	31	R	V	B
111	307	1	R	H	B
112	33	1	L	H	B
113	82	23	L	H	P
114	3	8	L	H	P
115	325	14	R	H	Y
116	53	30	R	V	B
117	22	13	L	H	B
118	61	12	L	H	B
119	311	9	L	H	Y
120	343	8	L	V	P
121	346	5	L	H	P

122	295	6	L	H	B
123	313	6	R	H	B
124	338	5	R	H	Y
125	326	5	L	H	Y
126	16	18	L	H	B
127	321	0	R	H	B
128	310	10	L	H	B
129	0	10	R	H	P
130	22	29	R	V	B
131	336	1	L	H	Y
132	299	28	R	H	Y
133	341	9	L	H	Y
134	41	3	R	H	B
135	307	5	L	H	Y
136	9	4	L	V	P
137	327	26	R	H	Y
138	312	5	L	H	B
139	314	10	R	H	B
140	327	8	L	H	Y
141	344	20	R	H	P
142	41	34	R	V	B
143	338	16	L	H	P
144	303	18	L	H	B
145	329	6	L	H	Y
146	311	10	L	H	Y
147	348	20	R	H	P
148	43	18	L	H	B
149	76	9	R	H	B
150	296	34	L	V	Y
151	38	25	R	H	B
152	38	11	R	H	B
153	38	16	R	H	B
154	1	4	L	H	P
155	340	11	L	H	Y
156	336	4	R	H	Y
157	355	2	R	H	P
158	320	18	R	H	Y
159	324	6	L	H	Y
160	322	11	L	H	Y
161	1	1	R	V	P
162	48	13	R	H	B

163	51	11	L	H	B
164	5	20	L	H	P
165	318	7	R	H	Y
166	38	28	R	H	B
167	65	36	R	V	B
168	325	13	L	H	Y
169	357	17	L	H	P
170	39	8	R	H	B
171	335	1	R	H	Y
172	327	19	R	H	Y
173	38	9	L	H	B
174	308	27	R	H	Y
175	337	8	R	H	Y
176	14	18	R	H	B
177	12	17	R	H	P
178	323	8	R	H	Y
179	36	13	L	H	B
180	334	14	R	H	Y
181	343	0	L	H	Y
182	13	23	L	V	P
183	342	23	L	H	P
184	328	19	L	H	Y
185	348	5	R	H	P
186	28	17	L	H	B
187	44	11	L	H	B
188	46	15	L	H	B
189	59	23	L	H	B
190	16	11	R	H	B
191	322	17	R	H	Y
192	26	6	L	H	B
193	328	12	L	H	Y
194	25	16	R	H	B
195	348	7	R	H	P
196	332	8	R	H	Y
197	53	20	L	H	B
198	330	8	R	H	Y
199	339	11	L	H	Y
200	332	17	R	H	Y

Sample GF19-3					
NO	I-V	N-S	L/R	H/V	COR
1	18	20	R	H	B
2	358	20	K	V	P
3	12	12	R	H	P
4	26	19	R	H	B
5	4	40	R	V	P
6	356	8	R	V	P
7	21	2	R	H	B
8	346	22	L	H	Y
9	23	1	L	H	B
10	26	17	R	H	B
11	317	8	R	H	Y
12	335	7	R	H	Y
13	302	28	L	H	Y
14	30	27	R	H	B
15	26	3	R	V	P
16	25	2	L	H	B
17	37	1	R	H	B
18	340	2	L	V	P
19	27	16	R	H	B
20	320	24	R	V	Y
21	6	30	L	H	P
22	329	2	R	H	Y
23	346	27	R	V	P
24	7	8	L	H	P
25	30	27	R	H	B
26	32	13	R	H	B
27	23	24	R	H	B
28	28	29	L	V	B
29	21	18	R	H	B
30	320	5	L	H	Y
31	32	25	L	H	B
32	330	19	R	V	P
33	43	3	L	H	B
34	300	17	R	H	Y
35	20	15	R	H	B
36	296	30	L	V	Y
37	46	26	L	H	B
38	28	3	R	H	B
39	327	23	R	H	Y

40	339	31	R	H	Y
41	26	19	L	H	B
42	25	16	L	H	B
43	309	14	L	H	Y
44	16	13	L	V	P
45	294	16	L	H	Y
46	21	22	R	H	B
47	43	19	L	H	B
48	21	20	L	V	B
49	83	7	L	V	P
50	23	6	L	H	B
51	29	17	L	H	B
52	296	23	R	V	Y
53	29	22	R	H	B
54	7	21	R	V	P
55	25	18	R	H	B
56	21	4	R	H	B
57	306	2	L	H	Y
58	68	7	R	H	B
59	355	13	L	H	P
60	19	12	L	H	B
61	344	0	L	H	Y
62	353	13	L	V	P
63	30	23	R	H	B
64	331	3	L	H	Y
65	2	30	R	H	P
66	30	6	L	H	B
67	312	17	L	H	Y
68	23	23	L	H	B
69	29	8	R	H	B
70	18	1	R	H	B
71	23	32	R	H	B
72	33	9	L	V	P
73	339	38	R	V	Y
74	58	5	R	H	B
75	33	9	L	H	B
76	357	26	R	V	P
77	42	3	R	H	B
78	87	17	R	H	P
79	301	2	R	V	P
80	318	1	R	H	Y

81	42	13	L	V	P
82	352	14	R	V	P
83	23	16	L	H	B
84	301	7	L	H	Y
85	26	9	R	H	B
86	25	11	R	H	B
87	28	10	L	V	P
88	19	26	L	V	B
89	39	13	R	H	B
90	318	11	R	V	P
91	22	15	L	H	B
92	349	6	L	H	Y
93	18	1	L	H	B
94	4	24	R	V	P
95	43	12	R	H	B
96	297	13	L	H	Y
97	329	9	L	H	Y
98	15	3	R	H	P
99	24	8	L	H	B
100	17	9	R	H	B

Sample GF19-4					
NO	I-V	N-S	L/R	H/V	COR
1	340	22	R	H	Y
2	344	17	L	H	Y
3	1	20	R	H	P
4	27	16	R	V	P
5	49	9	L	H	B
6	335	19	L	H	Y
7	9	19	R	V	P
8	352	25	R	H	P
9	345	8	R	H	P
10	358	19	R	H	P
11	29	9	R	H	B
12	342	1	R	H	Y
13	34	23	L	V	B
14	352	26	R	V	P
15	348	21	R	H	P
16	337	10	R	H	Y
17	21	3	L	H	B
18	343	28	R	V	P
19	57	20	L	H	B
20	331	13	R	H	Y
21	358	22	R	V	P
22	0	2	R	H	P
23	338	17	R	H	Y
24	33	1	L	H	B
25	351	28	R	H	P
26	349	18	R	V	P
27	323	10	L	H	Y
28	30	19	L	H	B
29	323	13	R	H	Y
30	359	30	R	V	P
31	339	10	L	H	Y
32	33	16	L	H	B
33	39	15	R	H	B
34	337	21	L	H	Y
35	71	25	L	H	P
36	36	7	L	H	B
37	35	4	L	H	B
38	346	19	R	V	P

39	346	20	L	H	P
40	351	8	R	H	P
41	331	5	L	H	Y
42	34	30	R	H	B
43	30	32	L	H	B
44	20	7	L	H	B
45	349	21	L	H	Y
46	344	9	R	H	Y
47	18	21	R	H	B
48	41	22	R	H	B
49	346	21	R	V	P
50	342	17	R	H	Y
51	1	11	R	H	P
52	359	35	R	V	P
53	21	26	R	H	B
54	334	19	R	H	Y
55	356	13	R	H	P
56	26	27	R	H	B
57	346	8	R	H	Y
58	2	23	L	V	P
59	313	18	R	H	Y
60	340	7	R	H	Y
61	18	19	L	H	B
62	338	19	L	H	Y
63	351	0	L	H	P
64	339	23	R	H	Y
65	28	8	L	H	B
66	350	37	R	V	P
67	346	17	L	H	Y
68	343	18	L	H	Y
69	341	0	L	H	Y
70	349	19	R	V	P
71	8	14	L	H	P
72	60	10	L	H	B
73	32	12	R	H	B
74	324	26	R	V	Y
75	32	19	R	H	B
76	37	36	R	V	B
77	356	13	R	H	P
78	7	27	R	V	P
79	342	3	R	H	Y

80	338	0	L	H	Y
81	342	17	R	H	Y
82	354	1	R	V	P
83	326	11	L	H	Y
84	40	11	R	H	B
85	319	20	R	V	Y
86	331	20	L	H	Y
87	5	18	R	H	P
88	19	19	R	V	B
89	329	13	R	H	Y
90	326	6	L	H	Y
91	357	21	L	V	P
92	357	14	L	H	P
93	16	27	L	H	B
94	348	21	R	H	Y
95	48	1	L	H	B
96	332	18	L	H	Y
97	42	19	L	V	B
98	349	24	R	V	P
99	331	17	L	H	Y
100	355	3	R	V	P
101	354	23	R	H	P
102	349	22	R	H	P
103	21	33	L	H	B
104	348	21	R	H	P
105	2	14	L	V	P
106	346	6	R	H	P
107	31	14	R	H	B
108	338	21	L	H	Y
109	334	28	R	V	Y
110	344	20	R	V	P
111	358	27	L	H	P
112	348	7	R	V	P
113	342	14	R	H	Y
114	313	29	L	H	Y
115	345	7	R	H	Y
116	332	3	R	H	Y
117	10	27	R	V	P
118	3	17	L	H	P
119	358	23	R	H	P
120	352	19	L	H	P

121	8	16	L	V	P
122	27	36	R	V	B
123	12	17	L	H	P
124	64	30	L	V	B
125	19	28	R	H	B
126	312	11	L	H	Y
127	30	25	L	H	B
128	332	8	L	H	Y
129	321	26	R	V	Y
130	327	9	L	H	Y
131	332	23	R	H	Y
132	7	5	L	H	P
133	27	9	L	H	B
134	4	15	R	V	P
135	358	26	R	V	P
136	6	32	L	V	P
137	338	6	L	H	Y
138	345	9	L	H	Y
139	334	18	L	H	Y
140	349	23	L	H	Y
141	340	20	R	V	P
142	6	9	R	H	P
143	344	19	R	H	Y
144	353	26	L	V	P
145	344	4	L	H	Y
146	41	23	L	H	B
147	6	24	L	H	P
148	352	29	R	H	P
149	339	16	L	H	Y
150	331	26	R	H	Y
151	32	26	L	H	B
152	5	24	R	V	P
153	343	18	R	H	Y
154	28	30	R	V	B
155	22	4	L	H	B
156	358	14	L	H	P
157	330	35	R	V	Y
158	14	20	R	H	P
159	337	5	L	H	Y
160	17	23	L	V	P
161	340	19	R	H	Y

162	331	37	R	H	Y
163	333	19	R	V	P
164	351	21	L	H	P
165	13	25	L	H	P
166	24	21	R	H	B
167	340	1	R	H	Y
168	27	13	R	H	B
169	349	12	R	V	P
170	20	21	L	V	B
171	348	4	R	H	P
172	356	33	R	V	P
173	350	26	R	V	P
174	2	29	R	V	P
175	34	4	R	H	B
176	355	14	R	H	P
177	351	26	R	V	Y
178	348	3	R	H	Y
179	355	18	R	H	P
180	15	32	R	H	P
181	346	28	R	H	P
182	339	26	L	H	Y
183	331	6	L	H	Y
184	0	21	L	H	P
185	342	1	R	H	Y
186	349	10	R	V	P
187	346	3	R	H	Y
188	343	33	R	V	P
189	22	20	L	V	P
190	347	18	R	H	Y
191	2	32	R	H	P
192	337	31	R	V	Y
193	341	11	L	H	Y
194	40	3	L	H	B
195	357	17	R	H	P
196	3	31	R	V	P
197	346	1	L	H	Y
198	346	14	R	H	Y
199	348	22	R	V	P
200	342	2	R	H	Y

Sample GF19-5					
NO	I-V	N-S	L/R	H/V	COR
1	128	16	L	H	B
2	61	9	R	H	Y
3	93	28	L	H	P
4	118	28	R	H	B
5	80	21	L	H	P
6	146	8	R	H	B
7	61	19	R	H	Y
8	69	21	R	H	Y
9	87	24	L	H	P
10	79	28	R	H	Y
11	115	40	R	V	B
12	97	27	L	V	P
13	132	19	L	H	B
14	142	4	R	H	B
15	61	11	R	H	Y
16	104	5	L	V	P
17	137	15	L	H	B
18	136	7	R	H	B
19	74	20	L	H	Y
20	131	3	R	H	B
21	76	16	R	H	Y
22	79	29	R	V	P
23	116	20	L	H	B
24	97	22	L	H	P
25	108	35	R	V	P
26	141	5	R	H	B
27	69	17	L	H	Y
28	73	23	L	H	Y
29	110	17	L	H	B
30	133	6	R	H	B
31	100	26	R	H	P
32	88	15	R	V	P
33	109	33	R	H	B
34	46	19	L	V	P
35	74	23	R	H	Y
36	95	25	R	V	P
37	128	9	R	H	B
38	137	2	L	H	B
39	90	1	R	V	P

40	98	16	R	V	P
41	153	4	R	H	Y
42	142	0	L	H	Y
43	121	7	R	H	B
44	89	18	R	V	P
45	109	5	R	H	B
46	121	25	L	V	B
47	134	24	R	H	B
48	63	1	R	H	Y
49	93	19	R	H	P
50	104	17	L	H	P
51	57	22	R	H	Y
52	61	17	L	H	Y
53	111	20	L	V	P
54	72	33	R	V	P
55	81	15	L	H	P
56	110	0	L	H	B
57	145	25	R	H	B
58	67	4	L	H	Y
59	131	0	L	H	B
60	96	2	R	H	P
61	52	12	R	H	Y
62	71	10	L	H	Y
63	105	22	L	H	B
64	98	27	R	V	P
65	116	2	L	H	B
66	50	1	R	H	Y
67	93	41	L	H	P
68	120	17	L	H	B
69	124	23	L	H	B
70	47	16	R	H	Y
71	123	14	R	H	B
72	90	37	R	H	P
73	59	11	R	H	Y
74	138	17	L	H	B
75	113	17	R	H	B
76	110	17	R	V	P
77	70	13	R	H	Y
78	120	42	R	V	B
79	113	12	R	H	B
80	54	16	L	H	Y

81	72	30	R	H	Y
82	68	23	L	H	Y
83	119	35	L	V	B
84	94	19	L	V	P
85	84	20	L	V	P
86	137	1	R	H	B
87	97	19	R	H	P
88	135	13	L	H	B
89	57	16	R	H	Y
90	68	9	R	H	Y
91	134	36	R	H	B
92	58	21	R	H	Y
93	147	25	L	H	B
94	86	3	R	H	P
95	64	9	R	H	Y
96	144	1	L	H	B
97	121	28	L	H	B
98	49	28	R	H	Y
99	53	17	R	H	Y
100	106	24	R	H	P

Sample GF05					
NO	I-V	N-S	L/R	H/V	COR
1	20	2	L	H	B
2	29	13	R	H	B
3	8	14	R	H	P
4	343	19	R	H	Y
5	3	40	R	H	P
6	35	12	R	H	B
7	305	20	L	H	Y
8	359	24	R	V	P
9	4	14	L	H	P
10	300	18	R	V	P
11	51	36	R	H	B
12	44	3	R	H	B
13	336	14	R	H	Y
14	297	30	L	H	Y
15	69	26	L	V	P
16	321	21	R	H	Y
17	300	25	L	H	Y
18	32	17	R	H	B
19	24	2	L	H	B
20	10	33	L	H	P
21	47	10	R	H	B
22	294	38	L	H	Y
23	337	13	R	V	P
24	21	15	R	H	B
25	349	2	R	H	P
26	333	17	R	H	Y
27	51	22	L	V	B
28	61	28	L	V	B
29	36	18	L	H	B
30	358	15	L	H	P
31	279	25	R	V	P
32	20	11	L	H	B
33	2	5	R	H	P
34	0	1	R	H	P
35	292	21	R	V	Y
36	80	32	L	V	P
37	39	17	L	H	B
38	314	17	R	H	Y

39	15	17	L	H	P
40	19	9	R	H	B
41	346	29	R	H	Y
42	23	2	L	H	B
43	327	32	R	V	Y
44	33	13	R	H	B
45	298	25	R	V	Y
46	359	20	R	V	P
47	23	17	R	H	B
48	297	24	L	H	Y
49	11	27	R	H	P
50	35	11	L	H	B
51	41	29	R	H	B
52	322	3	R	H	Y
53	12	33	R	H	B
54	333	15	L	H	Y
55	7	3	R	H	P
56	32	24	L	V	B
57	281	23	R	V	P
58	343	21	R	V	P
59	38	0	L	H	B
60	311	18	L	H	Y
61	346	3	R	H	Y
62	34	15	L	H	B
63	8	16	L	H	P
64	10	1	R	H	B
65	33	5	L	H	B
66	304	27	R	H	Y
67	30	24	R	H	B
68	324	1	L	H	Y
69	356	23	R	H	P
70	59	27	R	H	B
71	295	35	R	H	Y
72	281	22	L	H	P
73	15	7	R	H	B
74	328	26	L	H	Y
75	68	20	R	H	B
76	314	31	R	V	Y
77	31	7	R	H	B
78	358	2	L	H	P
79	359	0	L	H	P

80	26	5	L	H	B
81	325	24	R	H	Y
82	12	13	R	H	B
83	3	30	L	H	P
84	24	29	R	H	B
85	292	29	L	H	Y
86	52	22	R	H	B
87	23	28	L	H	B
88	348	19	R	H	P
89	1	18	L	H	P
90	17	17	L	H	B
91	295	26	R	V	P
92	303	19	L	H	Y
93	43	31	L	V	B
94	62	20	R	H	B
95	4	5	L	H	P
96	311	25	L	H	Y
97	15	3	L	H	P
98	336	30	R	V	Y
99	325	7	L	H	Y
100	63	13	R	H	B
101	338	24	L	H	Y
102	20	13	R	H	B
103	331	2	R	H	Y
104	33	26	L	H	B
105	27	18	L	H	B
106	25	12	L	V	P
107	42	6	R	H	B
108	8	26	L	H	P
109	336	5	R	H	Y
110	322	32	R	V	Y
111	44	17	R	H	B
112	42	26	R	H	P
113	302	19	R	V	P
114	304	15	R	H	Y
115	39	23	R	H	B
116	296	26	R	V	Y
117	357	35	L	H	P
118	25	13	L	H	B
119	292	3	R	H	Y
120	27	14	L	H	B

121	317	25	R	V	P
122	40	11	R	H	B
123	5	13	L	H	P
124	31	27	R	H	B
125	22	14	L	H	B
126	339	0	L	H	Y
127	39	18	R	H	B
128	348	14	R	H	P
129	310	14	L	H	Y
130	46	34	L	V	B
131	333	20	R	H	P
132	310	20	L	H	Y
133	40	28	R	H	B
134	304	34	R	V	Y
135	21	7	R	H	B
136	22	1	L	H	B
137	15	3	R	H	B
138	326	24	L	H	Y
139	6	16	L	H	P
140	315	28	L	H	Y
141	3	11	L	H	P
142	314	15	L	H	Y
143	344	25	L	H	Y
144	45	22	R	H	B
145	14	26	L	H	B
146	287	19	R	V	P
147	45	20	R	H	B
148	304	16	L	H	Y
149	29	36	R	H	B
150	13	9	L	H	P
151	14	4	L	H	B
152	33	13	R	H	B
153	312	32	R	V	Y
154	289	21	R	V	P
155	48	22	L	V	B
156	12	29	L	H	P
157	308	23	R	V	Y
158	33	17	L	H	B
159	50	11	R	H	B
160	324	29	R	H	Y
161	313	10	R	H	Y

162	21	24	L	H	B
163	14	13	L	H	B
164	0	10	R	H	P
165	30	9	R	H	B
166	41	11	R	H	B
167	20	12	L	H	B
168	337	28	L	H	Y
169	36	23	R	H	B
170	356	16	L	H	P
171	342	20	L	H	Y
172	41	7	L	H	B
173	289	21	L	H	P
174	71	7	R	H	B
175	33	6	R	H	B
176	15	20	R	H	P
177	355	23	L	H	P
178	329	26	L	H	Y
179	304	22	L	H	Y
180	280	25	L	H	P
181	23	16	L	H	B
182	345	29	L	H	P
183	317	18	L	H	Y
184	323	19	R	H	Y
185	8	3	L	H	P
186	15	15	L	H	B
187	306	23	L	H	Y
188	36	14	L	H	B
189	325	17	R	H	Y
190	46	17	L	H	B
191	349	1	R	H	P
192	342	14	L	H	Y
193	48	11	R	H	B
194	333	34	R	V	Y
195	52	29	R	H	B
196	47	17	R	H	B
197	341	24	L	H	Y
198	34	16	R	H	B
199	27	8	L	H	B
200	330	17	R	V	P

Sample XC03					
No	I-V	S-N	L/R	H/V	COR
1	33	42	R	V	B
2	13	25	L	H	B
3	320	3	R	H	Y
4	14	34	L	H	B
5	12	17	L	H	B
6	358	8	L	V	P
7	350	10	L	H	P
8	30	20	R	V	B
9	14	34	L	H	B
10	0	0	R	V	P
11	25	34	L	H	B
12	27	22	L	H	B
13	292	11	L	V	P
14	8	1	L	H	P
15	29	7	L	H	Y
16	45	19	R	V	B
17	355	10	L	H	P
18	26	8	L	H	B
19	30	13	L	H	B
20	344	24	L	V	P
21	23	24	L	H	B
22	340	24	L	V	P
23	23	36	R	H	B
24	11	3	L	H	Y
25	20	27	L	H	B
26	27	24	R	H	B
27	8	10	R	H	Y
28	23	14	R	H	B
29	11	6	L	H	Y
30	31	31	R	V	B
31	32	42	R	V	B
32	343	21	L	V	P
33	20	38	L	H	Y
34	27	33	R	V	B
35	357	32	L	V	P
36	11	13	R	H	Y
37	23	3	R	H	B
38	9	0	L	H	P
39	30	31	R	V	B

40	25	30	L	H	B
41	2	7	L	H	P
42	23	40	R	V	B
43	8	34	L	H	P
44	9	33	R	H	Y
45	25	20	L	H	B
46	346	20	L	V	Y
47	338	17	L	V	P
48	20	8	R	H	B
49	13	18	R	H	Y
50	28	31	R	V	B
51	2	20	L	V	P
52	349	15	L	V	P
53	26	28	R	V	P
54	31	32	R	V	B
55	26	31	L	H	B
56	357	12	L	V	P
57	17	26	L	H	B
58	30	15	L	H	B
59	21	27	L	H	B
60	18	4	L	H	B
61	354	37	R	H	P
62	14	9	L	H	B
63	20	35	R	V	P
64	29	20	R	V	B
65	24	21	L	H	B
66	12	21	L	H	Y
67	3	5	L	V	P
68	18	13	L	H	B
69	24	24	L	H	B
70	24	42	R	V	B
71	35	38	R	V	B
72	25	22	R	H	B
73	10	12	R	H	B
74	21	28	R	H	B
75	32	16	R	H	B
76	21	23	R	H	B
77	341	11	L	V	P
78	27	34	R	H	B
79	22	25	R	H	B
80	329	10	R	V	P

81	27	26	L	H	B
82	343	23	L	V	P
83	326	24	L	V	P
84	20	25	L	H	B
85	32	16	L	H	B
86	20	17	L	H	B
87	22	20	L	H	B
88	26	31	R	V	B
89	331	20	R	H	Y
90	30	18	L	H	B
91	30	24	L	H	B
92	335	18	R	H	Y
93	21	43	R	H	B
94	357	24	L	H	P
95	28	12	L	H	B
96	14	22	R	H	B
97	9	29	L	H	P
98	348	20	L	H	P
99	22	21	R	H	B
100	19	27	R	H	B

Appendix C: Raw data of titanium concentration

	Calibrated by ICPMSDataCal 10.8<<<<<<<<IndividualUser>>>>>>>>IndividualUser(11)			Uncertainty	Limit
	Contents (AYCF)		Ti	Ti	Ti
			47	47	47
			ppm	ppm	ppm
std	20210325A01	SRM 610	511.5092296	6.375373957	0.041315323
std	20210325A02	SRM 610	515.3435204	5.973859155	0.030089044
Rep	20210325A03	SRM 612	44.17611955	0.554363766	0.041419628
Rep	20210325A04	QZ	58.72008281	1.49769528	0.107124016
Rep	20210325A05	QZ-2	16.93928463	0.364540245	0.045691684
Rep	20210325A06	S14(W)	6.834104439	0.455578084	0.063296998
Rep	20210325A07	S14(W)	11.19433589	0.590332264	0.102221905
Rep	20210325A08	S14(W)	10.9323689	0.432399364	0.069528727
Rep	20210325A13	S14(W)	6.949601433	0.236782625	0.035567319
Rep	20210325A14	S14(W)	9.69580953	0.464214512	0.060173318
Rep	20210325A15	S14(W)	8.625974411	0.334508452	0.052174747
Rep	20210325A16	S14(W)	7.027756571	0.241584372	0.049287328
Rep	20210325A17	S14(W)	9.069058939	0.589591804	0.059233925
Rep	20210325A18	S14(r)	1.978798566	0.120360859	0.067652193
Rep	20210325A19	S14(W)	7.708099073	0.226050067	0.037841221
Rep	20210325A20	S14(W)	7.540646749	0.426881795	0.036157899
Rep	20210325A27	S14(r)	6.099756805	1.844393607	0.045042991

Rep	20210325A29	S14(r)	5.430886836	0.264020934	0.044070826
Rep	20210325A30	S14(r)	7.974196744	0.254143248	0.633846322
Rep	20210325A31	GF4	9.737190371	0.406078971	0.060460456
Rep	20210325A32	GF4	25.02860294	1.218050278	0.046008359
Rep	20210325A33	GF4	1.928730272	0.321887078	0.036457062
Rep	20210325A35	S13	4.56045716	0.40603417	0.046815978
Rep	20210325A37	S13	2.6815988	0.10355912	0.060912604
Rep	20210325A38	S13	2.50905839	0.084895085	0.037883135
Rep	20210325A39	S13	2.251942051	0.097218809	0.054867167
Rep	20210325A40	S13	5.686813082	0.411641463	0.057537992
std	20210325A41	SRM 610	514.1430939	4.95367036	0.020119678
std	20210325A42	SRM 610	512.6973742	4.692991267	0.032403341
Rep	20210325A43	SRM 612	43.56341725	0.49430317	0.028191307
Rep	20210325A44	QZ	58.72763922	1.376886381	0.072968753
Rep	20210325A45	QZ-2	16.16128587	0.407929606	0.032742558
Rep	20210325A46	S13	11.81873181	0.472607288	0.076303907
Rep	20210325A47	S13	1.402756525	0.109378279	0.075214173
Rep	20210325A48	S13	12.257115	2.102025978	0.039009789
Rep	20210325A49	S13	20.15196267	1.104247798	0.048176766
Rep	20210325A50	S13	1.59212383	0.095128659	0.050034451
Rep	20210325A51	S13	8.12173703	0.323077061	0.034559966
Rep	20210325A52	S13	13.43815782	1.05079885	0.055781949
Rep	20210325A53	S13	2.136520977	0.093772313	0.064203151
Rep	20210325A54	S13	1.538849638	0.102419186	0.072321514

Rep	20210325A55	S13	1.576061431	0.056187662	0.029985396
Rep	20210325A56	S13	2.1901952	0.133003168	0.066268414
Rep	20210325A57	S13	1.225155203	0.0568362	0.045592418
Rep	20210325A58	S13	1.350246279	0.062989424	0.055899787
Rep	20210325A59	S13	1.688461969	0.071405701	0.06283405
Rep	20210325A60	S13	1.902168967	0.0699493	0.058208779
std	20210325A61	SRM 610	513.6590326	5.389723666	0.020929853
std	20210325A62	SRM 610	513.1796239	5.699856747	0.024861751
Rep	20210325A63	SRM 612	44.53316118	0.495080291	0.029000151
Rep	20210325A64	QZ-2	16.10458018	0.376775516	0.050014001
Rep	20210325A65	QZ	59.04242958	2.328121015	0.110422832
Rep	20210325A66	S08	0.716392534	0.036341048	0.051886773
Rep	20210325A67	S08	0.754208152	0.044075721	0.05454806
Rep	20210325A68	S08	0.802211501	0.049780075	0.064720255
Rep	20210325A69	S08	0.807858722	0.044507835	0.052788873
Rep	20210325A70	S08	1.265425875	0.055793308	0.047966349
Rep	20210325A71	S08	1.556526351	0.105373987	0.047437064
Rep	20210325A72	S08	1.000347897	0.043569426	0.041983407
Rep	20210325A73	S08	0.991012185	0.066393935	0.068863766
Rep	20210325A74	S08	0.723907977	0.044177409	0.084162576
Rep	20210325A75	S08	0.78990388	0.050550463	0.050321896
Rep	20210325A76	S08	1.10548426	0.204099521	0.052140004
Rep	20210325A77	S08	1.200901557	0.083345604	0.044853146
Rep	20210325A78	S08	20.26879192	1.090906868	0.050214425

Rep	20210325A79	S08	17.63375018	0.546938626	0.058991934
Rep	20210325A80	S08	1.077760619	0.060035953	0.073548194
Rep	20210325A86	S08	1.13001651	0.070350122	0.075443754
Rep	20210325A87	S08	1.014537803	0.055734699	0.05953866
Rep	20210325A88	S08	1.300456017	0.070059428	0.082364793
Rep	20210325A89	S08	0.755982185	0.050820069	0.067991318
Rep	20210325A90	S08	1.863133334	0.101308442	0.048772102
Rep	20210325A91	S08	0.976079431	0.055486584	0.059048618
Rep	20210325A92	GF4	2.672621601	0.178976418	0.039109759
Rep	20210325A93	GF4	11.35225832	0.578030268	0.04177476
Rep	20210325A94	GF4	0.723976842	0.043429251	0.032966798
Rep	20210325A95	GF4	#DIV/0!	#DIV/0!	#DIV/0!
Rep	20210325A96	GF4	1.001132939	0.051974179	0.045864753
Rep	20210325A97	GF4	0.954825461	0.056748586	0.054902851
Rep	20210325A98	GF4	1.054523214	0.044091135	0.046103182
Rep	20210325A99	GF4	1.034415997	0.048383624	0.045172723
Rep	20210325A100	GF4	0.935817953	0.054011311	0.04138765
Rep	20210325A101	QZ-2	16.88799729	0.368985376	0.038697012
Rep	20210325A102	QZ	56.43917513	1.256582927	0.03858178
Rep	20210325A103	SRM 612	43.57109163	0.558916492	0.022160485
std	20210325A104	SRM 610	509.2549662	4.358521825	0.025265245
std	20210325A105	SRM 610	517.6521313	4.817215175	0.018370062
std	20210326A01	SRM 610	496.2539699	5.334165906	0.023282567
std	20210326A02	SRM 610	493.3876053	5.700158729	0.029924965

Rep	20210326A03	SRM 612	43.29039676	0.44044204	3.387216377
Rep	20210326A04	QZ	59.01650857	0.931420772	0.050292548
Rep	20210326A05	QZ-2	18.22006527	0.567731579	0.060069029
Rep	20210326A07	S09	2.550745909	0.124441442	0.057781953
Rep	20210326A08	S09	6.607549715	0.425556928	0.04104006
Rep	20210326A09	S09	4.130832477	0.268725689	0.07407198
Rep	20210326A10	S09	53.15818357	2.058320882	0.047649378
Rep	20210326A11	S09	1.71423792	0.059594768	0.045200066
Rep	20210326A14	S09	1.161790571	0.059062262	0.042613908
Rep	20210326A15	S09	1.253837119	0.060948521	0.062307768
Rep	20210326A16	S09	1.569402922	0.104507065	0.059508395
Rep	20210326A17	S09	1.290828298	0.080020306	0.04930682
Rep	20210326A18	S09	2.695875216	0.166857564	0.043621143
Rep	20210326A19	S09	1.150401099	0.057497257	0.037213643
Rep	20210326A20	S09	1.246608581	0.088301132	0.048337691
std	20210326A22	SRM 610	501.1311601	4.254546309	0.018060249
Rep	20210326A23	SRM 612	42.54781156	0.492680657	0.040437456
Rep	20210326A24	QZ	56.85320365	1.079246883	0.035839357
Rep	20210326A25	QZ-2	17.48280578	0.879125189	0.081075625
Rep	20210326A26	S09	1.238362455	0.060849856	0.048115224
Rep	20210326A27	S09	1.25578314	0.072082009	0.025998805
Rep	20210326A30	S09	1.706601857	0.116849006	0.087201419
Rep	20210326A32	GF19-5	4.811352111	0.174449436	0.037379995
Rep	20210326A33	GF19-5	0.571866217	0.040565346	0.042514864

Rep	20210326A34	GF19-5	0.922573989	0.049666039	0.029149642
Rep	20210326A35	GF19-5	0.745947808	0.033015407	0.033984449
Rep	20210326A36	GF19-5	0.808806949	0.051950965	0.034728614
Rep	20210326A37	GF19-5	0.85892615	0.032425127	0.037600055
Rep	20210326A38	GF19-5	0.925878052	0.049525107	0.046298922
Rep	20210326A39	GF19-5	0.941041844	0.04723447	0.029936845
Rep	20210326A40	GF19-5	1.232618778	0.063883339	0.032710819
Rep	20210326A41	GF19-5	6.586419651	0.342939482	0.036053602
Rep	20210326A42	GF19-5	1.498148048	0.104784119	0.03265928
Rep	20210326A43	GF19-5	1.125769677	0.048981289	0.029516381
Rep	20210326A44	QZ	48.08676645	0.539022752	0.030098034
Rep	20210326A45	QZ-2	16.36399304	0.55653604	0.085969873
std	20210326A46	SRM 610	496.5240291	4.686979591	0.025338037
std	20210326A47	SRM 610	493.117409	5.181108457	0.028292016
Rep	20210326A48	SRM 612	42.50571367	0.463396527	0.030123368
Rep	20210326A49	GF19-5	0.790073451	0.052920928	0.058414272
Rep	20210326A50	GF19-5	0.817662788	0.042140696	0.031358374
Rep	20210326A51	GF19-5	0.796073164	0.036993514	0.03982138
Rep	20210326A52	GF19-5	0.719851908	0.05415782	0.033476946
Rep	20210326A53	GF19-5	0.667852766	0.035735103	0.025253463
Rep	20210326A54	GF19-5	0.986825116	0.048661161	0.031994492
Rep	20210326A55	GF19-5	0.736864147	0.038012782	0.030396103
Rep	20210326A56	GF19-5	1.125893464	0.051414494	0.030987191
Rep	20210326A57	GF19-5	1.183904711	0.054115596	0.024325754

Rep	20210326A58	GF19-5	0.731997898	0.042611718	0.034683903
Rep	20210326A59	GF19-5	0.94589833	0.066441889	0.0421924
Rep	20210326A60	GF19-5	0.888950253	0.050556963	0.031048577
std	20210326A61	SRM 610	494.3093661	4.509769043	0.024401605
std	20210326A62	SRM 610	495.3332167	4.096685093	0.030847155
Rep	20210326A63	SRM 612	45.17733881	0.768254271	0.03784091
Rep	20210326A64	QZ	56.49488356	1.216257579	0.03771785
Rep	20210326A66	S15	3.375338668	0.142338484	0.023254778
Rep	20210326A67	S15	4.907571687	0.165056664	0.028714346
Rep	20210326A68	S15	5.960583638	0.243349585	0.045787041
Rep	20210326A69	S15	24.32082549	0.998415045	0.035320998
Rep	20210326A70	S15	8.965057713	0.348894265	0.027178274
Rep	20210326A71	S15	19.27082602	0.628901143	0.040157084
Rep	20210326A72	S15	10.35209192	0.413260008	0.031740483
Rep	20210326A73	S15	2.448914929	0.132454907	0.0335652
Rep	20210326A74	S15	8.07931909	0.334459648	0.032974067
Rep	20210326A75	S15	6.279108218	0.145457774	0.041531488
Rep	20210326A76	S15	12.99167605	0.796110453	0.033567554
Rep	20210326A77	S15	16.15873002	1.216999631	0.030270383
Rep	20210326A78	S15	15.69488176	0.786567757	0.028639421
Rep	20210326A79	S15	11.82254114	0.287630126	0.033656728
Rep	20210326A80	S15	16.89042353	0.417851475	0.030833467
std	20210326A81	SRM 610	495.8649467	5.90518632	0.0237671
std	20210326A82	SRM 610	493.7748037	5.772900426	0.026185918

Rep	20210326A83	SRM 612	44.64151714	0.571863865	0.026861086
Rep	20210326A84	QZ	54.7071137	0.979842794	0.034745407
Rep	20210326A85	QZ-2	16.99674253	0.525214122	0.055460208
Rep	20210326A86	S15	3.361432976	0.167474894	0.035795639
Rep	20210326A87	S15	7.09634474	0.266566374	0.034962335
Rep	20210326A88	S15	4.792595222	0.160166834	0.033471672
Rep	20210326A89	S15	7.50292722	0.24575421	0.052630956
Rep	20210326A90	S15	20.17036892	0.93115626	0.029735243
Rep	20210326A91	S15	14.05381397	0.724222943	0.045245681
Rep	20210326A92	S15	14.36752207	0.88047175	0.033042992
Rep	20210326A93	S14(W)	7.045924532	0.181144291	0.039979728
Rep	20210326A94	S14(W)	6.499808566	0.196257062	0.03712158
Rep	20210326A95	S14(W)	6.938033691	0.185736944	0.031515058
Rep	20210326A96	S14(W)	10.06735768	0.453238092	0.034618276
Rep	20210326A97	S14(W)	6.431540432	0.273000383	0.03991247
Rep	20210326A98	S14(W)	9.599220643	0.40509397	0.040074947
Rep	20210326A99	S14(r)	1.633375686	0.093733862	0.049504213
Rep	20210326_100	S14(r)	2.311865687	0.140371233	0.037424865
Rep	20210326_101	QZ-2	16.7292681	0.633469148	0.094581952
Rep	20210326_102	QZ	57.21099221	1.073914472	0.044654398
Rep	20210326_103	SRM 612	44.24997768	0.651658955	0.023298561
std	20210326_104	SRM 610	494.6949863	5.348409102	0.015358954
std	20210326_105	SRM 610	495.9582466	4.735876729	0.030425943
std	20210326B01	SRM 610	493.2096102	4.619882977	0.032562071

std	20210326B02	SRM 610	493.5762572	4.924639556	0.029173236
Rep	20210326B03	SRM 612	44.00846444	0.763607369	0.034936549
Rep	20210326B04	QZ	56.30472495	1.487420559	0.066077045
Rep	20210326B05	QZ-2	16.45965176	0.766827681	0.058256614
Rep	20210326B09	S14(r)	3.988919164	0.470243489	0.059497225
Rep	20210326B10	S14(r)	2.295619216	0.089666658	0.044292011
Rep	20210326B11	S14(r)	2.937390464	0.207872426	0.07345702
Rep	20210326B12	S14(r)	4.766488044	0.541607846	0.04105635
Rep	20210326B13	S14(r)	1.67488295	0.091430359	0.051297331
Rep	20210326B15	QZ-2	15.28901357	0.458757536	0.061801549
Rep	20210326B16	QZ	55.77101068	1.095989899	0.039840633
Rep	20210326B17	SRM 612	44.19910795	0.629760905	0.020480019
std	20210326B18	SRM 610	494.7023493	5.218745606	0.020919488
std	20210326B19	SRM 610	494.9400475	4.664897845	0.02609451

Appendix D: Raw data of dynamically recrystallized grainsize measurement

Grainsize of GF02				
Length	Width	Grain size	Actual Grain Size (micron)	Diameter (µm)
37.47	5.16	13.90486	37.35857727	74.71715453
29.42	6.24	13.5492	36.40300709	72.80601418
33.75	9.01	17.4381	46.85143694	93.70287388
21.56	10.69	15.18145	40.78841807	81.57683614
36.99	3.96	12.10291	32.51721854	65.03443708
38.07	12.01	21.38272	57.44954234	114.8990847
49.24	8.41	20.34965	54.67397517	109.3479503
32.67	8.89	17.04219	45.78772638	91.57545277
22.82	7.57	13.14334	35.31257528	70.62515056
26.18	4.92	11.34926	30.49235756	60.98471511
27.5	5.88	12.71613	34.164781	68.32956199
62.21	17.65	33.13618	89.02789127	178.0557825
42.51	16.21	26.25047	70.52785752	141.055715
34.59	7.81	16.43618	44.15952865	88.3190573
30.86	19.22	24.35424	65.43321865	130.8664373
37.83	6.49	15.66897	42.09826041	84.19652082
30.74	10.21	17.71596	47.59797032	95.19594063
40.2	11.53	21.52919	57.84306687	115.6861337
17.65	6.73	10.89883	29.28218757	58.56437513
33.87	9.49	17.92837	48.16863459	96.33726917
55.72	12.13	25.99776	69.84890232	139.6978046
40.59	11.77	21.85736	58.72477862	117.4495572
47.32	13.33	25.11525	67.47782473	134.9556495
50.32	7.53	19.4656	52.29876525	104.5975305
40.19	7.21	17.02263	45.73516673	91.47033346
53.32	8.05	20.71777	55.66300417	111.3260083
20.54	6.97	11.96511	32.14698443	64.29396886
54.4	17.41	30.77505	82.68418816	165.3683763
56.44	15.97	30.02244	80.66211251	161.324225
28.34	8.29	15.32771	41.18137275	82.36274551
20.54	5.76	10.87706	29.22369271	58.44738542
29.66	8.41	15.79369	42.43333856	84.86667712
22.45	5.76	11.37154	30.5522392	61.1044784
28.46	10.21	17.04631	45.7987843	91.59756861
48.4	8.89	20.7431	55.73104577	111.4620915
23.78	10.93	16.12189	43.31513151	86.63026302
29.9	8.91	16.32204	43.85287564	87.70575128

19.22	11.29	14.73071	39.57740306	79.15480612
25.7	8.17	14.49031	38.93150754	77.86301507
15.02	5.16	8.80359	23.65284841	47.30569681
31.7	11.05	18.7159	50.28453071	100.5690614
40.95	5.38	14.84288	39.87876701	79.75753401
33.99	5.76	13.99223	37.59330041	75.18660082
31.83	5.76	13.54034	36.379204	72.75840801
22.94	7.69	13.28189	35.68481979	71.36963958
28.1	5.76	12.72226	34.18125725	68.36251451
21.26	6.12	11.40663	30.64650632	61.29301263
22.22	13.93	17.59331	47.26843425	94.53686851
missing		4.2	11.28425578	22.56851155
		5.28	14.18592155	28.3718431
12.73	4.68	7.718575	20.73770822	41.47541643
5.76	1.92	3.325538	8.934813408	17.86962682
11.17	2.76	5.552405	14.91779926	29.83559852
3.48	2.04	2.664432	7.158603969	14.31720794
8.41	3.12	5.122421	13.76255052	27.52510103
12.37	5.04	7.895872	21.21405787	42.42811574
4.56	4.56	4.56	12.2514777	24.5029554
7.33	2.88	4.594606	12.34445334	24.68890668
9.13	2.76	5.019841	13.48694421	26.97388842
10.45	4.44	6.811608	18.30093428	36.60186856
15.85	4.92	8.830742	23.72579731	47.45159462
4.2	3	3.549648	9.536936781	19.07387356
2.4	2.4	2.4	6.448146158	12.89629232
19.58	7.33	11.98004	32.18710837	64.37421674
12.49	5.16	8.027976	21.56898464	43.13796928
13.21	3.24	6.542201	17.57711302	35.15422603
12.37	5.52	8.263317	22.20128029	44.40256059
8.77	3.24	5.330553	14.32174487	28.64348975
3.24	3.24	3.24	8.704997313	17.40999463
3.36	3.36	3.36	9.027404621	18.05480924
7.33	3.84	5.305393	14.25414692	28.50829383
18.73	5.64	10.278	27.61417494	55.22834989
7.93	3.24	5.068846	13.61860834	27.23721667
25.94	5.93	12.40259	33.32237625	66.6447525
17.17	4.2	8.491996	22.81568036	45.63136073
13.69	4.32	7.690306	20.66175601	41.32351201
12.13	6.85	9.115399	24.49059392	48.98118785
3.96	3.96	3.96	10.63944116	21.27888232
3.36	3.36	3.36	9.027404621	18.05480924

6.61	2.4	3.982964	10.70113842	21.40227684
4.44	4.44	4.44	11.92907039	23.85814078
7.93	2.88	4.778954	12.83974707	25.67949415
19.44	5.28	10.1313	27.22003772	54.44007545
20.66	8.41	13.18145	35.41496262	70.82992523
29.3	8.77	16.03	43.06825126	86.13650252
25.7	8.77	15.01296	40.33573634	80.67147269
7.18	3.12	4.733033	12.71636984	25.43273968
21.38	8.17	13.21645	35.50900556	71.01801112
4.44	2.52	3.344966	8.987013346	17.97402669
10.3	5.77	7.70915	20.71238691	41.42477382
10.21	5.88	7.748213	20.81733664	41.63467328
4.56	4.56	4.56	12.2514777	24.5029554
6.37	3.84	4.945786	13.28797981	26.57595962
17.53	9.49	12.89805	34.65354713	69.30709425
6.76	2.6	4.192374	11.26376687	22.52753374
8.17	5.16	6.492858	17.44453953	34.88907907
16.09	3.84	7.860382	21.11870411	42.23740822
5.28	6.49	5.853819	15.72761759	31.45523518
14.17	3.04	6.563292	17.63377715	35.26755431
11.05	4.92	7.37333	19.81012982	39.62025964
10.57	3.72	6.270598	16.84738866	33.69477731
12.01	3.73	6.693079	17.98247854	35.96495709
17.53	3.96	8.331795	22.38526202	44.77052404
3.12	2.28	2.667133	7.165860539	14.33172108
9.37	2.52	4.859259	13.05550565	26.1110113
17.05	5.88	10.01269	26.90137546	53.80275092
8.05	4.56	6.058713	16.27811052	32.55622103
18.94	5.76	10.44483	28.0624032	56.1248064
12.85	4.2	7.346428	19.73784982	39.47569964
7.81	3.5	5.228288	14.04698667	28.09397334
6	4.8	5.366563	14.41849314	28.83698628
3.24	3.24	3.24	8.704997313	17.40999463
10.81	5.64	7.808226	20.97857719	41.95715439
9.61	2.99	5.360401	14.40193741	28.80387482
14.77	4.2	7.876167	21.16111386	42.32222773
16.45	3	7.024956	18.87414163	37.74828327
12.49	2.28	5.336403	14.3374618	28.67492361
26.66	5.53	12.14207	32.62242711	65.24485421
15.37	4.8	8.589296	23.07709743	46.15419486
13.81	2.28	5.61131	15.07606128	30.15212255
7.09	3.6	5.052128	13.57369227	27.14738455

10.81	2.52	5.21931	14.02286486	28.04572971
26.42	5.52	12.07636	32.44588143	64.89176285
21.98	5.28	10.77285	28.94372589	57.88745177
19.7	5.16	10.08226	27.0882903	54.17658061
15.73	4.08	8.011142	21.52375669	43.04751338
11.65	3.72	6.58316	17.68715834	35.37431669
4.92	1.8	2.975903	7.995441226	15.99088245
11.65	3.72	6.58316	17.68715834	35.37431669
27.86	4.68	11.41862	30.67871139	61.35742278
6.73	3	4.493328	12.07234924	24.14469848
10.09	3.84	6.224596	16.72379466	33.44758932
3.48	3.48	3.48	9.349811929	18.69962386
35.43	4.44	12.5423	33.69773359	67.39546717
11.11	4.2	6.830959	18.35292568	36.70585135
8.89	4.56	6.366977	17.10633344	34.21266687
13.21	3.12	6.419907	17.24853987	34.49707975
15.01	5.52	9.102483	24.45589247	48.91178494
3.48	3.48	3.48	9.349811929	18.69962386
3.78	3.78	3.78	10.1558302	20.3116604
5.4	3.24	4.182822	11.23810321	22.47620642
16.57	2.4	6.306187	16.94300762	33.88601525
12.13	4.2	7.137647	19.17691207	38.35382413
5.04	3.12	3.965451	10.65408596	21.30817192
15.85	4.44	8.388921	22.53874601	45.07749202
6.12	4.8	5.419963	14.56196427	29.12392853
14.59	5.52	8.97423	24.11131051	48.22262102
15.13	6.97	10.26918	27.5904945	55.18098899
9.01	4.92	6.658018	17.88827975	35.7765595
11.83	4.32	7.148818	19.20692661	38.41385322
12.49	4.92	7.839056	21.06140802	42.12281604
10.33	3.6	6.098196	16.38419252	32.76838503
5.04	2.64	3.647684	9.800333683	19.60066737
9.25	3.96	6.052272	16.26080683	32.52161365
19.82	4.32	9.253237	24.86092765	49.7218553
13.45	4.08	7.407834	19.90283098	39.80566196
11.65	6.61	8.775335	23.57693378	47.15386755
4.02	4.02	4.02	10.80064481	21.60128963
8.29	4.44	6.066927	16.3001793	32.60035859
7.93	5.22	6.433864	17.28603852	34.57207703
9.85	4.56	6.70194	18.00628699	36.01257398
12.84	3.96	7.130666	19.15815736	38.31631471
15.01	4.44	8.163602	21.93337492	43.86674984

13.09	5.16	8.21854	22.08097801	44.16195603
14.41	5.28	8.72266	23.43541146	46.87082292
11.77	5.88	8.319111	22.35118358	44.70236716
11.77	4.88	7.57876	20.36206285	40.7241257
18.13	10.57	13.8432	37.19289867	74.38579734
9.61	4.68	6.706325	18.01806924	36.03613849
7.09	4.08	5.378401	14.4502989	28.90059779
9.37	6.97	8.081392	21.71249921	43.42499842

Grainsize of GF03				
Length	Width	Grain Size	Actual grain size (micron)	Diameter (μm)
8.11	4.59	6.101221	32.35005933	64.70011866
7.57	4.82	6.04048	32.02799636	64.05599272
10.36	4.05	6.4775	34.34517242	68.69034483
7.97	2.79	4.715538	25.00285337	50.00570674
7.16	5.31	6.166004	32.6935502	65.3871004
6.58	2.66	4.183635	22.18258104	44.36516207
12.61	3.96	7.066513	37.46825332	74.93650665
17.92	5.09	9.550539	50.63912647	101.2782529
19.19	5.09	9.883173	52.40282379	104.8056476
42.09	4.5	13.76245	72.97162731	145.9432546
18.43	5.16	9.751861	51.70658198	103.413164
20.12	6.06	11.04207	58.54753459	117.0950692
24.44	6.12	12.23	64.84621374	129.6924275
18.73	6.97	11.42576	60.58199759	121.1639952
11.53	6.24	8.48217	44.97438777	89.94877554
52.15	15.94	28.83177	25.82103768	51.64207535
60.26	18.37	33.27125	29.79692984	59.59385967
57.01	15.94	30.1453	26.99740711	53.99481421
48.37	28.37	37.04399	33.17569946	66.35139892
88.36	26.48	48.3712	43.32007706	86.64015411
49.18	17.29	29.16028	26.11524685	52.2304937
62.96	27.56	41.65546	37.30562693	74.61125385
75.12	26.21	44.37223	39.73870192	79.47740384
97.82	30.8	54.88949	49.15770103	98.31540207
147.36	39.99	76.7654	68.74923738	137.4984748
92.59	37.83	59.18344	53.00326088	106.0065218
104.12	43.59	67.36906	60.33410722	120.6682144
98.72	22.7	47.33861	42.39531617	84.79063234
107.27	19.73	46.00475	41.20074408	82.40148816
89.35	23.06	45.39175	40.89346879	81.78693757
70.98	36.03	50.57084	45.55931123	91.11862247
93.31	18.73	41.80546	37.66257457	75.32514915
98.36	23.78	48.36322	43.57046615	87.1409323
182.66	37.47	82.7301	74.53162573	149.0632515
56.92	27.02	39.21707	35.22913018	70.45826035
73.5	34.23	50.1588	45.05820862	90.11641723
118.17	22.7	51.79246	46.52574635	93.05149271
6.49	4.59	5.457939	28.93923209	57.87846417
3.15	2.7	2.916333	15.46306105	30.9261221

4.64	3.24	3.877319	20.55842344	41.11684688
2.7	1.58	2.06543	10.95137719	21.90275437
1.85	1.76	1.804439	9.567544915	19.13508983
2.43	1.89	2.143059	11.36298283	22.72596566
2.07	2.12	2.094851	11.1073745	22.21474899
4.59	2.12	3.119423	16.53988878	33.07977756
4.23	2.21	3.057499	16.21155344	32.42310687
2.97	2.52	2.735763	14.50563705	29.0112741
6.3	4.1	5.082322	26.94762621	53.89525243
2.48	1.58	1.979495	10.4957311	20.9914622
5.13	3.11	3.994283	21.17859711	42.35719422
6.62	4.5	5.458022	28.93966924	57.87933849
4.64	3.56	4.064283	21.54975321	43.09950641
2.48	1.85	2.141962	11.35716711	22.71433423
3.51	3.04	3.266558	17.32003087	34.64006173
4.82	3.15	3.896537	20.66032303	41.32064607
3.96	2.75	3.3	17.49734889	34.99469777
2.66	1.85	2.218333	11.76210343	23.52420686
4.32	2.61	3.357856	17.80411696	35.60823392
1.62	1.49	1.553641	8.237756549	16.4755131
5	1.65	2.872281	15.2294874	30.4589748
12.43	7.07	9.374439	49.70540111	99.41080223
4.5	2.34	3.244996	17.20570598	34.41141196
4.5	3.66	4.058325	21.51815895	43.0363179
3.06	1.74	2.307466	12.23470913	24.46941827
3.96	1.02	2.009776	10.65628901	21.31257802
6.18	4.08	5.021394	26.62457173	53.24914346
5.16	3	3.934463	20.8614163	41.7228326
2.94	2.52	2.721911	14.43219031	28.86438063
4.74	5.52	5.115154	27.12170709	54.24341417
3.42	4.56	3.949076	20.9388963	41.87779259
2.76	1.92	2.301999	12.2057218	24.4114436
39.61	20.18	28.27242	25.32009779	50.64019558
40.34	21.26	29.28529	26.22720154	52.45440308
10.27	8.38	9.276993	8.308250983	16.61650197
34.86	26.21	30.22715	27.07070576	54.14141151
19.46	10.81	14.50388	12.98932674	25.97865348
26.75	19.73	22.97341	20.57443	41.14886001
22.97	25.4	24.15446	21.63215232	43.26430465
13.24	13.36	13.29986	11.91103767	23.82207534
24.59	20	22.17656	19.86079546	39.72159091
29.45	20	24.26932	21.73501899	43.47003797

17.56	10	13.25142	11.86764734	23.73529468
29.99	18.64	23.64347	21.17451947	42.34903894
27.29	11.89	18.01328	16.13225476	32.26450951
13.24	13.24	13.24	11.85742432	23.71484865
21.98	27.02	24.37006	21.8252332	43.65046641
34.59	18.73	25.4533	22.79536477	45.59072954
33.51	8.65	17.02532	15.24746497	30.49492993
36.39	17.29	25.08352	22.4641971	44.9283942
24.86	30.62	27.59009	24.70902062	49.41804124
12.25	12.25	12.25	10.97080423	21.94160845
24.14	8.65	14.45029	12.94133451	25.88266902
44.68	23.42	32.34819	28.97026075	57.94052149
45.76	19.82	30.11583	26.97100996	53.94201993
24.5	9.73	15.43972	13.82744179	27.65488358
50.44	12.97	25.57747	22.90656157	45.81312313
72.42	18.01	36.11488	32.34361011	64.68722023
11.35	8.65	9.908456	8.873773943	17.74754789
9.19	7.84	8.488204	7.60183018	15.20366036
9.19	7.57	8.340761	7.469784485	14.93956897
9.19	5.4	7.044572	6.308948933	12.61789787
14.32	13.24	13.76942	12.33155596	24.66311192
29.54	21.26	25.06034	22.57687855	45.15375711
21.28	12.61	16.38111	14.75775772	29.51551545
32.43	15.85	22.67191	20.42514408	40.85028817
29.54	10.09	17.26437	15.55348984	31.10697968
17.65	8.65	12.35607	11.13159584	22.26319168
27.02	10.45	16.80354	15.13832549	30.27665098
14.77	13.69	14.21975	12.8105859	25.6211718
18.01	11.17	14.1835	12.77792881	25.55585762
28.1	17.65	22.27027	20.06330781	40.12661561
12.61	8.28	10.21816	9.205549824	18.41109965
47.56	10.81	22.67429	20.42729173	40.85458345
18.73	14.41	16.42861	14.80055156	29.60110313
35.67	11.17	19.96081	17.9827109	35.96542181
12.97	10.45	11.64201	10.48830129	20.97660258
21.98	14.05	17.57325	15.83175379	31.66350759
15.85	16.21	16.02899	14.44053096	28.88106192
11.71	17.65	14.37642	12.95173123	25.90346247
36.75	20.54	27.47444	24.75175015	49.50350031
64.49	19.82	35.75181	32.20883635	64.4176727
34.41	14.77	22.54408	20.30998512	40.61997024
45.76	17.29	28.12811	25.34063688	50.68127376

37.11	26.3	31.24089	28.14494295	56.28988589
19.1	14.41	16.59009	14.94602469	29.89204937
28.46	18.37	22.86504	20.59913801	41.19827601
14.77	11.17	12.84449	11.57161179	23.14322359
20.18	15.13	17.47351	15.74189699	31.48379398
17.65	18.73	18.18198	16.38016472	32.76032944
15.13	11.53	13.20791	11.89901848	23.79803695
19.82	10.09	14.14156	12.74014672	25.48029343
11.53	8.65	9.986716	8.997041601	17.9940832
17.65	18.01	17.82909	16.0622445	32.124489
10.09	8.29	9.145824	8.239481247	16.47896249
17.29	13.33	15.18143	13.6769605	27.35392099
36.39	15.85	24.01628	21.63628444	43.27256889
21.26	15.49	18.1471	16.34874275	32.6974855
14.05	26.66	19.35389	17.38581432	34.77162863
19.1	13.69	16.17031	14.52597225	29.05194449
32.07	26.3	29.04206	26.08880319	52.17760638
24.5	10.09	15.72275	14.12392581	28.24785162
34.23	13.69	21.64737	19.44607588	38.89215175
25.94	14.41	19.33379	17.36775878	34.73551756
28.46	13.33	19.47747	17.49682809	34.99365619
18.37	13.33	15.64839	14.05712333	28.11424666
32.79	20.54	25.95201	23.31297674	46.62595347
25.22	23.06	24.11583	21.66351853	43.32703706
26.66	14.05	19.35389	17.38581432	34.77162863
23.06	13.33	17.53254	15.74967254	31.49934508
7.39	6.94	7.161466	37.97171967	75.94343935
3.78	3.06	3.401	18.03287303	36.06574605
3.78	2.16	2.857411	15.15064377	30.30128755
2.52	2.43	2.474591	13.12084239	26.24168479
2.75	2.66	2.704626	14.34053906	28.68107813
2.12	2.79	2.432036	12.89520776	25.79041552
5.19	2.94	3.906226	20.71169565	41.4233913
4.08	2.76	3.355712	17.79274416	35.58548832
22.34	12.25	16.54282	14.81535305	29.6307061
44.31	18.1	28.3198	25.36252797	50.72505593
30.8	25.94	28.26574	25.31411336	50.62822672
35.4	41.88	38.50392	34.48318277	68.96636553
8.11	18.91	12.38386	11.09069004	22.18138009
11.35	13.24	12.25863	10.9785327	21.9570654
25.4	17.29	20.95629	18.7679454	37.53589081
16.21	9.19	12.20532	10.93079223	21.86158447

11.89	10.54	11.19467	10.0256747	20.05134941
21.35	11.62	15.75078	14.10601626	28.21203252
55.04	24.86	36.99046	33.12776611	66.25553222
33.87	23.06	27.94713	25.02877685	50.0575537
10.49	8.25	9.302822	8.331382906	16.66276581
23.42	12.61	17.18506	15.39052254	30.78104507
35.67	16.21	24.04601	21.53502789	43.07005578
67.37	24.5	40.62715	36.38469111	72.76938223
27.56	16.48	21.31171	19.08624906	38.17249813
26.75	20.81	23.5938	21.13003954	42.26007908
23.24	16.48	19.57026	17.52665516	35.05331033
19.46	12.97	15.88698	14.22799758	28.45599515
39.27	19.1	27.38717	24.6731248	49.3462496
34.59	25.22	29.53574	26.60877268	53.21754536
14.77	10.45	12.42363	11.19245647	22.38491295
19.1	24.14	21.47263	19.34471509	38.68943017
31.34	15.85	22.28764	20.07895704	40.15791408
22.34	18.73	20.45552	18.42839423	36.85678846
17.65	15.13	16.3415	14.7220687	29.4441374
15.85	14.05	14.92289	13.44404064	26.88808128
42.15	18.73	28.0975	25.31306296	50.62612593
24.86	12.97	17.95645	16.17698458	32.35396915
41.07	28.82	34.40403	30.99462319	61.98924638
23.42	14.05	18.13976	16.34212879	32.68425757
32.79	24.86	28.551	25.72161845	51.4432369
11.53	10.09	10.786	9.717113108	19.43422622
21.62	10.09	14.76976	13.30608977	26.61217954
21.62	11.17	15.54012	14.00011015	28.0002203
24.86	17.29	20.73233	18.67777245	37.35554489
20.9	34.95	27.02693	24.3485865	48.697173
24.14	15.13	19.11121	17.21730283	34.43460565
16.93	12.25	14.40113	12.97398957	25.94797915
29.9	15.13	21.26939	19.10653176	38.21306352
30.26	18.37	23.57703	21.17950679	42.35901357
6.03	3.51	4.600576	24.39329825	48.78659651

Grainsize of GF04				
Length	Width	Grain size	Actual Grain Size (micron)	Diameter (µm)
20.54	14.68	17.36454	92.02193	184.0439
31.34	6.21	13.95068	73.93046	147.8609
28.46	18.46	22.92099	121.4679	242.9357
33.15	4.05	11.58695	61.4041	122.8082
31.7	8.38	16.29865	86.37335	172.7467
16.93	5.76	9.875059	52.33206	104.6641
16.21	7.21	10.81083	57.29111	114.5822
16.66	4.05	8.214195	43.53045	87.06089
20.18	17.56	18.82447	99.75874	199.5175
16.3	13.6	14.88892	78.90261	157.8052
20.27	9.55	13.91325	73.73211	147.4642
12.34	12.16	12.24967	64.91611	129.8322
17.47	4.5	8.86651	46.98733	93.97467
12.52	8.9	10.55595	55.94036	111.8807
16.57	9.64	12.63862	66.97734	133.9547
12.97	8.57	10.54291	55.87126	111.7425
14.59	6.49	9.730832	51.56774	103.1355
17.96	3.51	7.939748	42.07604	84.15207
15.85	3.51	7.458787	39.52722	79.05444
34.11	5.46	13.647	72.32114	144.6423
8.11	2.64	4.627137	24.52113	49.04226
22.28	4.62	10.14562	53.76587	107.5317
78.18	32.07	50.07227	44.84352	89.68704
74.22	11.89	29.70649	26.60442	53.20884
95.49	31.34	54.70518	48.99264	97.98527
72.78	25.22	42.84287	38.36904	76.73808
114.93	29.9	58.62088	52.49944	104.9989
79.98	18.37	38.33057	34.32793	68.65587
89.74	27.02	49.242	44.09995	88.1999
108.81	23.78	50.86749	45.5557	91.1114
136.19	34.23	68.27726	61.14746	122.2949
144.29	22.93	57.52017	51.59685	103.1937
72.96	22.97	40.93765	36.72197	73.44394
45.67	18.1	28.75112	25.79039	51.58077
80.25	39.45	56.266	50.47183	100.9437
77.28	26.75	45.46691	40.78481	81.56963
61.34	14.86	30.19126	27.08222	54.16445
83.96	22.93	43.87713	39.35875	78.7175
15.4	4.41	8.240995	43.67247	87.34494

11.98	8.29	9.965651	52.81214	105.6243
12.52	4.77	7.727898	40.95335	81.9067
5.67	5.49	5.579274	29.5669	59.1338
10.99	5.85	8.018198	42.49178	84.98355
7.66	4.95	6.157678	32.6321	65.26421
10.78	3.78	6.383447	33.82855	67.6571
4.77	2.79	3.648054	19.33256	38.66512
4.14	3.06	3.55927	18.86205	37.72411
8.02	4.32	5.886119	31.193	62.386
5.67	1.71	3.113792	16.50128	33.00256
9.55	2.7	5.077893	26.90987	53.81975
2.16	2.08	2.119623	11.23276	22.46553
6.12	4.41	5.195113	27.53107	55.06214
9.73	2.61	5.039375	26.70575	53.4115
7.51	2.97	4.722785	25.02801	50.05602
10.27	3.96	6.377241	33.79566	67.59132
7.03	6.49	6.754606	35.79547	71.59095
10.9	5.49	7.735696	40.99468	81.98936
4.05	3.6	3.818377	20.23517	40.47034
7.3	6.49	6.883095	36.47639	72.95278
7.48	4.14	5.564818	29.49029	58.98058
8.29	4.41	6.046396	32.04237	64.08474
4.77	2.61	3.528413	18.69853	37.39707
4.77	3.34	3.991466	21.15244	42.30488
4.5	2.7	3.485685	18.4721	36.9442
9.19	7.12	8.089054	42.86727	85.73455
7.93	3.96	5.60382	29.69698	59.39396
10.72	4.05	6.589082	34.91829	69.83659
9.91	4.95	7.003892	37.11654	74.23309
4.5	4.41	4.454773	23.6077	47.2154
3.42	2.52	2.935711	15.55756	31.11512
4.14	2.88	3.452999	18.29888	36.59776
4.5	2.79	3.543304	18.77744	37.55489
3.87	2.07	2.830353	14.99922	29.99845
10.09	3.25	5.726474	30.34697	60.69394
7.03	3.28	4.801916	25.44736	50.89471
8.11	6.03	6.993089	37.0593	74.1186
9.19	3.16	5.388915	28.55811	57.11621
4.97	3.78	4.334351	22.96953	45.93907
9.1	3.44	5.594998	29.65023	59.30045
4.59	2.52	3.401	18.02332	36.04663
11.53	3.96	6.75713	35.80885	71.6177

7.48	4.32	5.684505	30.12456	60.24913
8.74	6.49	7.531441	39.91225	79.82449
7.03	4.14	5.394831	28.58946	57.17892
3.6	3.24	3.41526	18.09889	36.19777
3.6	2.52	3.011976	15.96172	31.92344
4.5	3.23	3.81248	20.20392	40.40784
8.56	3.69	5.620178	29.78367	59.56733
7.75	3.34	5.08773	26.962	53.92401
10.09	2.69	5.209808	27.60895	55.21789
6.21	2.43	3.884624	20.58624	41.17248
6.4	1.98	3.559775	18.86473	37.72947
3.15	2.7	2.916333	15.45487	30.90973
9.28	4.86	6.715713	35.58936	71.17873
5.31	2.43	3.592116	19.03612	38.07225
5.31	2.07	3.315373	17.56955	35.13909
9.96	3.24	5.680704	30.10442	60.20884
5.31	2.25	3.456516	18.31752	36.63504
8.83	2.43	4.632159	24.54774	49.09549
4.26	3.06	3.610485	19.13346	38.26693
13.87	3.42	6.887336	36.49887	72.99773
3.36	1.87	2.506631	13.28368	26.56737
10.99	2.28	5.005717	26.52738	53.05476
8.77	2.28	4.471644	23.69711	47.39421
4.68	4.14	4.401727	23.32659	46.65317
9.91	1.98	4.42965	23.47456	46.94913
6.67	2.52	4.099805	21.72658	43.45315
4.5	3.9	4.189272	22.2007	44.4014
6.24	3.55	4.706591	24.94219	49.88438
5.4	2.76	3.86057	20.45877	40.91754
11.89	3.6	6.542477	34.67131	69.34262
49.18	24.05	34.39155	30.80025	61.60049
36.21	24.86	30.00301	26.86997	53.73994
72.96	14.32	32.32317	28.94785	57.8957
22.46	17.83	20.01154	17.92185	35.84371
21.5	16.21	18.66856	16.71911	33.43822
29.45	17.29	22.56525	20.20889	40.41779
21.35	15.4	18.13257	16.23909	32.47818
53.68	20.54	33.20523	29.7378	59.4756
21.98	10.82	15.42153	13.81115	27.6223
18.37	12.97	15.43564	13.82378	27.64757
22.7	7.28	12.85519	11.5128	23.0256
10.9	11.53	11.21058	10.03992	20.07984

18.01	12.25	14.85337	13.30232	26.60463
30.98	19.1	24.32525	21.78511	43.57022
12.61	11.17	11.86818	10.62886	21.25771
21.26	13.69	17.06017	15.27868	30.55735
23.78	14.77	18.74115	16.78412	33.56824
21.26	12.25	16.138	14.4528	28.9056
30.98	13.34	20.32912	18.20627	36.41254
21.98	9.01	14.07266	12.60314	25.20627
21.98	9.73	14.62414	13.09702	26.19405
39.63	18.01	26.71584	23.92606	47.85213
19.1	12.25	15.29624	13.69894	27.39789
25.22	11.17	16.78414	15.03147	30.06294
19.82	10.81	14.63742	13.10892	26.21785
21.26	15.13	17.93499	16.06214	32.12428
26.66	14.05	19.35389	17.33288	34.66575
30.64	12.99	19.95028	17.86699	35.73397
21.62	11.51	15.77486	14.12758	28.25517
41.79	21.62	30.05827	26.91946	53.83893
25.05	14.46	19.03216	17.07226	34.14452
19.4	9.53	13.59713	12.19693	24.39385
35.98	14.46	22.80945	20.46057	40.92114
14.46	12.7	13.55146	12.15595	24.31191
15.52	10.23	12.60038	11.30282	22.60563
11.99	8.11	9.860979	8.845514	17.69103
31.75	11.99	19.51109	17.50187	35.00374
18.7	11.64	14.75358	13.23428	26.46856
24.34	13.41	18.06653	16.20607	32.41214
21.17	11.29	15.45993	13.86789	27.73578
14.11	9.88	11.80707	10.5912	21.18239
12.43	8.11	10.04028	9.006354	18.01271
15.4	8.65	11.54166	10.35312	20.70625
14.05	8.65	11.02418	9.888929	19.77786
18.64	12.43	15.22154	13.65405	27.3081
41.34	21.35	29.70874	26.64939	53.29877
20.81	10.54	14.81004	13.28493	26.56987
21.35	8.65	13.58961	12.19018	24.38036
25.4	10.81	16.57027	14.8639	29.7278
38.37	17.29	25.75689	23.10449	46.20899
21.35	10.54	15.00097	13.4562	26.91239
25.67	11.08	16.86486	15.12815	30.2563
31.89	16.21	22.73625	20.39491	40.78982
38.37	24.32	30.54764	27.4019	54.80381

17.83	7.84	11.82316	10.60564	21.21127
18.91	9.73	13.56445	12.16761	24.33522
31.34	12.43	19.73718	17.70468	35.40936
12.16	7.84	9.763934	8.758462	17.51692
31.4	18.34	23.99742	21.52621	43.05242
19.4	9.17	13.33784	11.96434	23.92867
10.58	7.76	9.060949	8.12787	16.25574
6.03	5.94	5.984831	31.71611	63.43223
4.77	4.77	4.77	25.27822	50.55644
10.63	6.58	8.363337	44.32081	88.64162
7.84	6.85	7.328301	38.83572	77.67145
11.35	10.18	10.74909	56.96393	113.9279
10.63	3.62	6.203273	32.87373	65.74747
9.62	5.13	7.024998	37.2284	74.45679
5.31	5.13	5.219224	27.65885	55.31769
2.34	1.98	2.152487	11.40693	22.81385
4.95	1.98	3.130655	16.59065	33.18129
11.98	5.31	7.975826	42.26723	84.53446
7.3	2.7	4.439595	23.52726	47.05453
3.96	6.03	4.886594	25.8961	51.7922
5.85	4.32	5.027126	26.64084	53.28168
3.54	2.34	2.878124	15.25238	30.50476
3.72	2.58	3.097999	16.41759	32.83518
38.55	13.69	22.9728	20.57388	41.14777
16.57	10.81	13.38364	11.98606	23.97212
16.57	13.15	14.76128	13.21985	26.4397
28.82	13.32	19.59292	17.54694	35.09389
29.55	27.74	28.6307	25.64096	51.28193
19.46	10.45	14.26033	12.77121	25.54241
27.38	15.13	20.35336	18.22798	36.45596
18.73	11.89	14.92313	13.36479	26.72958
22.93	14.82	18.43428	16.53595	33.0719
25.75	11.64	17.31271	15.52988	31.05976
63.15	13.05	28.70727	25.75105	51.5021
21.89	11.62	15.94872	14.30635	28.61271

Grainsize of GF05				
Length	Width	Grain Size	Actual Grain size (micron)	Diameter (µm)
135.47	85.03	107.3267	97.32197	194.6439
27.02	175.1	68.78373	62.3719	124.7438
123.58	26.66	57.39898	52.0484	104.0968
64.49	42.87	52.58028	47.67889	95.35779
82.14	23.42	43.86022	39.77169	79.54338
85.75	39.27	58.02932	52.61999	105.24
153.48	21.98	58.08176	52.66753	105.3351
92.49	33.87	55.96996	50.75259	101.5052
111.13	23.78	51.40692	46.61491	93.22981
82.14	15.13	35.25306	31.96687	63.93373
50.8	41.43	45.8764	41.59993	83.19985
231.66	71.34	128.5559	116.5723	233.1446
54.42	20.54	33.43332	30.31676	60.63351
91.87	35.31	56.95551	51.64627	103.2925
87.91	25.94	47.75338	43.30194	86.60388
208.24	49	101.0137	91.59745	183.1949
197.8	32.79	80.53485	73.02761	146.0552
165.37	32.07	72.82456	66.03605	132.0721
77.46	31.7	49.55282	44.93364	89.86728
176.99	41.34	85.5381	76.72955	153.4591
177.8	21.62	62.00029	55.61562	111.2312
182.12	32.99	77.51218	69.53013	139.0603
191.67	49.72	97.62086	87.56805	175.1361
49.72	47.56	48.62801	44.09504	88.19008
501.3	58.56	171.3363	153.6924	307.3848
29.18	18.01	22.92448	20.78752	41.57505
15.13	9.73	12.13321	11.00219	22.00438
21.26	18.01	19.56764	17.7436	35.4872
20.9	20.54	20.71922	18.78783	37.57566
25.58	22.7	24.09701	21.85075	43.70151
22.7	12.25	16.67558	15.12113	30.24226
9.73	9.73	9.73	8.822996	17.64599
23.42	12.25	16.93798	15.35906	30.71813
16.96	11.88	14.19453	12.87136	25.74272
27.38	14.77	20.10976	18.23519	36.47037
10.45	11.53	10.97673	9.953505	19.90701
10.45	11.17	10.804	9.796884	19.59377
19.82	11.53	15.11703	13.70786	27.41572
6.49	5.76	6.114115	5.544174	11.08835

17.65	12.25	14.70417	13.33348	26.66697
11.17	6.49	8.5143	7.72062	15.44124
10.45	9.37	9.895277	8.972866	17.94573
16.57	9.73	12.69748	11.51386	23.02772
11.53	7.93	9.562055	8.670707	17.34141
25.94	20.54	23.08263	20.93093	41.86185
15.85	15.49	15.66897	14.20835	28.4167
14.05	14.75	14.39575	13.05381	26.10763
11.53	16.57	13.82216	12.5337	25.06739
11.17	14.77	12.84449	11.64716	23.29432
18.76	14.41	16.44176	14.90911	29.81822
9.37	7.57	8.422048	7.636968	15.27394
11.17	9.73	10.42517	9.453361	18.90672
15.13	7.93	10.95358	9.932517	19.86503
11.89	10.45	11.14677	10.1077	20.2154
36.39	19.46	26.61108	24.13046	48.26093
13.69	11.53	12.56367	11.39252	22.78503
15.13	12.61	13.81265	12.52507	25.05015
20.84	13.69	16.89081	15.3163	30.6326
10.45	10.09	10.26842	9.311228	18.62246
24.14	15.13	19.11121	17.32971	34.65942
22.7	19.1	20.82234	18.88134	37.76268
17.29	12.61	14.76573	13.38931	26.77863
12.97	19.46	15.88698	14.40604	28.81208
25.94	10.09	16.17821	14.67012	29.34025
10.45	10.45	10.45	9.47588	18.95176
7.57	12.61	9.770246	8.85949	17.71898
14.77	19.82	17.10969	15.51477	31.02954
9.37	9.37	9.37	8.496554	16.99311
10.45	10.45	10.45	9.47588	18.95176
19.1	12.61	15.51937	14.0727	28.1454
10.81	7.57	9.046088	8.202836	16.40567
11.17	7.21	8.974168	8.137621	16.27524
16.21	7.55	11.0628	10.03155	20.06311
21.98	7.21	12.58872	11.41523	22.83046
8.29	6.85	7.535682	6.833226	13.66645
7.93	7.93	7.93	7.190787	14.38157
10.45	12.25	11.31426	10.25958	20.51915
13.33	7.93	10.28139	9.322983	18.64597
13.69	10.81	12.16507	11.03107	22.06215
40.71	12.27	22.34976	20.26638	40.53275
17.29	10.09	13.20818	11.97695	23.9539

9.01	7.93	8.452769	7.664825	15.32965
14.05	11.53	12.72778	11.54134	23.08267
19.46	8.65	12.97417	11.76475	23.5295
19.1	10.81	14.3691	13.02965	26.0593
15.26	10.09	12.4086	11.25191	22.50381
10.45	7.93	9.103214	8.254637	16.50927
29.9	15.13	21.26939	19.28672	38.57343
16.57	9.37	12.46037	11.29885	22.5977
11.53	10.09	10.786	9.780555	19.56111
11.17	10.45	10.804	9.796884	19.59377
24.5	12.61	17.57683	15.93837	31.87673
13.69	8.65	10.88203	9.867634	19.73527
16.21	11.89	13.88297	12.58884	25.17768
9.37	7.21	8.219349	7.453164	14.90633
15.49	13.69	14.56221	13.20476	26.40953
18.01	6.12	10.49863	9.519975	19.03995
14.05	15.13	14.58	13.2209	26.44179
9.73	9.37	9.548304	8.658237	17.31647
21.26	13.69	17.06017	15.46987	30.93974
15.13	11.53	13.20791	11.97671	23.95341
17.65	9.01	12.61057	11.43505	22.8701
21.26	9.01	13.84025	12.5501	25.1002
8.88	8.65	8.764246	7.947267	15.89453
9.01	8.65	8.828165	8.005228	16.01046
10.45	10.45	10.45	9.47588	18.95176
34.23	15.13	22.75741	20.63603	41.27206
8.65	7.93	8.28218	7.510138	15.02028
15.49	14.05	14.75244	13.37726	26.75452
19.46	21.62	20.51159	18.59955	37.19911
7.93	5.76	6.758461	6.128456	12.25691
9.73	8.29	8.981186	8.143984	16.28797
18.37	8.65	12.60557	11.43052	22.86103
10.81	10.45	10.62848	9.637718	19.27544
21.26	12.61	16.37341	14.84713	29.69425
20.18	12.61	15.95211	14.4651	28.9302
12.91	10.09	11.41323	10.34932	20.69865
14.77	9.37	11.76414	10.66752	21.33503
21.98	12.61	16.64836	15.09644	30.19289
12.61	9.73	11.07679	10.04424	20.08849
22.77	15.85	18.99749	17.22659	34.45319
8.29	9.73	8.981186	8.143984	16.28797
25.22	16.93	20.66336	18.73718	37.47436

31.16	14.77	21.45305	19.45325	38.9065
11.89	10.81	11.33715	10.28033	20.56066
14.61	13.69	14.14252	12.82419	25.64839
9.37	7.57	8.422048	7.636968	15.27394
9.19	8.65	8.915913	7.997769	15.99554
9.19	8.38	8.77566	7.871959	15.74392
12.16	7.84	9.763934	8.758462	17.51692
35.13	16.86	24.33705	21.83086	43.66173
14.05	8.65	11.02418	9.888929	19.77786
20	8.92	13.35665	11.9812	23.96241
13.51	10.54	11.93295	10.70412	21.40824
14.32	10.54	12.28547	11.02034	22.04067
14.32	10.81	12.44183	11.1606	22.32119
10.27	8.38	9.276993	8.321666	16.64333
9.46	5.67	7.32381	6.569618	13.13924
6.49	8.11	7.254922	6.507824	13.01565
25.13	10.81	16.48197	14.78469	29.56937
23.42	12.61	17.18506	15.41537	30.83075
23.42	14.41	18.37069	16.47891	32.95782
17.69	18.37	18.02679	16.17043	32.34086
9.37	11.53	10.39404	9.425137	18.85027
20.54	11.53	15.38916	13.95462	27.90925
14.41	9.01	11.39448	10.33231	20.66463
18.37	9.37	13.11971	11.89673	23.79346
19.82	17.29	18.51183	16.78621	33.57241
11.17	10.09	10.61628	9.626655	19.25331
13.78	9.73	11.57927	10.38685	20.77371
11.89	9.46	10.60563	9.513483	19.02697
11.08	7.86	9.332138	8.371132	16.74226
11.33	9.73	10.49957	9.418341	18.83668
20.9	18.37	19.59421	17.76769	35.53538
9.73	11.52	10.58724	9.600324	19.20065
21.26	13.69	17.06017	15.46987	30.93974
17.65	10.81	13.81291	12.52531	25.05062
15.49	23.42	19.04667	17.2712	34.54239
19.1	15.13	16.9995	15.41485	30.82971
11.53	9.01	10.19241	9.242305	18.48461
10.09	15.49	12.50176	11.33638	22.67277
16.57	15.85	16.206	14.69532	29.39065
9.37	19.1	13.37785	12.13081	24.26162
6.85	9.37	8.011523	7.264711	14.52942
12.25	24.14	17.19637	15.59337	31.18674

14.77	11.17	12.84449	11.64716	23.29432
19.82	16.03	17.82455	16.16299	32.32599
10.45	8.65	9.507497	8.621234	17.24247
13.33	13.33	13.33	12.08741	24.17483
9.37	7.57	8.422048	7.636968	15.27394
8.83	7.57	8.175763	7.413641	14.82728
11.17	10.09	10.61628	9.626655	19.25331
10.81	9.01	9.869048	8.949082	17.89816
10.09	22.7	15.13417	13.7234	27.4468
13.69	9.73	11.54139	10.46553	20.93107
8.65	9.01	8.828165	8.005228	16.01046
10.09	11.17	10.61628	9.626655	19.25331
20.18	21.62	20.88759	18.94051	37.88102
14.41	14.77	14.58889	13.22895	26.45791
10.09	10.09	10.09	9.149438	18.29888
15.13	14.77	14.94892	13.55542	27.11084
12.25	11.53	11.88455	10.7767	21.55341
22.7	8.65	14.01267	12.70645	25.4129
19.1	12.97	15.73935	14.27217	28.54433
12.97	14.77	13.84077	12.55057	25.10114
9.01	9.01	9.01	8.170112	16.34022
16.57	11.89	14.03629	12.72786	25.45572
11.35	9.19	10.21306	9.161334	18.32267
38.64	23.78	30.31269	27.19115	54.38229
10.81	8.92	9.819633	8.808426	17.61685
23.78	17.56	20.4347	18.33037	36.66074
18.31	17.83	18.06841	16.20776	32.41551
11.17	10.69	10.92736	9.802085	19.60417
26.3	21.26	23.6461	21.21107	42.42214
20.54	12.97	16.32188	14.64108	29.28217
13.69	12.97	13.32514	11.95294	23.90588
16.21	15.85	16.02899	14.37835	28.75671
14.05	9.73	11.69216	10.48812	20.97624
18.1	10.54	13.8121	12.38975	24.77951
12.59	8.65	10.43568	9.361037	18.72207

Grainsize of GF19-3				
Length	Width	Grain size	Actual grain size (micron)	Diameter (μm)
6.76	4.59	5.570314	4.969945	9.93989
9.19	5.67	7.218539	6.440523	12.88105
6.62	2.97	4.434118	3.956208	7.912416
5.94	5.94	5.94	5.299786	10.59957
4.93	3.68	4.25939	3.800312	7.600624
5.17	3.18	4.054701	3.617685	7.235369
12.16	8.11	9.930639	8.860314	17.72063
10.2	4.86	7.040739	6.281887	12.56377
15.94	15.93	15.935	14.21752	28.43504
19.19	14.05	16.42009	14.65033	29.30067
11.62	5.67	8.116982	7.242133	14.48427
17.5	7.84	11.71324	10.45079	20.90157
12.23	6.76	9.092568	8.11257	16.22514
9.73	9.19	9.456146	8.436961	16.87392
7.9	5.67	6.692757	5.971411	11.94282
13.24	8.38	10.53334	9.398053	18.79611
49.18	19.27	30.78471	27.46673	54.93346
31.67	6.21	14.02393	12.51243	25.02486
6.62	6.08	6.344257	5.660472	11.32094
10.61	7.03	8.636452	7.705614	15.41123
18.1	8.65	12.51259	11.16398	22.32797
11.01	5.67	7.901057	7.04948	14.09896
20.54	10.61	14.76243	13.17133	26.34267
15.4	9.39	12.02522	10.72914	21.45829
33.24	12.97	20.7635	18.5256	37.05121
34.59	7.57	16.18167	14.4376	28.87521
14.86	7.3	10.41528	9.292717	18.58543
23.78	10.81	16.03315	14.30509	28.61018
12.5	9.9	11.1243	9.925319	19.85064
16.08	7.3	10.83439	9.666657	19.33331
12.7	6.49	9.078711	8.100206	16.20041
12.43	6.76	9.166613	8.178634	16.35727
11.35	10.54	10.9375	9.758658	19.51732
11.89	10.54	11.19467	9.988105	19.97621
34.56	13.51	21.608	19.27909	38.55817
8.98	7.51	8.212174	7.327064	14.65413
10	7.9	8.888194	7.930223	15.86045
17.02	5.4	9.586866	8.553592	17.10718

10.27	7.11	8.545157	7.624158	15.24832
9.46	3.92	6.089598	5.43326	10.86652
12.63	6.49	9.053657	8.077852	16.1557
12.06	7.84	9.723703	8.675681	17.35136
12.7	8.79	10.56565	9.426884	18.85377
11.01	2.76	5.512495	4.918357	9.836715
6.76	6.49	6.623624	5.909729	11.81946
35.32	21.35	27.46055	24.50085	49.0017
28.83	12.16	18.72359	16.70556	33.41112
7.57	5.61	6.516725	5.814351	11.6287
5.61	5.13	5.364634	4.786433	9.572866
8.71	6.01	7.23513	6.455326	12.91065
10.54	10.27	10.40412	9.282766	18.56553
12.94	8.58	10.53685	9.401186	18.80237
41.15	13.24	23.34151	20.82576	41.65151
13.51	8.73	10.86012	9.689618	19.37924
16.48	7.03	10.76357	9.603469	19.20694
10.29	8.74	9.483385	8.461265	16.92253
7.03	6.21	6.607291	5.895157	11.79031
8.16	6.35	7.198333	6.422496	12.84499
7.7	6.49	7.069158	6.307243	12.61449
9.25	5.67	7.242065	6.461514	12.92303
17.77	14.05	15.8009	14.09788	28.19576
28.96	9.91	16.94089	15.11499	30.22999
9.12	4.05	6.077499	5.422466	10.84493
7.35	3.78	5.270958	4.702853	9.405707
10.79	6.49	8.36822	7.466292	14.93258
14.81	10.38	12.3987	11.06237	22.12474
7.77	5.76	6.689933	5.968891	11.93778
9.47	7.63	8.500359	7.584189	15.16838
9.47	8.38	8.908344	7.948202	15.8964
38.03	11.75	21.13889	18.86053	37.72107
14.32	7.71	10.50748	9.374985	18.74997
16.9	10.88	13.55994	12.09845	24.1969
33.39	19.46	25.49057	22.7432	45.48639
9.19	7.84	8.488204	7.573344	15.14669
18.1	10.32	13.66719	12.19414	24.38827
34.32	10.71	19.17204	17.10568	34.21135
18.64	8.11	12.29514	10.96997	21.93993
9.46	6.76	7.996849	7.134948	14.2699
15.39	13.46	14.39269	12.84144	25.68288
13.23	6.73	9.43599	8.418977	16.83795

11.35	6.73	8.73988	7.797894	15.59579
31.07	7.97	15.7362	14.04015	28.08029
47.02	19.46	30.24912	26.98886	53.97773
62.15	21.06	36.17843	32.27912	64.55823
132.08	28.69	61.5579	54.92318	109.8464
13.24	9.21	11.04266	9.852483	19.70497
18.64	12.97	15.54866	13.87282	27.74564
26.48	12.16	17.94427	16.01023	32.02047
22.16	11.89	16.23214	14.48264	28.96528
12.87	10.54	11.64688	10.39158	20.78315
53.49	14.05	27.41413	24.45943	48.91886
13.19	7.57	9.992412	8.915428	17.83086
21.35	12.16	16.1126	14.37598	28.75197
33.78	12.43	20.49111	18.28257	36.56514
45.4	16.8	27.61739	24.64078	49.28156
72.09	18.43	36.45022	32.52161	65.04322
36.37	10.27	19.32666	17.24363	34.48726
21.89	5.4	10.87226	9.700445	19.40089
13.24	5.94	8.868235	7.912416	15.82483
14.78	10.44	12.42188	11.08305	22.1661
9.19	5.67	7.218539	6.440523	12.88105
8.38	8.38	8.38	7.476802	14.9536
9.73	7.03	8.270544	7.379144	14.75829
19.22	11.3	14.73723	13.14885	26.2977
23.78	5.46	11.39468	10.16656	20.33312
34.32	11.89	20.20061	18.02339	36.04678
12.97	7.84	10.08389	8.997045	17.99409
17.83	8.65	12.41892	11.0804	22.16081
9.51	7.03	8.176509	7.295244	14.59049
18.54	8.65	12.66377	11.29886	22.59773
10.81	4.32	6.833681	6.097146	12.19429
10.91	7.57	9.087833	8.108345	16.21669
17.02	7.3	11.14657	9.94519	19.89038
9.73	7.24	8.393164	7.488547	14.97709
25.67	14.32	19.17275	17.10631	34.21262
16.75	7.08	10.8899	9.716188	19.43238
14.05	7.57	10.31303	9.201486	18.40297
21.89	9.46	14.39025	12.83927	25.67854
20.7	7.3	12.29268	10.96777	21.93555
10.49	5.49	7.588814	6.770891	13.54178
25.4	9.18	15.26997	13.62417	27.24834
18.37	10.61	13.96086	12.45616	24.91232

42.69	15.13	25.41456	22.67537	45.35074
18.37	10.81	14.09183	12.57301	25.14602
12.97	8.38	10.42538	9.301733	18.60347
11.08	9.19	10.09085	9.003254	18.00651
16.48	8.38	11.7517	10.4851	20.9702
13.78	6.21	9.250611	8.253579	16.50716
38.64	18.91	27.03114	24.11772	48.23543
21.35	6.49	11.77121	10.50251	21.00502
11.08	10.27	10.66731	9.51759	19.03518
18.37	6.73	11.11891	9.92051	19.84102
14.86	11.08	12.83155	11.44857	22.89714
11.35	5.54	7.929628	7.074971	14.14994
39.72	20	28.1851	25.14731	50.29462
47.83	20.54	31.34371	27.96548	55.93096
25.4	13.24	18.33838	16.36186	32.72372
16.21	10.81	13.23745	11.81072	23.62143
50.12	19.46	31.23036	27.86434	55.72869
32.64	11.62	19.47503	17.37601	34.75202
20	9.19	13.55729	12.09608	24.19216
20.81	14.37	17.29276	15.42895	30.8579
29.18	13.03	19.49911	17.3975	34.79499
28.1	7.57	14.58482	13.01287	26.02573
16.21	7.3	10.8781	9.705654	19.41131
62.15	9.1	23.78161	21.21842	42.43685
18.37	15.07	16.63839	14.8451	29.6902
25.4	11.35	16.9791	15.14909	30.29819
13.24	6.76	9.460571	8.440909	16.88182
27.29	8.38	15.12251	13.4926	26.9852
25.48	7.03	13.38374	11.94124	23.88247
17.61	10	13.27027	11.84	23.67999
7.57	6.21	6.856362	6.117382	12.23476
42.06	8.65	19.07404	17.01824	34.03647
24.59	8.92	14.81023	13.21398	26.42796
7.92	6.86	7.37097	6.576526	13.15305
11.89	7.57	9.487218	8.464684	16.92937
18.94	10.63	14.18916	12.65985	25.3197
17.26	10.63	13.54525	12.08534	24.17068
20.81	8.29	13.13449	11.71886	23.43771
19.19	8.11	12.47521	11.13063	22.26126
19.13	12.43	15.42031	13.7583	27.51661
12.43	10.54	11.44606	10.2124	20.4248
15.4	6.49	9.9973	8.919789	17.83958

11.62	8.21	9.767303	8.714581	17.42916
16.21	6.49	10.25685	9.151362	18.30272
8.35	6.21	7.200937	6.424819	12.84964
10.2	6.49	8.136215	7.259293	14.51859
14.57	8.38	11.04973	9.858791	19.71758
28.21	9.19	16.10124	14.36585	28.73169
10.54	9.73	10.1269	9.035425	18.07085
14.1	8.11	10.6935	9.540955	19.08191
12.15	6.49	8.879949	7.922867	15.84573
10.27	10.06	10.16446	9.068931	18.13786
11.49	6.7	8.773996	7.828333	15.65667
12.75	6.76	9.283857	8.283241	16.56648
17.02	10.27	13.22102	11.79606	23.59211
23.51	8.11	13.80819	12.31994	24.63988
7.84	5.94	6.824192	6.08868	12.17736
14.59	9.19	11.57938	10.33135	20.66271
19.73	8.92	13.26618	11.83635	23.6727
15.62	7.03	10.47896	9.349536	18.69907
13.51	4.32	7.639581	6.816186	13.63237
14.55	6.49	9.717484	8.670132	17.34026
27.72	10.27	16.87259	15.05406	30.10812
45.94	20.54	30.7182	27.40738	54.81477
17.91	11.57	14.39509	12.84359	25.68718
22.06	6.7	12.15738	10.84706	21.69412
28.5	9.19	16.18379	14.4395	28.87899
12.43	10.81	11.59173	10.34238	20.68475
16.81	7.02	10.86307	9.692243	19.38449
12.97	12.16	12.55847	11.20492	22.40983
18.46	10.81	14.12631	12.60377	25.20755
28.13	10	16.772	14.96431	29.92862
6.2	5.13	5.639681	5.031835	10.06367
11.81	8.02	9.732225	8.683284	17.36657
11.19	7.94	9.425954	8.410023	16.82005
9.65	8.65	9.136329	8.151614	16.30323
11.08	7.3	8.993553	8.024227	16.04845
11.24	7.03	8.889162	7.931087	15.86217

Grainsize of GF19-5				
Length	Width	Grain Size	Actual grain size (micron)	Diameter (µm)
21.62	17.29	19.33416	17.45275	34.90551
58.01	11.89	26.26288	23.70724	47.41448
23.78	9.37	14.92711	13.47455	26.94911
25.94	10.09	16.17821	14.60391	29.20782
43.77	18.91	28.76961	25.97004	51.94009
88.63	16.75	38.52989	34.78055	69.5611
58.01	9.73	23.75789	21.44601	42.89202
37.83	21.62	28.59868	25.81574	51.63149
16.21	14.41	15.28352	13.79628	27.59257
36.75	18.37	25.98264	23.45427	46.90854
10.45	10.09	10.26842	9.269202	18.5384
47.56	21.98	32.33216	29.18592	58.37184
70.26	12.97	30.18729	27.24976	54.49952
18.73	12.25	15.14736	13.67337	27.34674
16.08	7.57	11.03293	9.959318	19.91864
18.73	19.1	18.9141	17.07356	34.14713
23.78	11.89	16.815	15.17873	30.35746
13.33	13.33	13.33	12.03286	24.06572
24.59	10.81	16.30392	14.71739	29.43478
19.55	9.46	13.59937	12.27602	24.55204
98.73	25.49	50.166	45.28435	90.5687
23.87	12.35	17.16958	15.49881	30.99762
15.85	11.17	13.30581	12.01102	24.02204
47.92	10.14	22.04334	19.8983	39.7966
13.05	12.61	12.82811	11.57981	23.15962
16.21	9.73	12.55879	11.3367	22.6734
15.13	12.97	14.00843	12.64527	25.29054
32.29	19.46	25.06718	22.62789	45.25578
50.8	11.89	24.57666	22.1851	44.3702
21.08	11.89	15.83165	14.29107	28.58215
39.99	11.89	21.80553	19.68363	39.36727
63.77	22.7	38.04706	34.3447	68.68941
15.13	12.61	13.81265	12.46854	24.93708
15.13	7.57	10.70206	9.660643	19.32129
47.92	19.82	30.81841	27.81947	55.63894
12.39	11.53	11.95227	10.78919	21.57839
20.12	10.81	14.74779	13.31268	26.62536
34.95	26.66	30.52486	27.55449	55.10897

31.45	10.81	18.4384	16.64416	33.28831
45.04	32.79	38.42996	34.69034	69.38068
10.81	8.65	9.669876	8.7289	17.4578
13.53	10.81	12.09377	10.91693	21.83385
13.33	9.52	11.26506	10.16886	20.33772
97.75	14.41	37.53102	33.87888	67.75776
20.18	26.66	23.1948	34.24092	68.48185
16.21	9.44	12.37022	18.26133	36.52265
47.92	13.69	25.61298	37.81072	75.62144
19.46	13.33	16.10596	23.77614	47.55227
21.83	11.37	15.75459	23.25744	46.51488
42.15	16.21	26.13908	38.58736	77.17473
13.48	13.33	13.40479	19.78859	39.57718
16.28	10.81	13.266	19.5837	39.16741
14.95	13.87	14.39988	21.25757	42.51514
42.51	13.69	24.12389	35.61247	71.22494
25.94	19.11	22.26462	32.86776	65.73552
29.97	8.29	15.76234	23.26888	46.53776
19.85	9.73	13.8975	20.51594	41.03189
30.8	13.51	20.39873	17.97561	35.95123
23.78	8.65	14.34214	12.63847	25.27695
65.93	23.24	39.14349	34.49374	68.98748
61.61	15.13	30.53128	26.90455	53.8091
25.22	14.92	19.398	17.09376	34.18752
63.41	10.45	25.74169	22.6839	45.3678
17.15	20.54	18.76862	16.53914	33.07828
19.1	11.53	14.83991	13.07712	26.15423
27.59	8.65	15.44841	13.61334	27.22667
39.12	12.61	22.21043	19.57211	39.14422
46.48	25.56	34.46779	30.37345	60.7469
54.76	39.37	46.43168	40.91618	81.83236
12.61	7.93	9.999865	8.812007	17.62401
20.9	9.07	13.76819	12.1327	24.2654
15.49	10.81	12.94013	11.403	22.80601
47.7	22.34	32.6438	28.76613	57.53226
50.08	12.25	24.76853	21.82634	43.65268
16.57	11.78	13.97121	12.3116	24.6232
14.95	7.93	10.88823	9.594843	19.18969
21.26	10.3	14.79791	13.0401	26.0802
17.65	8.65	12.35607	10.88833	21.77665
11.17	9.73	10.42517	9.186788	18.37358
20.18	15.49	17.68016	15.57998	31.15996

18.73	13.69	16.01292	14.11079	28.22158
19.1	10.81	14.3691	12.66223	25.32446
28.46	12.25	18.67177	16.4538	32.9076
58.73	20.54	34.73203	30.6063	61.21261
10.09	8.47	9.244582	8.146442	16.29288
18.73	12.78	15.47157	13.63374	27.26748
57.1	20.18	33.94522	29.91295	59.82591
21.47	8.61	13.5962	11.98114	23.96229
12.39	8.69	10.37637	9.143789	18.28758
47.65	17.29	28.70311	25.29354	50.58708
15.16	13.76	14.44305	12.72739	25.45479
13.76	10.81	12.19613	10.74738	21.49477
23.22	8.29	13.87421	12.22613	24.45226
52.06	18.81	31.29295	27.57574	55.15148
47.56	25.58	34.87958	30.73632	61.47264
23.78	16.21	19.63349	17.30127	34.60255
44.31	20.81	30.36595	26.75886	53.51772
23.1	19.1	21.005	18.50987	37.01974
11.88	7.93	9.706101	8.553138	17.10628
29.54	10.81	17.86973	15.74703	31.49407
29.54	7.21	14.59395	12.86037	25.72075
19.25	11.89	15.12886	13.33174	26.66349
42.51	18.7	28.19463	24.84546	49.69092
13.33	10.31	11.72315	10.33059	20.66118
13.32	11.89	12.58471	11.0898	22.1796
30.93	10.81	18.28533	16.11326	32.22652
24.83	23.57	24.1918	21.31812	42.63623
13.36	12.97	13.16356	11.59989	23.19978
17.16	11.17	13.84475	12.20017	24.40034
15.93	9.52	12.31477	10.85193	21.70386
27.98	30.28	29.10729	25.64971	51.29942
26.84	5.76	12.43376	10.95679	21.91357
12.97	12.25	12.60486	11.10756	22.21512
10.81	7.66	9.099703	8.018773	16.03755
11.65	6.85	8.933225	7.87207	15.74414
17.93	14.05	15.87188	13.9865	27.973
21.62	11.89	16.03315	14.47296	28.94592
32.43	19.46	25.12146	22.67689	45.35378
19.46	16.75	18.05422	16.29737	32.59474
41.07	27.02	33.31233	30.07071	60.14142
28.89	16.21	21.6404	19.53457	39.06915
14.09	12.43	13.234	11.9462	23.8924

25.4	14.5	19.19114	17.32365	34.64731
13.93	13.89	13.90999	12.55641	25.11281
27.02	17.29	21.61425	19.51097	39.02194
19.46	18.01	18.72097	16.89923	33.79846
15.51	14.7	15.09957	13.63023	27.26046
54.58	31.53	41.48382	37.44703	74.89406
31.34	22.16	26.35326	23.78883	47.57765
31.34	15.13	21.77554	19.65656	39.31313
24.06	18.91	21.33013	19.2545	38.509
21.62	15.67	18.40612	16.61502	33.23005
18.91	16.06	17.42684	15.73103	31.46206
45.4	20.49	30.49993	27.53199	55.06397
25.94	20.81	23.23384	20.97296	41.94591
11.89	10.54	11.19467	10.10532	20.21063
22.9	9.46	14.71849	13.28624	26.57247
15.52	12.43	13.88933	12.53776	25.07553
27.56	17.83	22.16743	20.01031	40.02063
25.4	14.59	19.25061	17.37733	34.75467
14.86	8.38	11.15916	10.07326	20.14652
22.7	10.81	15.66483	14.14049	28.28098
11.93	8.92	10.31579	9.311964	18.62393
15.94	12.16	13.9223	12.56752	25.13504
18.37	13.24	15.59547	14.07788	28.15576
15.67	8.65	11.6424	10.50948	21.01896
18.64	19.46	19.04559	17.19226	34.38452
25.13	15.4	19.67237	17.75805	35.5161
14.05	9.44	11.5166	10.39592	20.79183
41.14	9.73	20.0073	18.06039	36.12079
32.97	10	18.15764	16.39072	32.78145
10.81	8.74	9.720051	8.774193	17.54839
23.51	14.44	18.4251	16.63216	33.26431
60.94	28.06	41.35186	37.32791	74.65582
54.2	37.47	45.06522	40.67992	81.35985
21.98	10.45	15.15556	13.68077	27.36155
16.93	10.76	13.49692	12.18353	24.36707
22.67	10.09	15.12416	13.65243	27.30486
20.9	16.57	18.60949	16.77135	33.54269
15.49	6.89	10.33083	9.310411	18.62082
27.02	18.73	22.49632	20.27426	40.54853
21.98	15.49	18.45183	16.62927	33.25853
21.98	16.21	18.8758	17.01135	34.02271
23.78	12.25	17.06766	15.38181	30.76363

53.68	20.95	33.535	30.2226	60.4452
15.85	12.25	13.93422	12.55788	25.11575
20.9	11.53	15.52343	13.99012	27.98023
43.89	16	26.49981	23.88231	47.76462
20.18	12.25	15.72275	14.16975	28.3395
18.73	8.34	12.49833	11.26381	22.52763
33	13.69	21.25488	19.15545	38.31089
24.5	18.16	21.09313	19.00967	38.01933
18.73	17.65	18.18198	16.38607	32.77214
25.58	15.49	19.90563	17.93947	35.87893
23.42	13.25	17.61576	15.87578	31.75155
31.67	16.34	22.74836	20.5014	41.00281
14.12	10.6	12.23405	11.02564	22.05128
22.29	12.35	16.59161	14.95278	29.90557
20.21	11.89	15.50151	13.97036	27.94072
15.85	11.89	13.72795	12.37198	24.74395
18.73	10.09	13.74721	12.38934	24.77867
15.32	12.97	14.09611	12.70378	25.40756
13.69	9.51	11.41017	10.28313	20.56627
81.78	10.81	29.73284	26.796	53.592
19.82	8.07	12.64703	11.39783	22.79566
16.57	20.9	18.60949	16.77135	33.54269
19.82	9.73	13.88699	12.51532	25.03063
23.07	12.97	17.29792	15.58933	31.17865
28.1	25.94	26.99841	24.33166	48.66332
25.94	11.53	17.29417	15.58595	31.17189
26.51	15.85	20.49838	18.47366	36.94733
35.31	19.46	26.21321	23.62402	47.24804
24.14	12.61	17.44722	15.72388	31.44776
22.44	9.01	14.21916	12.81467	25.62934
27.02	20.18	23.35088	21.04441	42.08882
34.59	26.01	29.99476	27.03205	54.0641
20.9	12.25	16.00078	14.42031	28.84063
20.18	12.25	15.72275	14.16975	28.3395
15.28	11.53	13.27322	11.96217	23.92434
32.07	24.14	27.82391	25.07562	50.15124

Grainsize of S15				
Length	Width	Grainsize	Actual grain size (micron)	Diameter (µm
65.39	17.75	34.06864	26.88074	53.76147
133.53	41.07	74.05455	58.43029	116.8606
64.45	9.19	24.33712	19.2024	38.4048
55.66	9	22.38169	17.65953	35.31906
85.68	20.9	42.31681	33.38867	66.77735
279.94	31.34	93.666	73.90406	147.8081
17.29	11.08	13.841	10.92078	21.84156
17.56	5.49	9.818574	7.747021	15.49404
7.57	5.94	6.705654	5.290874	10.58175
19.46	5.94	10.75139	8.483029	16.96606
14.41	6.23	9.47493	7.47588	14.95176
11.23	10.54	10.87953	8.584134	17.16827
10.09	12.97	11.43972	9.026136	18.05227
8.41	4.68	6.273659	4.950023	9.900046
11.89	6.12	8.530346	6.730587	13.46117
10.74	7.93	9.228662	7.28157	14.56314
18.73	15.13	16.83404	13.28234	26.56468
18.73	15.13	16.83404	13.28234	26.56468
9.41	4.32	6.375829	5.030637	10.06127
18.76	8.86	12.89239	10.17231	20.34462
10.08	7.73	8.82714	6.964762	13.92952
8.65	5	6.576473	5.188948	10.3779
17.79	8.65	12.40498	9.787738	19.57548
9.87	7.95	8.858132	6.989216	13.97843
16.55	7.21	10.92362	8.618922	17.23784
13.02	10.45	11.66443	9.203435	18.40687
10.99	8.65	9.750051	7.692955	15.38591
11.4	5.76	8.103333	6.393666	12.78733
8.79	4.58	6.344935	5.006261	10.01252
3.24	2.16	2.645449	2.087304	4.174608
4.7	3.09	3.810905	3.006869	6.013737
14.23	8.65	11.09457	8.753804	17.50761
9.01	5.98	7.340286	5.79161	11.58322
17.78	5.67	10.04055	7.922162	15.84432
9.74	7.57	8.586722	6.775069	13.55014
9.73	5.52	7.328683	5.782455	11.56491
6.73	6.06	6.38622	5.038835	10.07767
9.59	7.03	8.210828	6.478482	12.95696

25.5	7.57	13.8937	10.96237	21.92473
12.53	9.39	10.84697	8.55844	17.11688
5.94	5.37	5.647814	4.45622	8.912441
10.74	3.75	6.346259	5.007305	10.01461
5.67	3.24	4.286117	3.381819	6.763638
5.67	3.38	4.377739	3.45411	6.90822
4.37	2.7	3.434967	2.710247	5.420494
2.67	1.92	2.264155	1.786457	3.572914
3.78	3.33	3.547873	2.799331	5.598663
4.32	3.78	4.04099	3.188409	6.376819
4.86	2.25	3.306811	2.60913	5.21826
21.89	13.96	17.48097	13.79278	27.58556
13.31	4.41	7.661403	6.044977	12.08995
8.83	7.9	8.352066	6.589921	13.17984
11.15	10.3	10.71658	8.455559	16.91112
13.51	6.12	9.09292	7.174468	14.34894
12.17	4.86	7.690657	6.068058	12.13612
10.09	5.4	7.381463	5.824099	11.6482
8.46	5.22	6.645389	5.243324	10.48665
16.26	9.01	12.10383	9.550123	19.10025
7.37	4.86	5.984831	4.722133	9.444265
15.67	5.67	9.425969	7.437249	14.8745
8.92	6.49	7.6086	6.003314	12.00663
14.32	7.57	10.41165	8.214966	16.42993
8.38	6.21	7.213862	5.691859	11.38372
11.53	10	10.73778	8.472293	16.94459
10.15	6.49	8.116249	6.403858	12.80772
11.15	6.76	8.68182	6.850103	13.70021
8.92	7.31	8.074974	6.371291	12.74258
12.17	5.48	8.166493	6.4435	12.887
7.3	4.45	5.699561	4.49705	8.9941
17.37	8.84	12.39156	9.777151	19.5543
10.27	9.08	9.656687	7.619289	15.23858
8.65	8.11	8.375649	6.608529	13.21706
12.7	13.33	13.01119	10.26605	20.53209
13.51	5.94	8.958203	7.068173	14.13635
11.89	5.67	8.210743	6.478415	12.95683
3.78	3.24	3.4996	2.761243	5.522487
4.32	3.76	4.030285	3.179963	6.359926
14.32	10	11.96662	9.441865	18.88373
6.76	5.94	6.33675	4.999803	9.999605
8.41	8.38	8.394987	6.623786	13.24757

8	6.21	7.048404	5.56131	11.12262
4.86	3.24	3.968173	3.130956	6.261912
14.32	9.46	11.63904	9.183397	18.36679
11.69	8.38	9.897586	7.809362	15.61872
17.65	10.45	13.58096	10.71561	21.43121
11.98	5.4	8.043134	6.346168	12.69234
9.72	8.29	8.97657	7.082665	14.16533
13.56	5.39	8.549175	6.745444	13.49089
15.85	9.73	12.41855	9.798449	19.5969
15.85	12.61	14.13749	11.15471	22.30943
27.45	17.49	21.9112	17.2883	34.57661
18.01	11.17	14.1835	11.19102	22.38204
19.46	11.53	14.97911	11.81877	23.63754
19.72	6.49	11.31295	8.926107	17.85221
5.76	4.32	4.988306	3.935858	7.871716
5.4	4.68	5.027126	3.966488	7.932975
22.45	7.58	13.04496	10.29269	20.58539
10.17	6.49	8.124242	6.410164	12.82033
7.21	5.76	6.444346	5.084698	10.1694
17.29	8.29	11.97222	9.446285	18.89257
11.17	9.73	10.42517	8.225633	16.45127
17.65	9.37	12.86003	10.14678	20.29357
9.73	7.57	8.582313	6.77159	13.54318
6.76	6.12	6.432045	5.074992	10.14998
26.3	13.33	18.72375	14.77336	29.54672
18.37	9.73	13.36937	10.54866	21.09732
13.33	6.12	9.032143	7.126513	14.25303
14.77	9.93	12.11058	9.555451	19.1109
6.12	5.76	5.937272	4.684608	9.369216
9.73	8.29	8.981186	7.086307	14.17261
10.81	6.12	8.133708	6.417633	12.83527
22.43	9.01	14.21599	11.21665	22.43331
10.24	1.08	3.325538	2.623905	5.247811
36.13	15.03	23.30309	18.38653	36.77306
23.41	12.61	17.18139	13.55641	27.11281
11.17	9.01	10.03203	7.915444	15.83089
10.09	6.85	8.313633	6.559597	13.11919
11.89	5.76	8.275651	6.529628	13.05926
23.78	10.5	15.80158	12.46772	24.93543
9.73	7.5	8.542541	6.740209	13.48042
19.31	11.89	15.15242	11.95552	23.91103
19.84	5.4	10.35065	8.166839	16.33368

16.93	9.37	12.595	9.93767	19.87534
15.49	8.53	11.49477	9.069566	18.13913
17.82	10.5	13.67882	10.79282	21.58563
11.93	6.85	9.039939	7.132665	14.26533
23.86	8.65	14.36625	11.33521	22.67042
26.3	10.83	16.87688	13.31614	26.63228
11.89	7.93	9.710185	7.6615	15.323
27.56	11.89	18.10217	14.28291	28.56583
30.62	10.09	17.57714	13.86866	27.73732
27.74	9.05	15.84446	12.50155	25.0031
40.35	15.13	24.70821	19.49519	38.99039
28.67	8.65	15.74787	12.42534	24.85068
22.04	7.57	12.91676	10.19155	20.38309
12.36	6.21	8.761027	6.912598	13.8252
11.35	5.4	7.828793	6.17705	12.3541
7.39	1.08	2.825102	2.229053	4.458106
14.91	9.15	11.68018	9.215856	18.43171
8.86	6.61	7.652751	6.03815	12.0763
12.48	9.74	11.02521	8.699075	17.39815
9.91	4.32	6.543027	5.162559	10.32512
13.69	8.65	10.88203	8.586103	17.17221
13.44	7.03	9.720247	7.669439	15.33888
8.29	4.32	5.98438	4.721777	9.443553
5.79	4.61	5.16642	4.076393	8.152786
15.83	6.15	9.866838	7.785102	15.5702
8.67	6.12	7.284257	5.747402	11.4948
10.13	7.39	8.652208	6.826738	13.65348
10.45	7.44	8.817483	6.957143	13.91429
15.49	11.32	13.24186	10.44805	20.8961
11.32	8.47	9.791854	7.725938	15.45188
6.76	5.58	6.141726	4.845926	9.691851
4.42	4.36	4.389897	3.463703	6.927406
4.81	4.46	4.631695	3.654486	7.308971
12.61	7.01	9.40192	7.418274	14.83655
11.35	7.39	9.158411	7.226141	14.45228
10.63	9.19	9.88381	7.798493	15.59699
9.46	5.21	7.020442	5.539247	11.07849
7.23	6.92	7.073302	5.580955	11.16191
12.97	6.76	9.36361	7.388047	14.77609
8.53	4.86	6.438618	5.080178	10.16036
6.76	5.13	5.888871	4.646419	9.292837
11.35	4.97	7.510626	5.926011	11.85202

11.89	7.05	9.155572	7.223901	14.4478
13.78	7.03	9.842429	7.765842	15.53168
12.04	8.65	10.20519	8.052071	16.10414
7.03	4.59	5.680467	4.481984	8.963968
15.67	7.21	10.62924	8.386648	16.7733
10.81	10.04	10.41789	8.21989	16.43978
11.17	11.09	11.12993	8.781701	17.5634
11.89	6.79	8.98516	7.089443	14.17889
17.6	11.17	14.02113	11.06291	22.12581
7.57	6.49	7.00923	5.530401	11.0608
7.57	5.76	6.603272	5.210093	10.42019
23.42	6.12	11.97207	9.446163	18.89233
14.09	12.61	13.32947	10.51718	21.03436
14.05	6.49	9.549058	7.534368	15.06874
27.74	13.6	19.42328	15.3253	30.6506
14.41	8.29	10.92973	8.623738	17.24748
9.73	5.4	7.248586	5.719257	11.43851
13.69	5.04	8.306479	6.553953	13.10791
6.49	4.32	5.294979	4.177828	8.355655
7.57	6.12	6.806497	5.370441	10.74088
8.29	5.76	6.910166	5.452238	10.90448
22.7	13.33	17.39514	13.72506	27.45012
9.73	8.29	8.981186	7.086307	14.17261
5.76	5.76	5.76	4.544737	9.089475
8.3	7.57	7.926601	6.254222	12.50844
7.57	6.64	7.089767	5.593946	11.18789
8.29	7.93	8.108002	6.397351	12.7947
11.53	7.67	9.403994	7.41991	14.83982
10.09	6.49	8.092225	6.384902	12.7698
6.85	6.67	6.759401	5.333281	10.66656
7.78	6.87	7.310855	5.768388	11.53678
7.57	7.21	7.387808	5.829105	11.65821
9.01	7.1	7.998187	6.310705	12.62141
11.53	10.09	10.786	8.510333	17.02067
8.86	5.78	7.156172	5.646341	11.29268
7.21	5.76	6.444346	5.084698	10.1694

Curriculum Vitae

Name:	Xueke Chang
Post-secondary Education and Degrees:	McMaster University Hamilton, Ontario, Canada 2015-2019 B.A
	The University of Western Ontario London, Ontario, Canada 2019-2022 M.A.
Related Work Experience	Teaching Assistant The University of Western Ontario 2019-2021
Scholarship	Charles Murray Ball Award 2016